DEVELOPMENT OF A HYBRID POWERED 2D BIPED WALKING MACHINE DESIGNED FOR ROUGH TERRAIN LOCOMOTION

by

Bryce C. Baker

Submitted to the Department of Mechanical Engineering and the Graduate Faculty of the University of Kansas in partial fulfillment of the requirements for the degree of Doctor of Philosophy.

_____

Terry N. Faddis, Chair

_____

Carl W. Luchies, Committee Member

_____

Sarah L. Kieweg, Committee Member

_____

Robert C. Umholtz, Committee Member

_____

James R. Miller, Committee Member

Date Defended: _____

The Dissertation Committee for Bryce C. Baker

certifies that this is the approved version of the following dissertation:

DEVELOPMENT OF A HYBRID POWERED 2D BIPED WALKING MACHINE DESIGNED FOR ROUGH TERRAIN LOCOMOTION

_____

Terry N. Faddis, Chair

_____

Carl W. Luchies, Committee Member

_____

Sarah L. Kieweg, Committee Member

_____

Robert C. Umholtz, Committee Member

_____

James R. Miller, Committee Member

Date Approved: _____

ABSTRACT

Biped robots hold promise as terrestrial explorers because they require a single discrete foothold to place their next step. However, biped robots are multi-input multi-output dynamically unstable machines. This makes walking on rough terrain difficult at best. Progress has been made with non-periodic rough terrain like stairs or inclines with fully active walking machines. Terrain that requires the walker to change its gait pattern from a standard walk is still problematic. Most walking machines have difficulty detecting or responding to the small perturbations induced by this type of terrain. These small perturbations can lead to unstable gait cycles and possibly a fall. The Intelligent Systems and Automation Lab at the University of Kansas has built a three legged 2D biped walking machine to be used as a test stand for studying rough terrain walking. The specific aim of this research is to investigate how biped walkers can best maintain walking stability when acted upon by small perturbations caused by periodic rough terrain.

The first walking machine prototype, referred to as Jaywalker has two main custom actuation systems. The first is the hip ratchet system. It allows the walker to have either a passive or active hip swing. The second is the hybrid parallel ankle actuator. This new actuator uses a pneumatic ram and stepper motor in parallel to produce an easily controlled high torque output. In open loop control it has less than a 1° tracking error and 0.065 RPM velocity error compared to a standard stepper motor.

Step testing was conducted using the Jaywalker, with a passive hip, to determine if a walker with significant leg mass could walk without full body actuation. The results of testing show the Jaywalker is ultimately not capable of walking with a passive hip. However, the walking motion is fine until the terminal stance phase. At this point the legs fall quickly towards the ground as the knee extends the shank. This quick step phenomenon is caused by increased speeds and forces about the leg and hip caused by the extension of the shank. This issue can be overcome by fully actuating the hip, or by adding counterbalances to the legs about the hip.

SUMMARY OF WORK

Biped walking robots and machines require self contained high torque, low speed joint actuators. Pneumatic actuators have the high force-to-weight ratio desired for walking. However, they require expensive complex control systems to perform intermediate motions. Electric motors are easy to control with simple cost effective control systems. Unfortunately, electric motors are typically high speed low torque devices that require substantial gear reduction to achieve the torques and speeds required by biped walkers.

The Hybrid Parallel Ankle Actuator (HPAA) was developed for the Jaywalker walking machine. It optimizes the performance of pneumatic and electric actuators, and combines them into one actuator for biped joint propulsion. This design is based on macro-micro actuators for manipulator arms, and consists of a pneumatic ram and stepper motor attached in parallel to the ankle joint. The pneumatic ram acts as a counterbalance to the required system torque; allowing the stepper motor to move and control the joint. The properties of the HPAA that make it unique are:

- Macro-micro actuator controlled entirely by the micro actuator.
- Produces a very large band of operational torque, with a relatively small footprint. The HPAA configuration tested on the Jaywalker has a 18:1 mass-to-torque ratio.
- It is possible to maintain or increase torque output with increased speed. This improves the walker's ability to catch itself before falling.

Currently the HPAA is capable of motion in only the plantarflexion direction. In the future a pulse pressure feedback system will be introduced to allow the HPAA to move in the dorsiflexion position.

The Jaywalker walking machine was developed as a test platform to study biped walking on rough terrain. It is one of the few walkers that use both pneumatic and electric power for joint actuation. Based on the literature reviewed, it may be the only hybrid powered walker that allows passive hip swing. While in the tests the Jaywalker struggled to walk with a passive hip; several important observations were recorded about

the performance. The outside legs suffered from a behavior termed quick step. Quick step occurs during the terminal swing phase when the knee is extending in preparation for heel strike. A combination of the hip pin joint and inertia effects cause the walker to take a smaller than expected step length. The observations of note about the quick step behavior are:

- The inertia effects of the leg only affect the terminal stance phase. Problems were also expected just after toe-off when the knee flexes.
- Based on a relative energy analysis with the inside leg, the outside legs passive performance can be improved by adding a counterweight to the legs just above the hip.

Currently the Jaywalker's hip is being transitioned to an all time active hip. While further study on implementing passive joint capable active walkers is important, it is currently out of the scope of the projects direction for studying rough terrain motion.

ACKNOWLEDGEMENTS

I offer special thanks to my advisor, Dr. Terry N. Faddis, for his support, guidance and encouragement during my research. I would also like to thank my committee members, Dr. Carl W. Luchies, Dr. Sarah L. Kieweg, Dr. James R. Miller and Professor Robert C. Umholtz, for their assistance and support during this research. In addition, I would like to thank Dr. Sara E. Wilson for her time and advice in developing this research.

Thank you to Madison and Lila Self Graduate Fellowship for providing four years of generous funding.

Finally, I would like to thank my family and friends for the support they have shown me throughout my research. I would especially like to thank my parents, Georgianna and Jim, for all the support and encouragement. To my brothers Andy and Tyler and my godmother Jan Beck your encouragement is very much appreciated. Thanks.

TABLE OF CONTENTS

LIST OF FIGURES

LIST OF TABLES

NONMENCLATURE

C-ATGRF	Center of Actual Total Ground Reaction Force
C_{et}	Transport specific energy cost
C_{mt}	Mechanical specific energy cost
HPAA	Hybrid Parallel Ankle Actuator
HRS	Hip Ratchet System
iHD	Independent Hip Drive
IPM	Inverted Pendulum Model
ISAL	Intelligent Systems and Automation Laboratory
LEGS	Leg Extension Guidance System
Li-Ion	Lithium Ion
MMIPM	Multiple Mass Inverted Pendulum Model
SPI	Serial Peripheral Interface
TMIPM	Two Mass Inverted Pendulum Model
ZMP	Zero Moment Point

INTRODUCTION

Biped robots and walkers inspired by human locomotion have the potential to better transverse unstructured and irregular terrain than wheeled mobile robots. This is because wheeled robots require a continuous path to move across terrain, whereas bipeds require discrete isolated footholds. To put this in perspective, only about half of the earth's land mass is accessible by existing wheeled or track vehicles, whereas animals on foot can reach a much larger fraction of the surface [1]. Biped research started in the early 1970's. Since then significant progress in the field has improved the performance of biped locomotion. Today, biped robots are capable of walking on flat surfaces and non-periodic rough terrain; like stairs and inclined surfaces. Recently bipeds have shown the capability to carry heavy loads [2]. However, biped locomotion over unstructured rough terrain still has not been achieved. The three areas of research that need to be addressed to achieve unstructured rough terrain walking are: 1) control systems, 2) actuator development and 3) joint compliance.

No single advancement in one area will produce a robust rough terrain walking biped. Trajectory based control algorithms based on the inverted pendulum model (IPM) or zero moment point (ZMP) to great affect for controlling biped motion [3-4]. However, path planners require knowledge of the terrain, in order to generate the trajectory. Control algorithms based on intelligent techniques like fuzzy logic and neural networks have shown promise for rough terrain walking [5-7]. This is because intelligent controllers are not dependent on knowledge of the terrain prior to making a decision.

Regardless of how effective a control method may be in adapting to rough terrain; the biped is still limited by its physical ability to respond to the control commands.

Actuator development and joint compliance work together to increase the biped's mobility and agility. However, this is not an equal partnership. The physical characteristics of current actuator technology do more to restrict a biped's mobility than joint compliance limitations. This is because actuators cannot efficiently transmit power through flexible drives. Bipeds are high torque systems relative to their size, and typically cannot accommodate the larger actuators required to compensate for the power loss by the flexible drive. This effect leads most actuators to use rigid drive systems or compliant actuators. Typical compliant actuators used in biped develop consist of antagonistically paired pneumatic muscles [8-9]. Smart wire has been successful as a compliant actuator for small bipeds [10]. However, many bipeds still use electric motors or actuators with rigid drive systems. The Series Elastic Actuator developed at MIT is one example of this type of actuator [11]. All of this does not mean that joint compliance is trivial, or should be neglected. The more energy that can be absorbed or transferred back to the environment; means less energy available to cause instability in the biped.

The scope of work discussed in this dissertation encompasses the development of a biped walking machine to be used as a test platform for studying rough terrain locomotion. While the long range goal of this project is to develop and improve control systems and compliant joints for rough terrain walking. The development of the biped walker focused on actuation. Chapter 1 discusses the design and construction of the biped walking machine; emphasizing the different actuator systems used to improve the walking performance. Chapter 2 details the unique actuator used to power the ankle

joint introduced in Chapter 1. Finally, Chapter 3 discusses the struggles of teaching the biped to walk with a passive hip, but actively controlled knee and ankle.

References

[1] Raibert, M. H., 1986, *Legged Robots That Balance*, MIT Press, Cambridge, Mass. , pp. 1-3, Chap. 1.

[2] Choi, H.-S., You, S.-S., Lee, S.-J., Kim, B.-G., Lim, G.-W., Ko, D.-Y. and Moon, W.-J., 2006, "A study on a new biped robot supporting heavy weight," Busan, South Korea, pp. 1180-1184.

[3] Albert, A. and Gerth, W., 2003, "Analytic path planning algorithms for bipedal robots without a trunk," Journal of Intelligent and Robotic Systems: Theory and Applications, **36**(2), pp. 109-127.

[4] Ito, S., Amano, S., Sasaki, M. and Kulvanit, P., 2008, "A ZMP feedback control for biped balance and its application to in-place lateral stepping motion," Journal of Computers, **3**(Compendex), pp. 23-31.

[5] Bebek, B. and Erbatur, K., 2003, "A Fuzzy System for Gait Adaptation of Biped Walking Robots," *in Proceedings of IEEE Conference on Control Applications (CCA)*, Istanbul, Turkey, **1**, pp. 669-673.

[6] Tabrizi, S. S. and Bagheri, S., 2004, "Robustness of A biped robot controller developed by human expertise extraction against changes in terrain," *Proceedings of the IASTED International Conference on Artificial Intelligence and Applications (as part of the 22nd IASTED International Multi-Conference on Applied Informatics, Febrary 16, 2004 - Febrary 18, 2004*, Innsbruck, Austria, pp. 68-73.

[7] Zhe, T., Meng, J. E. and Geok, S. N., 2007, "Humanoid robotics modeling by dynamic fuzzy neural network," *2007 International Joint Conference on Neural Networks, IJCNN 2007, August 12, 2007 - August 17, 2007*, Orlando, FL, United states, pp. 2653-2657.

[8] Sardellitti, I., Park, J., Shin, D. and Khatib, O., 2007, "Air muscle controller design in the Distributed Macro-Mini (DM2) Actuation approach," *2007 IEEE/RSJ International Conference on Intelligent Robots and Systems, IROS 2007, October 29, 2007 - November 2, 2007*, San Diego, CA, United states, pp. 1822-1827.

[9] Spampinato, G. and Muscato, G., 2006, "DIEES biped robot: A bio-inspired pneumatic platform for human locomotion analysis and stiffness control," Genoa, Italy, pp. 478-483.

[10] Tu, K.-Y., Lee, T.-T., Wang, C.-H. and Chang, C.-A., 1999, "Design of a fuzzy walking pattern (FWP) for a shape memory alloy (SMA) biped robot," Robotica, **17**(pt 4), pp. 373-382.

[11] Robinson, D. W., Pratt, J. E., Paluska, D. J. and Pratt, G. A., 1999, "Series elastic actuator development for a biomimetic walking robot," IEEE/ASME International Conference on Advanced Intelligent Mechatronics, AIM, pp. 561-568.

1. DESIGN OF A 2D BIPED WALKING MACHINE TEST PLATFORM FOR UNDERSTANDING ROUGH TERRAIN LOCOMOTION

1.1 Introduction

Only about half of Earth's land mass is accessible to wheeled and tracked vehicles, whereas animals can reach a much larger fraction. The reason that legs provide better mobility on rough terrain than wheels or tracks is that they use discrete footholds that optimize support and traction, whereas wheels and tracks require a continuous path [1]. Biped robots offer the potential to transverse the largest segment of rough terrain than any other configuration of legged robot. This increased mobility is due to bipeds needing a single foothold in a path to place the next step, whereas quadruped and hexapod robots require two and three footholds in the path respectively. This makes biped robots ideal for terrestrial exploration. Their ability to move similar to humans also makes them ideal as service robots. This is because they can navigate rooms designed for human occupancy better than other types of robots. The psychology of human-robot interactions is also beneficial for using biped robots as service robots. A humanoid robot is more likely to be psychologically accepted by the user than non-humanoid robots [2].

Much progress has been made over the past 40 years in the area of biped robotics. Honda's ASIMO exemplifies this progress in motion with its ability to walk, run, use stairs, and transverse inclines. The Honda robot is powered by a 51.8 V Li-Ion battery with a one hour runtime [3]. It also exemplifies the difficulties that still need to be overcome if biped robots are going to reach their potential as service bots and terrestrial explorers. The two prevailing difficulties in the field of biped robotics are energy

efficiency and rough unstructured terrain walking. ASIMO is not capable of walking on rough unstructured terrain, like walking through the woods. However, it still demonstrates the upper limits to current biped motion. If biped robots are going to reach their potential as terrestrial explorers, rough unstructured terrain walking will have to be achieved. The two focal areas of rough terrain walking research are adaptive controllers and compliant mechanisms. Adaptive control research focuses on developing robust control systems that can adapt the bipeds gait cycle dynamically to different terrain inputs. The compliant mechanisms research area focuses on improved compliance and dexterity of joints and limbs to reduce the terrain disturbances or improve their ability to reach stable footholds. Often these research areas overlap; adaptive controllers and compliant mechanisms work hand-in-hand to improve walking.

The Intelligent Systems and Automation Laboratory (ISAL) in the Department of Mechanical Engineering at the University of Kansas is interested in developing fuzzy logic walking machines that can transverse rough unstructured terrain. ISAL's current focus is on developing a biped test platform that can be used to develop and evaluate new compliant mechanisms that will aide biped robots in rough terrain walking. The scope of this paper will be discussing the design and development of the biped test platform named Jaywalker.

1.2 Human Gait Analysis

Tracing the hip position during human walking shows the limb movement generates periodic motion about this point. One period of this periodic motion is called a

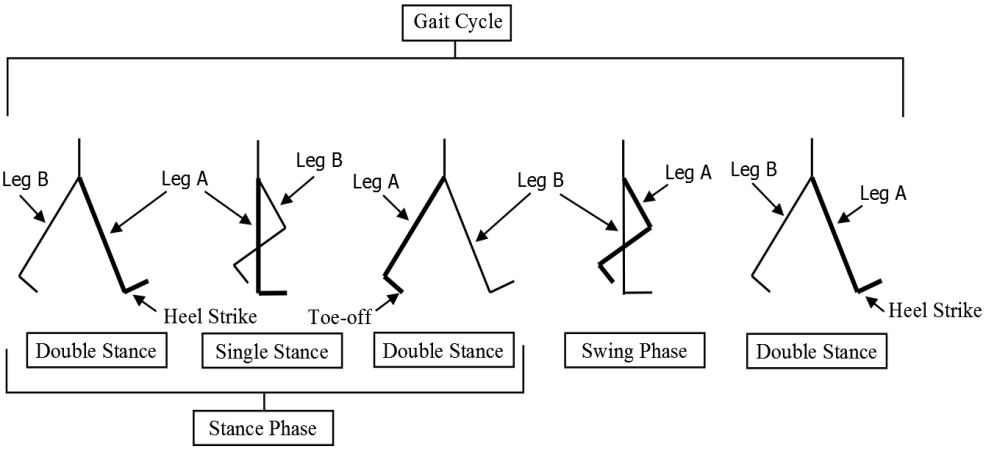

Figure 1.2.1: One gait cycle of human walking starting at the heel strike of one leg and ending at the next heel strike of the same leg.

gait cycle and can be divided into double and single stance phases. Figure 1.2.1 shows a complete gait cycle of human walking starting at heel strike of one leg and ending on heel strike of the same leg. The gait cycle starts at the beginning of the double stance phase with the heel strike event of Leg A. This leg rolls through the double stance phase while Leg B toes-off. Once Leg B breaks contact with the ground, single stance phase begins; Leg A supports the body while Leg B swings forward. Leg B heel strikes the ground and it rolls through the intermediate double stance interval, while Leg A toes-off. Then Leg A swings forward during Leg B's single stance phase. The gait cycle is concluded when Leg A heel strikes the ground. A person will take two steps or one stride during the gait cycle. From Perry [4], the customary walking speed is 80 m/min (262.5 ft/min) and the time duration is approximately 60% for stance and 40% swing. The stance phase can be further segmented to 10% for each double stance phase and 40% for single limb support.

1.3 Human Joint Range of Motion

The overall range of motion for the ankle during a gait cycle is 30°. The peak dorsiflexion angle is 10 degrees and the peak plantarflexion angle is 20° [5]. Ankle dorsiflexion moves the foot towards the lower leg. Ankle plantarflexion moves the foot away from the lower leg. Figure 1.3.1a shows the peak dorsiflexion and plantar flexion angles of the foot relative to the neutral axis.

The knees total range-of-motion is 70°. Starting with 0° at full extension and moving to 70° of flexion during a gait cycle. The exact limits vary depending upon walking speed, individual behavior and obstacles in the path [6]. Knee flexion[1] moves the lower leg towards the thigh. Knee extension[2] moves the lower leg away from the thigh. Figure 1.3.1b shows the flexion and extension range-of-motion during the gait cycle from the lower legs neutral axis.

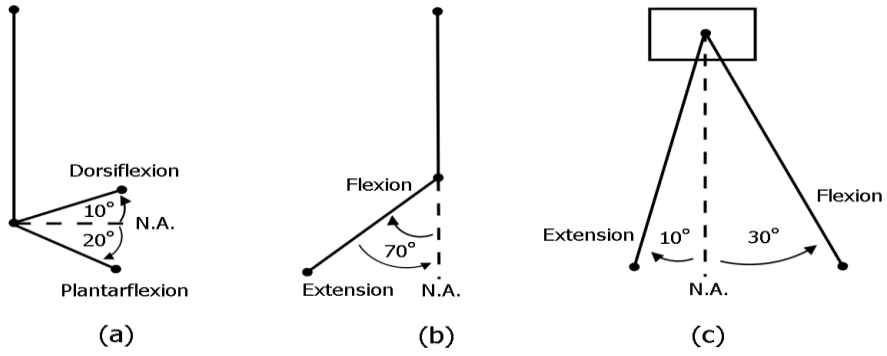

Fig. 1.3.1: (a) Ankle range of motion for human walking. The dorsiflexion and plantar flexion angles are measured from the neutral axis. (b) Knee range of motion for human walking. When the shank moves from 0° to 70° the knee is in flexion. When the shank is moving from 70° to 0° the knee is in extension. (c) Hip range of motion for human walking measured from the neutral axis.

[1] Flexion describes to the bending of a joint.
[2] Extension describes the straightening of a joint.

The hip range-of-motion during the gait cycle is approximately 40°; with a peak flexion of 30° and peak extension of 10° [7]. The hip flexion moves the thigh up towards the body. It moves in the opposite direction as the knee flexion. Hip extension moves the thigh away from the upper body. Figure 1.3.1c shows the peak extension and flexion angles of the hip from the neutral axis. It should be noted the thigh also has a total range-of-motion of 40°, but its peak flexion and extension are both 20° [7].

1.4 Biped Walking Machine Review

There are two fundamental types of walking machines: active walkers, and dynamic walkers. Active walkers depend on actuators to control joint position or force for walking. Dynamic walkers rely on the natural dynamics and gravitational force to walk down inclined paths, or minimal actuation to walk on flat ground.

Most active walker's control architecture is based on generating stable leg trajectories for locomotion. The two most common trajectory generating algorithms, actually implemented on physical walkers, are the inverted pendulum model (IPM) and the zero moment point (ZMP). Kajita et al. created one of the first trajectory controlled active walkers based on the dynamics of a 2D IPM in the sagittal[3] plane [8-9] . The problem with IPM is that it assumes a large mass located at the hip and infinitesimally small mass at the feet. This is an insufficient assumption for active walkers as their legs have significant mass due to the actuators. The advantage of the IPM is its simplicity and

[3] The sagittal plane travels the length of a body and divides it into left and right portions.

its closed analytic solution for trajectories [10]. Advanced IPM models were developed to increase model accuracy and gait stability. Albert discusses two of these advanced models: the two mass inverted pendulum model (TMIPM), and the multiple mass inverted pendulum model (MMIPM) [10]. Both of these advanced models apply a mass or masses to the swing leg to improve the model accuracy and gait stability. This is because the inertia effects of the swing leg have the most impact on the overall walker stability in the sagittal plane.

Another approach to generating stable gait trajectories is to control the robot with the zero moment point (ZMP). The ZMP is the location on the ground where all the forces acting on the robot are summed to zero. If this location is within the foot profile during single stance phase, or within the polygon created by both feet contacting the ground during double stance phase, then the robot is said to be stable. ZMP controllers generate trajectories that satisfy this condition to maintain stable walking. Honda's approach to implementing ZMP control is to use two controllers: a Ground Reaction Force controller that modifies the desired position and posture of the feet and acts to control the Center of Actual Total Ground Reaction Force (C-ATGRF), and a Model ZMP controller to change the ideal body trajectory to shift the desired ZMP to an appropriate position [11]. The difference between the desired ZMP and C-ATGRF is the tipping moment arm. Honda's new generation walker, ASIMO, uses a predictive movement controller added to these earlier controllers to anticipate movement and smooth walking[12]. The BIP2000 control method involves monitoring the ZMP with an original non specified proprietary approach [13]. Both of these robots are powered with

electric actuators. In the past 5 years, microprocessors have become powerful enough to utilize the ZMP approach with pneumatic actuators. An example this is the Lucy pneumatic biped walking robot developed by Vanderborght et al. [14]. It uses a single controller to calculate the joint trajectories required to maintain the ZMP inside the base of support. These trajectories are then used by joint trajectory tracking unit to compute the torque required for locomotion.

The advantage of tracking planners is that they are stable throughout the gait cycle. This helps to prevent falls under normal walking conditions. It also allows them to transverse terrain like stairs and inclines. Trajectory generation is performed either pre-walk offline on a separate computer, or dynamically during the walking cycle. Regardless of how the trajectories are planned, trajectory planning methods have problems when unexpected events occur. The computational power required to produce trajectories and the constraints placed on motion, diminishes the reaction time of the robot. This makes active walkers unresponsive to unplanned perturbations and susceptible to falls.

The first dynamic walkers were passive using gravity to move down inclined surfaces. McGeer's work with a 2D passive walker is the foundation for most of the natural dynamic research to date [15-16]. Since then researchers have expanded this area to include minimally actuated robots. Researchers at Cornell and Delft have both developed minimally actuated walkers. Cornell's walker uses actuated ankles with a passive hip to walk on flat ground. Delft uses an active hip with passive ankles to walk on flat ground. Both use primitive control systems that turn the actuators on or off

depending on feedback from a ground tactile sensor [17]. The primary focus of these walkers is to study human locomotion by comparing morphology, gait, energy consumption, and control. This research has yielded energy efficient walking machines that require minimum control to produce a walking gait. For example, Table 1.4.1 shows the transport specific energy cost (C_{et}) and mechanical specific energy cost (C_{mt}) of Cornell's robot compared to a human [17]. Looking at these results it is easy to see that the natural dynamic walk of Cornell's walker is approximately as energy efficient as a human walk, and significantly more energy efficient than Honda's ASIMO, whose C_{et} and C_{mt} the authors approximated to be 3.2 and 1.6 respectively. These results suggest that human's rely on natural dynamics to minimize muscle activation during a normal gait cycle to reduce energy consumption. Therefore, for biped robots to truly mimic human motion and maximize energy efficiency they must take advantage of natural dynamics to reduce energy consumption of actuators. Dynamic walkers, like McGeer's passive walker, Cornell's walker and Deflt's walker are often referred to as limit cycle walkers. This is because the nonlinear dynamics of walking will converge to a single periodic behavior regardless of modest deviations to the initial conditions. Takuma and Hosoda developed a limit cycle style walker with pneumatic muscle actuation at the hip and knee [18]. They were able to adjust the walking period by

Table 1.4.1: Cornell walker transport specific energy cost and mechanical specific energy cost ratio compared to a human walking at 0.4 m/s.

	C_{et}	C_{mt}
Cornell Walker	0.2	0.55
Human	0.2	0.50

controlling the duty cycle of the pneumatic solenoid valves, while still achieving a walking cycle with only ground tactile sensors to trigger locomotion.

Energy efficiency is important for wide spread implementation of biped robots. The limit cycle dynamic walker approach is limited for rough terrain walking when compared to more actively controlled walkers. Certain rough terrain environments may prevent the use of a periodic gait. Non-periodic gait locomotion requires more control over limb motion than periodic locomotion. Since methods like ZMP always control the position of the limbs, even during periodic motion, it makes them easily adaptable to rough terrain. Limit cycle walkers are incapable of non-periodic motion. Energy requirements for locomotion will also increase with non-periodic gaits because the natural dynamics cannot be exploited to reduce consumption. Thus more fully actuated walkers with more powerful actuators will be required to compensate for the increase in required joint torque.

Recently dynamic walkers have been evolving into more articulated walkers to address the limitations of rough terrain walking. These articulated walkers utilize the natural dynamic mechanisms of the limit cycle walkers, like knee limits and curved feet, to reduce the complexity of the actuator control. Pratt and Krupa have developed one example of these articulated walkers that incorporates knee limits, compliant ankles and a passive swing phase, all allowing the robot to use soft control techniques that do not require high precision. [19].

1.5 Rough Terrain Review

Rough terrain can be defined as either non-periodic or periodic because of the type of gait used to transverse it. Non-periodic terrain requires a walker to significantly change its motion away from a normal gait cycle to successful transverse the terrain. Stairs are a common example of non-periodic terrain. Periodic terrain is any small disturbance that may cause a local perturbation in the walking motion, but does not dramatically alter the periodic gait cycle. It is this classification of rough terrain that is of most interest because it is more likely to cause instability problems with biped walking machines. This is because non-periodic terrain is typically observed and compensated for in the walking motion, and periodic terrain is small unobserved disturbances that are not compensated for in the walking motion. Anecdotally this can be explained by asking, "How often have you fallen down stairs compared to fallen down in a yard due to small elevation changes in the terrain."

Many have investigated rough terrain locomotion using simulations. One example is the study by McCown-McClintick et al. where they developed a biped simulation that looked at walking stability for sinusoidal surfaces with maximum vertical ground steps ranging from ± 1.0 to ± 3.0 cm (± .40 in. to ± 1.2 in.) [20]. Huang et al. developed a control strategy for rough terrain incorporating real time sensor data into a walking pattern generator to adjust to unknown terrains. This controller was simulated on unknown rough terrain with ground height of ± 2.0 cm (.79 in.) [21]. Similar to Huang, Ogino et al. developed a controller based on kinetic energy compensation, and used a simulation to test its performance on 2.3 cm (.91 in.) high ground [22]. Huang and

Ogino's research is more typical of rough terrain simulation research, where a simulation is developed to test a new controller. With increasing frequency more research is being done on physical prototypes. Yamaguchi and Takanishi were some of the first researchers to experimentally study rough terrain biped walking [23]. They built a compliant foot that was able to adaptively walk across terrain that deviated ± 1.6 cm (.63 in.) and ± 3° tilt angle. Tabrizi and Bagheri developed a fuzzy logic rough terrain controller and implemented on MIT's Spring Flamingo, that was capable of walking on sinusoidal ground with a maximum height of 2.5 cm (.98 in) [24].

1.6 Jaywalker Walking Machine

The purpose of the Jaywalker walking machine is to provide a vehicle to study biped locomotion across periodic rough terrain, with specific interest in developing compliant mechanisms for damping terrain perturbations. The Jaywalker 2D biped active walking machine is modeled after McGeer's passive walker [16]. The principle reason for this design choice was to balance the lateral forces without building a torso to shift the walker's center-of-mass over the stance foot. While this design will constrain terrain study to 2D objects and motion response, the increased

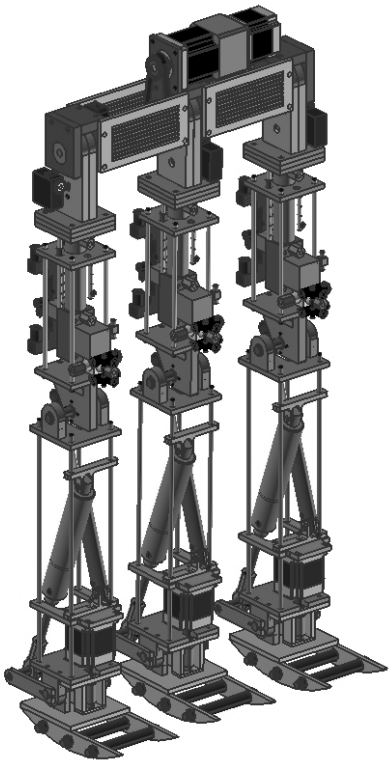

Figure 1.6.1: Isometric view of the Jaywalker 2D biped walking machine test stand prototype.

simplicity will expedite vehicle development reducing the time to rough terrain testing. When 2D terrain testing has been exhausted, converting the Jaywalker to a two legged walking machine requires the development of a torso and the removal of the middle leg.

Another design constraint placed on the Jaywalker was maintaining anthropomorphic leg lengths. The reasons for this constraint are:

1. Anthropomorphic robots are more aesthetically pleasing to humans.
2. If new compliant mechanisms are already in close anthropomorphic relation to humans, it will be easier to develop new prosthetics based on these mechanisms.
3. The gait dynamics of the walker can diverge noticeably from a human gait, if the leg lengths vary too much from their proper proportions.

The anthropomorphic relations were taken from Winters book on biomechanics [25]. It was decided the equivalent full body height of the walking machine would be the size of an average 10 year old boy, approximately 140 cm (55 in.). Table 1.6.1 shows the desired anthropomorphic lengths and actual lengths of the thigh and shank[4] for the Jaywalker. The percent error between the desired anthropomorphic length and the actual

Table 1.6.1: The desired anthropomorphic leg lengths from Winter's relations and the actual lengths for the Jaywalker walking machine given the desired fully body height of the robot is 140 cm (55 in).

Anthropomorphic Leg Lengths [cm (in.)]			
Body Segment	**Desired Length**	**Actual Length**	**% Error**
Thigh	34.22 (13.47)	35.22 (13.86)	2.9
Shank	34.36 (13.53)	36.96 (14.55)	7.5

[4] The shank refers to the lower leg between the knee and ankle. Human anatomy defines this body segment as the leg.

length of the body segment can be attributed to packaging issues with the walker's actuators. However, the body segment masses are not anthropomorphic. This is because of the weight constraints the actuators place on the walking machining. It was not possible to find lighter actuators that would provide the position control and force necessary for walking without exceeding budget limits. The total walker mass based on the modeled prototype was estimated to be 20 kg (45 lb).

The sections 1.7-1.12 will discuss the design and development of the individual components for the Jaywalker walking machine. Section 1.7 will discuss the active hip design as well as the Hip Ratchet System. Section 1.8 will discuss the Leg Extension Guidance System located in the thighs. Section 1.9 will discuss the knee. Section 1.10 will discuss the importance of the ankle and foot to walking. Section 1.11 discusses the control system. Section 1.12 will discuss the differences between the initial design and manufactured prototype.

1.7 The Jaywalker Hip

The hip has two main functions: The first is help keep the torso upright during walking. The second is to move the swing leg during the single support phase of the gait cycle. Since the Jaywalker does not have a torso, the primary function of its hip is to move the swing leg. Controlling the swing leg angular position and velocity modify the step length of the gait cycle. Two different hip designs have been developed for the Jaywalker. The first is the hip ratcheting system (HRS) implemented on the current Jaywalker prototype, and the second is the independent hip drive (iHD). Both designs

meet the minimum design constraints of achieving at least the same range of motion as a human, and rotating the swing leg at approximately 17 rpm[5].

The first hip design developed for the Jaywalker walking machine was the HRS. Energy efficiency was not a main focus for the overall design of the Jaywalker. However, the HRS is designed to take advantage of passive swing dynamics of the leg, thereby increasing energy efficiency. The HRS is powered with a stepper motor connected to the drive shaft by a timing belt with approximately a 60:1 gear reduction. The legs are attached to the drive shaft using a ratchet and pawl. The ratchet is fixed to the drive shaft, and a RC servo motor is used to engage and disengage the pawl to the ratchet. When the leg needs hip power, the servo will rotate the pawl clockwise or counterclockwise depending upon the desired direction of motion. Moving the servo to the neutral position will disengage the pawl from the ratchet and allow the leg to free swing. Figure 1.7.1 shows an isometric view of the HRS. The ratchet and pawl mechanism can be seen in the nearest leg.

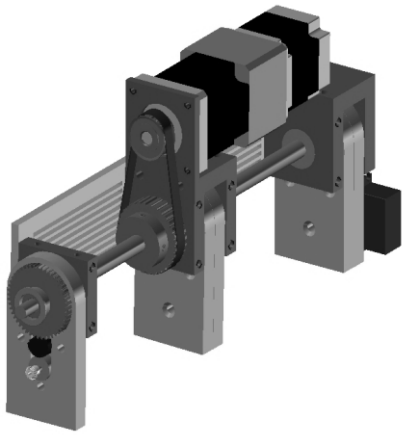

Figure 1.7.1: The hip ratchet system (HRS) for the Jaywalker walking machine.

Unfortunately for the HRS, the passive leg dynamics do not allow a large enough step length to successfully walk. This is due to the hip mass being only 13% heavier than

[5] This angular velocity is what is required to attain the customary walking speed of 80 m/min stated in section 1.2.

the leg mass. Therefore, the inertia forces generated during the swing leg affected the hip motion. Refer to Chapter 3 for step testing results and analysis. This means the Jaywalker's hip will always need to be actively controlled to combat these forces. A new hip prototype, the iHD, has been designed, but not implemented to resolve the issues of a passive hip swing phase. The new hip prototype always actively controls the hip swing, and allows the outside legs to be independently controlled. The iHD, shown in Figure 1.7.2, consists of two stepper motor drives with approximately a 60:1gear reduction directly attached to the outside legs. The larger gear is mounted to the leg and not shown in Figure 1.7.2. The motors are rigidly attached to the hip frame along with the center leg. Therefore the motors will either move the outside legs or the inside leg depending up which are in swing phase. The stepper motors on the iHD can be synchronized to move the outside legs together, or controlled independently to change the step lengths allowing the walker to perform gradual turns.

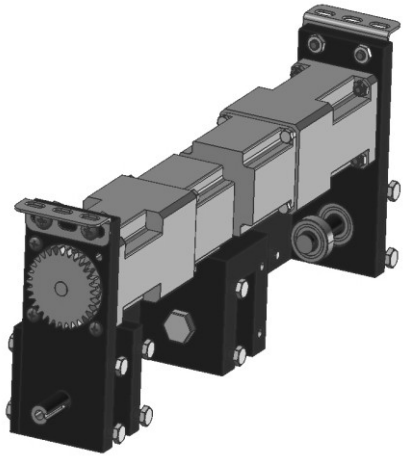

Figure 1.7.2: The independent hip drive (iHD) for the Jaywalker walking machine.

1.8 The Jaywalker Leg Extension Guidance System

The leg extension guidance system (LEGS) is located in the thigh, and is used to vary the Jaywalker's leg length. It can extend the thigh 5 cm (2 in.) with a resolution of 0.63 cm (.25 in.). In general, the smaller the change in the hip potential energy from one

step to another; the more stable the walking motion. The LEGS increasing and decreasing the leg length provides an extra degree-of-freedom to control the potential energy of the Jaywalker. This will allow the Jaywalker to respond to the changes in potential energy during rough terrain walking; improving the walker's stability. The LEGS consists of an air cylinder and rod lock controlled by a solenoid valve. The air cylinder extends or retracts the thigh until the manually adjusted limits on the guide rails are reached. The rod lock is a pneumatic clamp that will hold the air cylinders rod firmly at the desired position. This will prevent the thigh from sagging and other issues related to the compressibility properties of air. Figure 1.8.1 shows the LEGS installed in the thigh of the walking machine's leg.

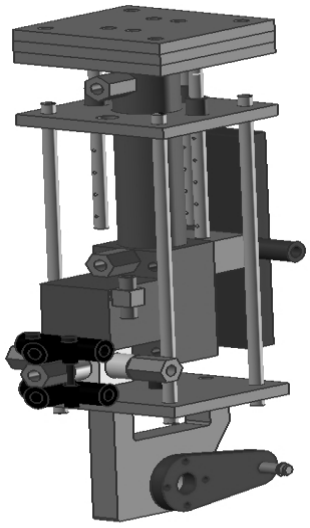

Figure 1.8.1: The leg extension guidance system (LEGS) for the Jaywalker walking machine.

1.9 The Jaywalker Knee

As stated previously by Pratt, natural dynamic mechanisms, like knee limits, are important to reduce the complexity of the control system. This is because it is easier to move an actuator to a limit than it is to have a motor continuously hold a position. McGeer and Collins have effectively used mechanical knee limits with suction-cups to lock the knees during walking [16,26]. While suction-cups are not a reasonable solution

for the much heavier Jaywalker, a knee mechanism comprising physical limits and an actuator will provide the proper performance.

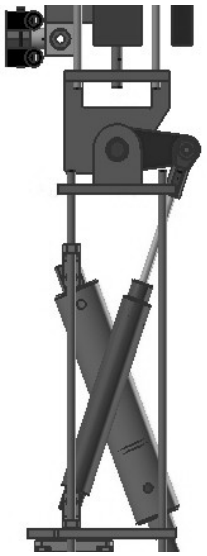

Figure 1.9.1: Illustrates how the knee mechanism is attached to the shank and thigh on the Jaywalker walking machine

It was decided that a pneumatic ram would be the best choice to actuate the knee, because it is a state mechanism. This means the knee is either extended or flexed; no intermediate positions are required so long as the knee flexes enough for the leg to clear the floor, or an obstacle in its path. Typically a human will flex their knees about 70° during walking, with a total range-of-motion greater than 90°s. After careful mechanism synthesis the Jaywalker knee with a pneumatic ram having a 6.3 cm (2.5 in.) stroke, and a 5.1 cm (2.0 in.) lever arm is able to obtain approximately 75° range-of-motion. While a range-of-motion closer to 90° would have been preferred, the physical constraints of the system simply would not allow it. However, the 75° exceeds the minimum requirement of 70° and will provide sufficient range-of-motion. Figure 1.9.1 shows the knee mechanism for the Jaywalker walking machine. Because of the LEGS the knee ram had to be mounted in the shank and pinned to a lever arm that is rigidly attached to the thigh, about the knee joint. The limits of motion are defined by the pneumatic ram position. When the ram is fully extended the leg is fully extended, and when the ram is flexed the leg is fully flexed. The front of the

lower thigh clevis was machined flat for a mechanical stop, if one is determined necessary during testing.

The required peak knee torque for the walking machine was approximated using joint moment-of-force profiles from Winter for the stance phase [27]. Refer to Appendix A.6 for more detailed discussion of approximation. The moment-of-force profile by Winter was given for an adult. Since the Jaywalker is child sized, the knee torque was scaled using a body weight approximation. The weight and sex of Winter's test subject was not provided. Therefore, it was assumed the subject was male and weighed[6] 75.5 kg (166 lb). Based off of these assumptions about the subject, a linear regression was performed to determine the knee torque for the walking machine. This regression yielded a peak knee torque approximation of 8.1 Nm (71.7 lb-in.) for the Jaywalker. This corresponds to a pneumatic ram having a minimum bore diameter of 17 mm (.685 in.) to generate the necessary stance torque at the standard maximum air pressure of 827.4 kPa (120 psi). A pneumatic ram with a bore diameter of 19 mm (.75 in.) was selected for the knee because it was the largest bore over the minimum that would fit within the allotted space in the shank.

1.10 Jaywalker Ankle and Foot

The ankle of the Jaywalker is a simple hinge joint like the knee. The difference is that the ankle needs to be able to move to intermediate positions to perform tasks like standing or adjusting the amount of plantarflexion before toe-off. The other difference is

---

[6] This is the average of a man at the 5th percentile weight and a man at the 95th percentile weight.

that while the knee is responsible for lifting the leg to clear the toe during walking, the ankle is responsible for providing the thrust for motion. This means the torque requirements are substantially greater at the ankle than the knee. Based on Winter's ankle moment-of-force profile, the regression analysis approximates 16.2 Nm (144 lb-in.) for the ankle torque. However, because the Jaywalker will be used for rough terrain walking the required ankle torque could be substantially larger than this value depending upon the type of terrain and gait required for motion.

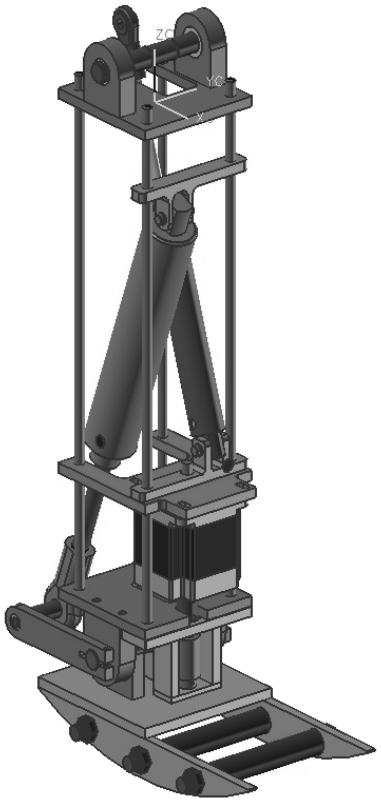

Figure 1.10.1: The lower leg assembly of the Jaywalker walking machine showing the stepper motor and pneumatic ram configured in parallel.

The Hybrid Parallel Ankle Actuator (HPAA) was developed to address the issues of intermediate motion and large torque loads for the ankle. Chapter 2 discusses this actuator in more detail. It consists of a pneumatic ram and stepper motor attached, in parallel, to the ankle shaft. The HPAA functions by the pneumatic ram supplying enough torque to the system, so that the stepper motor can control the speed and position of the ankle. Figure 1.10.1 shows the HPAA attached to the lower leg of the Jaywalker. The procedure for selecting the proper components for the HPAA was as follows:

1. Determine the overall torque required by the ankle.
2. Specify the stepper motor torque for the system.
3. Select an appropriate motor and gearing to match the selected motor torque.
4. Select the desired bore diameter and stroke of the pneumatic ram.
5. Design and synthesize the pneumatic ram mechanism, to ensure that it is capable of a range-of-motion of 10° dorsiflexion and 20° plantarflexion from the neutral axis. Without interfering with the motor and gearing system.
6. Calculate the pneumatic ram torque about the ankle over the range-of-motion as a function of air pressure. Verify that the air pressure for the pneumatic ram does not exceed 120 psi.

This was an iterative process and was performed several times to properly size and package all the components of the HPAA. To account for the high uncertainty in rough terrain ankle loading, the largest stepper motor and pneumatic ram were selected that could be packaged into the shank. This corresponds to a NEMA 23 stepper motor with a 15:1 worm gear and a pneumatic ram with a 31.7 mm (1.25 in.) diameter bore and 76 mm (3.0 in.) stroke. The lever arm attaching the pneumatic ram to the ankle is also 76 mm (3.0 in.). This configuration of components allows the HPAA to produce 37.1 Nm (328 lb-in.) of torque, and have a range-of-motion of 14 degrees dorsiflexion and 47 degrees plantar flexion.

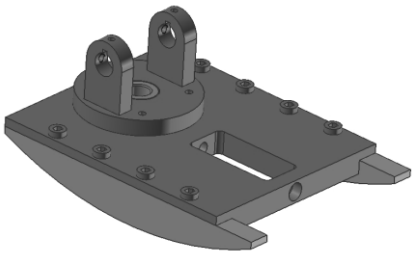

Figure 1.10.2: Baseline foot that will be used to benchmark the Jaywalkers performance across rough terrain.

The foot, shown if Figure 1.10.2, is the baseline foot that will be used for rough terrain testing. This foot has no compliance and will permit the walking machine to feel

every disturbance caused by rough terrain. The foot is curved because it has been shown that less work is needed to walk with larger radius of curvatures [28]. This curvature also allows the walker to have a more natural appearing gait. The reason is that a curved foot provides more toe-off than a flat foot, and therefore does not require the march like high knee lift that is associated with flat foot walkers. The normalized radius of curvature[7] is approximately 0.2 or 0.3 for human walking depending upon whether the foot is being evaluated by the transitional work criteria or center of pressure criteria [28]. Table 1.10.1 shows the expected anthropomorphic dimensions of the foot and the actual dimensions of the foot.

Table 1.10.1: The expected anthropomorphic dimensions for the foot and the actual dimension of foot given the height of the walker is 140 cm (55 in). Note the radius of curvature is a dimensionless number as it is normalized with respect to the leg length.

Foot Dimensions [cm (in)]		
Dimension	**Anthropomorphic**	**Actual**
Length	21.2 (8.36)	17.8 (7.0)
Width	7.7 (3.025)	12.7 (5.0)
Height	5.4 (2.145)	5.9 (2.34)
R.C.*	0.2/0.3	0.25

The foot was widened to provide a larger base of support for the middle leg. The radius of curvature (R.C.) for the actual foot is 0.25. This value is between the radius of curvature values for both evaluating criteria.

[7] The radius of curvature is normalized to leg length

1.11 Jaywalker Control System

There are two primary control approaches to solving the problem of biped walking. The first is conventional[8] techniques like IPM or ZMP that are based on mathematical models. The second is intelligent techniques like fuzzy or neural networks that rely on learning algorithms. A disadvantage to using conventional techniques is that they do not allow the robot to adapt to changing conditions. Therefore if there are changes to the terrain, the model used may no longer be sufficient [29]. Also humans learn to walk from experience. Based on these key points it was decided to use a fuzzy logic controller for the Jaywalker.

The fuzzy logic control system for the Jaywalker operates similar to those used for limit cycle walkers. Contact sensors in the feet register a heel strike or toe-off event, and then the controller triggers the appropriate knee and ankle response. However, additional sensing is needed to track the swing leg relative to the hip, and trigger knee extension. Encoders cannot be used with the HRS because it is possible to decouple the leg from the drive shaft. This will cause the encoder to be blind to the position of the leg. Therefore

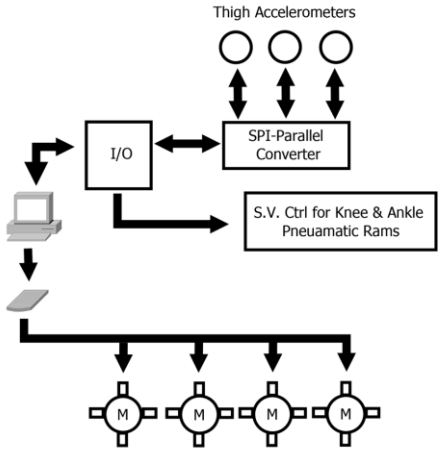

Figure 1.11.1: The basic communication structure of the Jaywalker fuzzy control system.

[8] Conventional techniques are also referred to as classical modeling techniques.

accelerometers attached to the legs were used to trigger knee extension. The Jaywalker has four stepper motors (1 hip, 3 ankles) that are driven by a 10 micro-step drive using a motion control card. A fifth stepper motor with the same control setup is required for the iHD. The contact sensors and solenoid valves for the pneumatic rams are connected to an I/O board. The accelerometers cannot be read directly by the I/O board because it is incapable of reading SPI protocol devices. Therefore a translator circuit was built to read the serial communication from the accelerometers and convert it to parallel communication to be read by I/O board. The motion control card and I/O board are connected to the test computer. The control program must be able to control the inside and outside legs simultaneously to allow the Jaywalker to successfully walk. Consequently, C# was used to write the control program because of its relative ease to multithread tasks. Figure 1.11.1 shows the diagram of the Jaywalker control system.

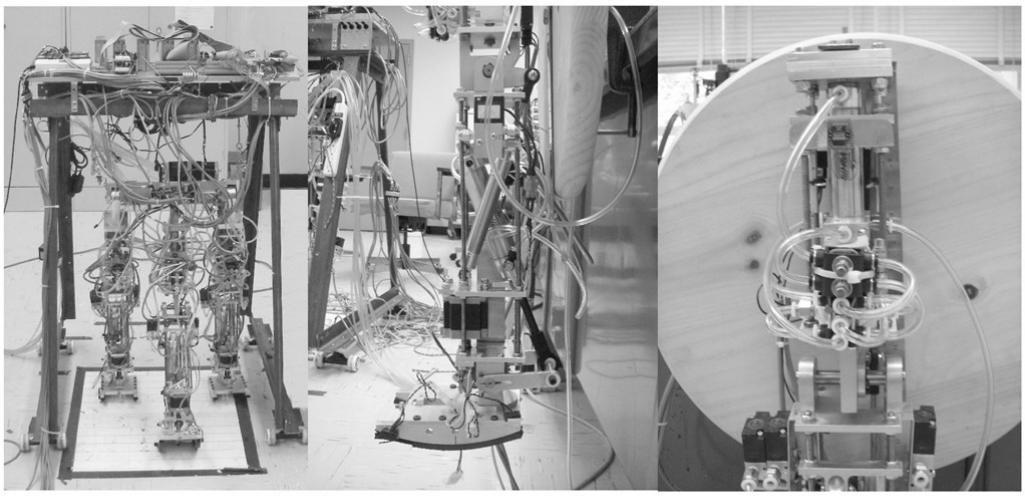

Figure 1.12.1: The Jaywalker prototype walking machine. (a) The Jaywalker connected to the safety tether. (b) The lower leg assembly showing the knee and ankle joints mechanisms. (c) The thigh containing the pneumatic ram and rod lock for the LEGS.

1.12 Jaywalker Construction

The construction of the Jaywalker walking machine, Figure 1.12a, was accomplished with minimal changes to the original design. Rubber soles, Figure 1.12.1b, where installed on the bottom of the feet to help absorb the vibration from the heel impact, and to compensate for machining inaccuracies between the three legs. Figure 1.12.1c shows the front of the thigh LEGS. The biggest concern about the prototype was weight. Throughout the design process the weight of the walker was targeted as 20.5 kg (45 lb). The total weight of the Jaywalker skeleton is 25 kg (55 lb). However, once the walker was completely wired it weighed 28 kg (61 lb). This is 7.5 kg (16 lb) more than the target mass. Because the final prototype mass varies significantly from the target mass, the joint torques where reevaluated with the new masses. This analysis showed that the originally designed actuators are sufficient to power the walker.

1.13 Conclusions

Bipeds hold tremendous promise as mobile robot vehicles because of their potential to travel across a larger percentage of rough terrain than other types of mobile robots. However, bipeds are Multi Input/Multi Output (MIMO) dynamically unstable systems; which makes the task of walking across rough terrain difficult. Progress has been made by robots like Honda's ASIMO traveling across non-periodic rough terrain, like slopes and stairs. Still bipeds struggle with periodic rough terrain that induces disturbances during the periodic walking cycle.

The Jaywalker walking machine was designed and constructed to be a platform for studying periodic rough terrain walking. It is a hybrid machine that utilizes both pneumatic and electric actuation to provide power for its joints. In the case of the ankle, it uses both energy forms together, in a novel way, to provide power to the joint. The primary concern with the prototype was the increased weight, but it was determined the previously selected actuators where sufficient to power the walker. The next phase in developing the Jaywalker rough terrain platform is to teach it to walk on flat ground.

Prototype I of the Jaywalker consists of the HRS, LEGS, knee limit actuator, HPAA and curved foot. These components were controlled using a general computer with interface cards. Prototype II future research recommendations are:

- Implement the iHD for active hip walking tests.
- Replace the general computer controller with an embedded distributed control system.
- Develop a compliant foot with a variable radius of curvature to allow the walker to stand and walk.

1.14 References

[1] Raibert, M. H., 1986, *Legged Robots That Balance*, MIT Press, Cambridge, Mass. , pp. 1-3, Chap. 1.

[2] Hara, F., 2004, "Artificial emotion of face robot through learning in communicative interactions with human," Okayama, Japan, pp. 7-15.

[3] Honda, "ASIMO's Function," at http://asimo.honda.com/InsideAsimo.aspx (last visited on March, 14 2010).

[4] Perry, J., 1992, *Gait Analysis: Normal and Pathological Function*, Slack, Thorofare, N.J., pp. 4-6, Chap. 1.

[5] Perry, J., 1992, *Gait Analysis: Normal and Pathological Function*, Slack, Thorofare, N.J., pp. 52-53, Chap. 4.

[6] Perry, J., 1992, *Gait Analysis: Normal and Pathological Function*, Slack, Thorofare, N.J., pp. 90-91, Chap. 5.

[7] Perry, J., 1992, *Gait Analysis: Normal and Pathological Function*, Slack, Thorofare, N.J., pp. 112-113, Chap. 6.

[8] Kajita, S. and Tani, K., 1991, "Study of dynamic biped locomotion on rugged terrain--Derivation and application of the linear inverted pendulum mode," *Proceedings of the 1991 IEEE International Conference on Robotics and Automation, April 9, 1991 - April 11, 1991*, Sacramento, CA, USA, **2**, pp. 1405-1411.

[9] Kajita, S. and Tani, K., 1995, "Experimental Study of Biped Dynamic Walking in the Linear Inverted Pendulum Mode," *Proceedings of the 1995 IEEE International Conference on Robotics and Automation. Part 3 (of 3), May 21-27 1995*, Nagoya, Jpn, **3**, pp. 2885-2891.

[10] Albert, A. and Gerth, W., 2003, "Analytic path planning algorithms for bipedal robots without a trunk," Journal of Intelligent and Robotic Systems: Theory and Applications, **36**(2), pp. 109-127.

[11] Hirai, K., Hirose, M., Haikawa, Y. and Takenaka, T., 1998, "Development of Honda Humanoid Robot," *Proceedings of the 1998 IEEE International Conference on Robotics and Automation. Part 2 (of 4), May 16-20 1998*, Leuven, Belgium, **2**, pp. 1321-1326.

[12] Honda, "ASIMO's Walking Control," at http://world.honda.com/ASIMO/technology/walking_02.html (last visited on March, 28 2010).

[13] Espiau, B. and Sardain, P., 2000, "Anthropomorphic Biped Robot BIP2000," *ICRA 2000: IEEE International Conference on Robotics and Automation, Apr 24-Apr 28 2000*, San Francisco, CA, USA, **4**, pp. 3996-4001.

[14] Vanderborght, B., Verreist, B., Van Damme, M., Van Ham, R., Beyl, P. and Lefeber, D., 2006, "Locomotion control architecture for the pneumatic biped lucy consisting of a trajectory generator and joint trajectory tracking controller," Genoa, Italy, pp. 240-245.

[15] McGeer, T., 1990, "Passive dynamic walking," International Journal of Robotics Research, **9**(2), pp. 62-82.

[16] McGeer, T., 1990, "Passive walking with knees," *Proceedings of the 1990 IEEE International Conference on Robotics and Automation, May 13-18 1990*, Cincinnati, OH, USA, pp. 1640-1645.

[17] Collins, S., Ruina, A., Tedrake, R. and Wisse, M., 2005, "Efficient bipedal robots based on passive-dynamic walkers," Science, **37**, pp. 1082-1085.

[18] Takuma, T. and Hosoda, K., 2006, "Controlling the walking period of a pneumatic muscle walker," International Journal of Robotics Research, **25**(9), pp. 861-866.

[19] Pratt, J. and Krupp, B., 2008, "Design of a bipedal walking robot," Orlando, FL, United States, **6962**, pp. 69621.

[20] McCown-McClintick, B. E. and Moskowitz, G. D., 1998, "Behavior of a biped walking gait on irregular terrain," International Journal of Robotics Research, **17**(1), pp. 43-55.

[21] Huang, Q., Kaneko, K., Yokoi, K., Kajita, S., Kotoku, T., Koyachi, N., Arai, H., Imamura, N., Komoriya, K. and Tanie, K., 2000, "Balance control of a biped robot combining off-line pattern with real-time modification," San Francisco, CA, USA, **4**, pp. 3346-3352.

[22] Ogino, M., Toyama, H., Fuke, S., Mayer, N. M., Watanabe, A. and Asada, M., 2008, "Compliance control for biped walking on rough terrain," Atlanta, GA, United states, **5001 LNAI**, pp. 556-563.

[23] Yamaguchi, J. i. and Takanishi, A., 1996, "Multisensor Foot Mechanism with Shock Absorbing Material for Dynamic Biped Walking Adapting to Unknown Uneven Surfaces," *Proceedings of the 1996 IEEE/SICE/RSJ International Conference on Multisensor Fusion and Integration for Intelligent Systems, Dec 8-11 1996*, Washington, DC, USA, pp. 233-240.

[24] Tabrizi, S. S. and Bagheri, S., 2004, "Robustness of A biped robot controller developed by human expertise extraction against changes in terrain," *Proceedings of the IASTED International Conference on Artificial Intelligence and Applications (as part of the 22nd IASTED International Multi-Conference on Applied Informatics, Febrary 16, 2004 - Febrary 18, 2004*, Innsbruck, Austria, pp. 68-73.

[25] Winter, D., 1990, *Biomechanics and Motor Control of Human Movement*, Wiley, New York, N.Y., pp. 52-56, Chap. 3.

[26] Collins, S. H., Wisse, M. and Ruina, A., 2001, "A three-dimensional passive-dynamic walking robot with two legs and knees," International Journal of Robotics Research, **20**, pp. 607-615.

[27] Winter, D., 1990, *Biomechanics and Motor Control of Human Movement*, Wiley, pp. Chap.

[28] Adamczyk, P. G., Collins, S. H. and Kuo, A. D., 2006, "The advantages of a rolling foot in human walking," Journal of Experimental Biology, **209**(20), pp. 3953-3963.

[29] Doerschuk, P. I., Nguyen, V., Simon, W. and Kwong, F., 1996, "Intelligent ballistic control of a jointed leg," *Proceedings of the 1996 IEEE International Joint Symposia on Intelligence and Systems, November 4, 1996 - November 5, 1996*, Rockville, MD, USA, pp. 117-124.

2. DEVELOPMENT OF A POSITION CONTROLLED HYBRID MACRO-MICRO PARALLEL ANKLE ACTUATOR

2.1 Introduction

Actuator selection for biped walking robots is a challenging process. This is because biped robot's have to be self supporting with the actuators located on the robot itself. The joint torque is a function of the robot's body weight including the weight of the actuators. Thus the actuators themselves affect the required joint torque for the robot. This relationship between joint torque and actuator weight can lead to a problematic design cycle; where the actuator weight increases the required joint torque beyond the torque capacity of the actuator. This is why the selection of actuators with suitable force-to-weight ratios is important for biped robots.

Electric motors are popular choices for biped robots because they offer highly controllable, cost effective, single level direct control solutions for the actuator. The ASIMO, BWR and M2V2 biped robots show some of the ways electric motors are used to power biped robots. Arguably the most famous and advanced biped robot, Honda's ASIMO uses servo motors with harmonic drives to power the joints [1]. The BWR developed at the Maritime University, in Korea, uses a four-bar-link mechanism to power the leg joints [2]. This four-bar-link mechanism is actuated by an electric motor coupled to a ball screw using a belt drive. The M2V2 developed by Yobotics uses a series elastic electric actuator to power the leg joints [3]. A series elastic actuator has a spring in series with the electric motor and transmission. The spring helps to reduce impact loading during walking and acts as a force sensor [4]. These actuators operate well for their

stated applications. However, electric motor torque curves behave similar to low pass filter frequency response curves. Where the torque will stay approximately constant up to a specific motor speed and then the torque will start to roll-off with increased motor speed. Thus standard electric motors have the characteristic of reducing output torque with increased motor speed. Large gear reductions exacerbate this behavior by having the motor work only on the torque roll-off slope. This will be an impediment to developing fall avoidance strategies, because stabilizing strategies typically require both high torque and high speed response.

Pneumatic actuators do not suffer from the same decrease in torque with increased speed characteristic as electric motors. This allows them to have a larger force range at a given velocity. Other advantages of pneumatic actuators are their natural compliance and large force-to-weight ratios. The disadvantage of pneumatic actuators is their controllability. Unlike electric motors, pneumatic actuators cannot produce intermediate movements between full extension and retraction without expensive control systems that use a sequence of devices to indirectly control the actuator. For a pneumatic actuator to perform like an electric motor a multilevel control system is required. While there are differences, most pneumatic control systems have three basic levels. The first level computes the torque based on a trajectory analysis. The second level calculates the appropriate actuator pressure to achieve the desired torque. Finally the third level uses a bang-bang controller to actuate the control valves. The Lucy biped robot and the DIEES biped robot have similar three level control systems [5-6]. The biped robot developed by Yong et al. at Tsinghua University is also of similar design, but incorporates stiffness as an extra constraint to improve energy efficiency [7].

The University of Kansas, Intelligent Systems and Automation Laboratory (ISAL) is interested in developing adaptive walking machines using fuzzy control logic. The initial step has been to build a biped robot testbed; referred to as the Jaywalker. Most biped robots are designed for a particular terrain or range of terrains. This allows the designer to select actuators that will optimize performance over a predictable torque range. Since the Jaywalker will be used to study the response to a wide range of terrains, it is difficult to predict the required torque for each instance. Therefore it has been important to design the Jaywalker's actuators to generate a wide band of torque to accommodate the unknown loading of the different terrains; particularly for the ankle actuator which provides the thrust for the walking machine. A hybrid parallel ankle actuator with a wide torque band is being proposed for the Jaywalker. Sections 2.2-2.3 describe the actuator design guideline and operation. Sections 2.4-2.6 present the experimental performance of the actuator. Sections 2.7-2.9 discuss actuator design and testing on the Jaywalker. Section 2.10 summarizes the results from the previous sections and discusses future work on the actuator.

2.2 Hybrid Parallel Ankle Actuator Background

Hybrid pneumatic-electric actuators are generally implemented to improve system control over that of pneumatic actuators. There are two configurations for hybrid actuators, series and parallel. Control performance improvements can be seen in both configurations. James Mills proposed a hybrid actuator that utilizes pneumatic muscles in series with servo motors to independently control torsional stiffness and position control [8]. Takemura et al. proposed placing a small electric motor in parallel with a

pneumatic motor to gain improved damping and position control, by switching control of the load between the two actuators [9]. Shin et al. developed the hybrid macro-micro actuator utilizing antagonistic pairs of pneumatic muscles and a servo motor to develop a parallel macro-micro actuator for safe human-robot interactions [10]. The concept of a parallel macro-micro actuator system to improve force control was first proposed by Morrell and Salisbury, and used large (macro) and small (micro) electric motors [11]. Shin's hybrid macro-micro actuators replace the heavy electric macro actuator with a light weight, powerful pneumatic muscle. This decrease in actuator weight decreases the manipulator inertia, which in turn decreases the impact loading. This makes the manipulator safer for human-robot environments.

Hybrid macro-micro actuators are attractive for weight critical applications. This is because the pneumatic macro-actuator increases the force-to-weight ratio and decreases the weight of the actuator compared to electric motors with gearheads or electric macro-micro actuators. This makes them potentially a good choice for walking robots.

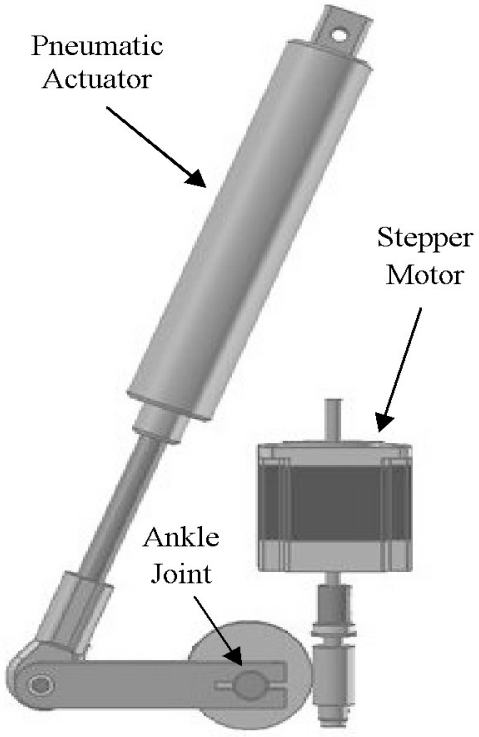

Figure 2.3.1: CAD rendering of the hybrid parallel ankle actuator (HPAA) for use with 2D biped walking machine.

2.3 Design Concept

The Hybrid Parallel Ankle Actuator (HPAA) utilizes a pneumatic ram and a stepper motor in a macro-micro actuator configuration coupled in parallel to a joint, as shown in Figure 2.3.1. The pneumatic macro-actuator provides the gross torque for motion. The micro-actuator stepper motor provides the remaining torque to control motion. The HPAA is position controlled to match the control strategy selected for the Jaywalker testbed. Position control was selected because its performance is equivalent to force control when studying known terrain environments, but is more affordable and easier to implement.

The HPAA macro-actuator acts like a counterbalance that reduces the required torque for motion. When the macro-actuator torque is properly set, the required system torque will be reduced to less than the micro-actuator torque output. Thus making it possible for the stepper motor to move the load, and hence control the actuator. For the macro-actuator to be correctly set, the pneumatic ram torque must be less than the required system torque, but the summation of the pneumatic ram torque and stepper motor torque must be larger than the required system torque. Mathematically, this relationship can be expressed as the following two inequalities;

$$\tau_p < \tau_s \tag{2.3.1}$$

and

$$\tau_p + \tau_m > \tau_s . \tag{2.3.2}$$

Where τ_s is the system torque including the inertial torque, τ_p is the pneumatic actuator torque, and τ_m is the stepper motor torque. Figure 2.3.2 shows the lower and upper bounds of the HPAA torque. The lower torque bound of the HPAA is the maximum

torque the pneumatic actuator can exert on the system. The upper bound is the summation of the pneumatic actuator torque and stepper motor torque. Notice for the actuator to work, the pneumatic ram torque is less than the system torque, and the sum of the pneumatic ram and motor torque is greater than the system torque.

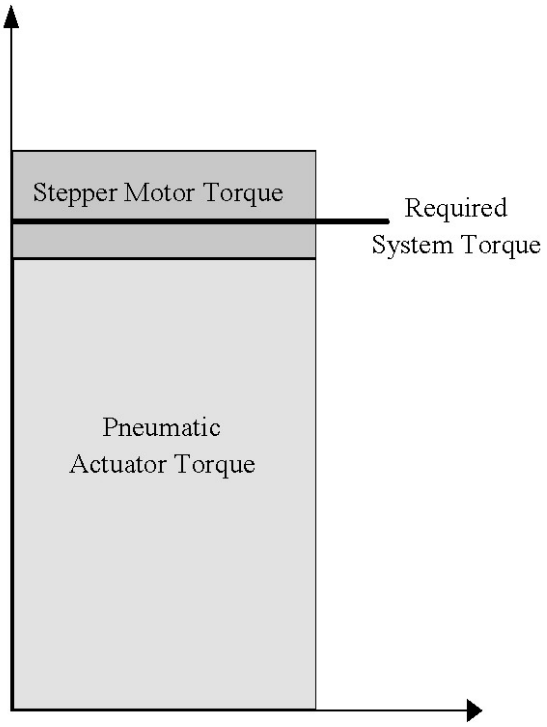

Figure 2.3.2: Distribution chart of how the HPAA develops torque.

A properly selected macro-actuator torque will ensure the HPAA moves the load, but does not guarantee the HPAA will move at the desired speed of the micro-actuator. The pneumatic actuator is rigidly attached to the joint shaft. Meaning the rod velocity of the cylinder is proportional to the rotational velocity of the stepper motor moving the joint. If the volumetric rate of change of the air piston exceeds the air flow rate; system pressure cannot be maintained. This pressure drop could cause the stepper motor to stall, because not enough pressure is being provided to maintain a proper torque level. Once the stepper motor stalls, the pressure will build in the air cylinder and the stepper motor will move again until the stepper motor out runs the air flow rate. This behavior will cause the HPAA to surge and possibly damage the stepper motor. Therefore care should be taken in selecting the components for the pneumatic system to

ensure the flow rate is sufficient to maintain the proper pressure over the entire range of operating speeds.

Electric motors have a faster response time to a system input, compared to pneumatic actuators. This characteristic causes a time lag between stepper motor and pneumatic actuator actuation. The HPAA open-loop controller has to compensate for this time lag. Otherwise the stepper motor will skip steps as it tries to lift a load beyond its capacity, and positional accuracy will be lost.

The pneumatic latency is a property of the mechanical system. It is the time to pressurize the pneumatic circuit downstream of the control valve to the set pressure. It is the pneumatic latency that causes the time lag between the stepper motor and pneumatic actuator. The pneumatic latency can be approximated by dividing the volume of the downstream circuit by the flow rate. Because the air cylinder cannot lift the load by itself, the downstream circuit can be modeled as a reservoir. Depending upon the application, the latency may be critical for the actuator to function properly. Reducing latency is a function of either decreasing the downstream volume or increasing the flow rate. Volume reduction can occur by decreasing the air cylinder diameter, or shortening air line length. Since the air cylinder diameter is constrained by system force requirements, this is not a viable method for reducing system volume. Minimizing the air line length is the preferred method for reducing the downstream pneumatic circuit volume.

Increasing the flow rate to decrease pneumatic latency is best achieved by selecting a control valve capable of increased flow rates. Calculating the actual flow rate is difficult. This is because the flow rate varies inversely with the change in downstream

pressure. Since the downstream pressure is continually increasing as air fills the pneumatic circuit; the flow rate is also continually decreasing. There are several methods that can be implemented in a stepwise approach to analytically calculating the flow rate. Methods can range in difficulty from simply approximating the flow as half the maximum flow rate to using the Fanno flow equations. The discussion of how to apply these or other methods is beyond the scope for this paper. Regardless of what method is used to calculate the flow rate, some level of uncertainty will exist in the calculation. Therefore it is best to use the analytical solution as the initial guess in tuning the lag time in the controller.

This paper's investigation of pneumatic latency for the HPAA is focused on how the cylinder fill time varies with system air pressure. If the fill time varies significantly with pressure, the controller will need to dynamically adjust the controller lag time to optimize the response time of the HPAA. On the other hand, if the fill time does not vary significantly with pressure, the controller can utilize a fixed lag time without affecting response time of the HPAA. The fixed lag time is the preferred condition because it optimizes the response time and computational efficiency for the controller. As long as the actual air flow rate through the circuit is constant, the fill time should be constant. This is because the ratio of air mass at a given pressure to the atmospheric mass is the same as the ratio of air density at a given pressure to atmospheric density. For example, air at 240 kPa (35 psi), 310 kPa (45 psi) and 380 kPa (55 psi) has 2.4, 3.0 and 3.7 times the mass and density of atmospheric air. This means that if the flow rate is constant at these pressures the mass flow rate increase in the system will match the needed increase in mass, thereby causing the pneumatic latency to be constant.

2.4 Benchmark Apparatus Description

The lever arm testbed, shown in Figure 2.4.1, is used to benchmark the performance of the HPAA to that of a standard stepper motor. The performance testing will compare the position and velocity control of the HPAA with a stepper motor. The testbed is designed for the HPAA to lift a load to a set position and hold it. The micro-actuator for the testbed uses a US Digital MS23 stepper motor connected to the output shaft by a timing belt with a 7.2:1 mechanical advantage. The macro actuator is a Parker SR series linear pneumatic ram with a 27 mm (1.1 in.) bore and a 305 mm (12.0 in.) stroke connected to the back of the lever arm, 165 mm (6.50 in.) away from the output shaft. The stepper motor and pneumatic actuator are driven by a US Digital MD1 micro-step drive and Humphrey 310 series solenoid valve respectively through microprocessors that interface with the test computer.

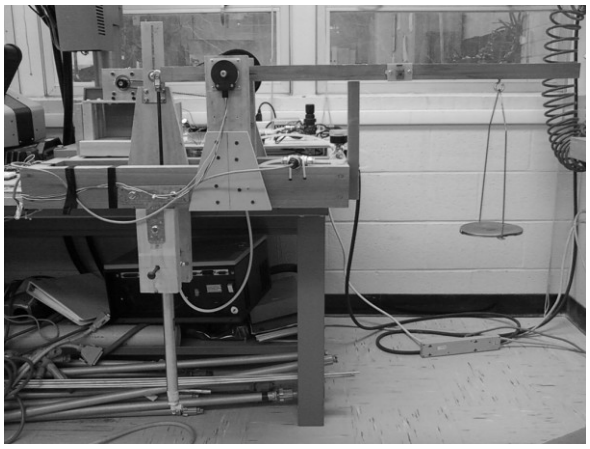

Figure 2.4.1: HPAA proof-of-concept test stand.

The angular position and air pressure are measured, using a US Digital E-3 optical encoder and a Honeywell MLH series pressure transducer respectively. Data acquisition is performed by a NI USB-6210 DAQ hub. The encoder provides the position performance data of the actuator. The velocity performance is determined by differentiating the encoder data with respect to time. The pressure sensor is used to validate that the air pressure is set at the desired test pressure.

2.5 Benchmark Test Procedure

The HPAA performance is benchmarked by comparing the open-loop step response to that of a baseline stepper motor step response. The step response will track an input signal that has the lever arm move 30 degrees at 2 and 4 RPM. Thirty degrees was selected because it is the typical range of motion for a foot during walking [12]. For this experiment the micro-actuator stepper motor used by the HPAA will be the baseline. Performance testing for the HPAA will be done at air pressures of 140 kPa (20 psi), 210 kPa (30 psi) and 280 kPa (40 psi). Loads were applied to the lever arm that produce torques equal to 25% of the total torque capacity of the baseline motor and HPAA at the set pressures. For example, the load for baseline testing produces a torque of 1.4 Nm (12 lb-in.), which is 25% of the stepper motor torque capacity at the output shaft. The Tested torque for the HPAA was 13.3 Nm (118 lb-in.), 19.3 Nm (170 lb-in.) and 25.2 Nm (223 lb-in) respectively for the test pressures of 140 kPa (20 psi), 210 kPa (30 psi) and 280 kPa (40 psi). Another way to look at the loading is that the HPAA is being tested at 9.5, 13.8 and 18 times the baseline torque.

The pneumatic latency was tested by locking the lever arm to the testbed preventing the pneumatic ram from lifting it. The DAQ recorded the air pressure rise over time at pressures of 140 kPa (20 psi), 210 (30 psi) kPa, 280 kPA (40 psi), 350 kPa (50 psi), 410 kPa (60 psi), and 480 kPA (70 psi).

2.6 Benchmark Test Results and Discussion

The effectiveness of the HPAA to be controlled by the micro-actuator is shown by the experimental results in Figure 2.6.1. Refer to Appendix B.4 for higher resolution performance plots. The HPAA step response compared to the baseline step response is shown in the upper plots of Figure 2.6.1a and Figure 2.6.1b for actuator speeds of 2 and 4

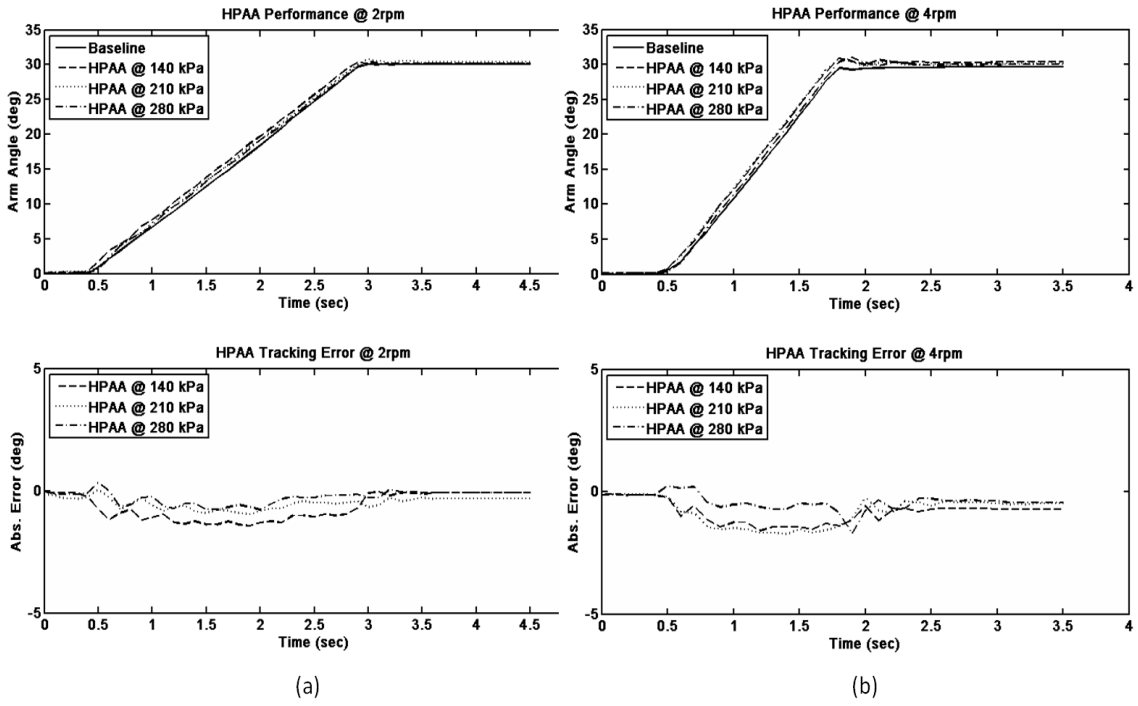

Figure 2.6.1: (a) HPAA step response and tracking error compared to baseline at 2 RPM. (b) HPAA step response and tracking error at 4 RPM.

RPM respectively. The difference between the HPAA position and baseline position at any given time is shown in the lower plot of Figure 2.6.1a and Figure 2.6.1b. This difference is the tracking error of the HPAA. Table 2.6.1 shows the root-mean-square and final position tracking errors with respect to the baseline performance for the HPAA. Table 2.6.1 also shows the absolute velocity error of the HPAA compared to the baseline

motor. The negative sign in front of the error indicates that the HPAA is moving slower than the baseline motor.

Table 2.6.1: RMS tracking error and abs. velocity error for the HPAA on the test stand.

HPAA Testing Errors				
	RMS Tracking Error (deg)		Abs. Velocity Error (RPM)	
HPAA	2 RPM	4 RPM	2 RPM	4 RPM
@ 140 kPA	0.850	0.957	-0.005	0.061
@ 210 kPA	0.544	0.975	-0.016	0.016
@ 280 kPA	0.379	0.543	0.005	-0.016

Theoretically, the HPAA step response should match the baseline step response because the same stepper motor configuration was used for the micro-actuator of the HPAA as for the baseline testing. However, a RMS tracking error less than 1º and a constant velocity error less than 0.07 RPM is a good result for an open-loop control system; considering that the HPAA is lifting 9.5, 13.8 and 18 times the baseline load. Based on these test results, it can be stated that the HPAA is successfully controlled by its micro-actuator stepper motor.

The pneumatic latency for the HPAA downstream pneumatic circuit is 0.101 ± 0.005 seconds for all tested pressures. Therefore, to fill a volume of 23.5 mL (1.43 in^3), the constant HPAA testbed flow rate is 232 mL/s (14.2 $in^{\wedge 3}$/s). The deviation is small compared to the overall fill time. Therefore a static lag time can be used in the HPAA controller to compensate for pneumatic latency.

2.7 Jaywalker Testbed Development - Ankle Loading

The ankle torque has a cyclical loading pattern. This loading cycle can be separated into loading that occurs during the stance phase and loading that occurs during swing phase of the gait cycle. A large torque is generated by the ankle during the stance

phase starting at heel strike and increases in magnitude, while plantarflexing the foot, until toe-off to provide thrust for walking. After toe-off has occurred, the torque generated by the ankle drastically diminishes during the swing cycle. This is because the ankle during the swing phase, dorsiflexes the foot, to position it for the next heel strike. Simply stated the ankle must generate a large torque during the stance phase to propel the entire body forward, but generates significantly less torque during the swing phase when it only has to reposition the foot.

To actuate the ankle for standard flat ground walking, the HPAA will engage both its micro-actuator and macro-actuator during the stance cycle, to generate the necessary torque for motion. However, during the swing cycle only the micro-actuator will be used to reset the foot for heel strike. The peak ankle torque for stance phase was approximated based on data from Winters [13]. From this approximation, the peak torque for the stance phase is 22 Nm (200 lb-in.) for the 28 kg (61 lb) Jaywalker. The swing phase torque of 2.0 Nm (14 lb-in) was approximated by calculating the foot moment due to its mass about the midline of the foot.

2.8 Jaywalker Testbed Development - Ankle Design

The micro-actuator of the HPAA is the same MS23 stepper motor used in the baseline testing, with a 15:1 worm gear attached to the ankle joint. The expected speed of the ankle joint is between 8 and 12 RPM. The main design focus for the HPAA was to maximize the torque output while minimizing the weight without affecting the open-loop position control. To achieve a maximized torque output the micro-actuator torque needs to be maximized. The 15:1 worm gear is the largest drive that can fit into the physical

constraints of the Jaywalker shank. This powertrain configuration allows the micro-actuator to produce 11.6 Nm (103 lb-in) of torque up to 33 RPM at the ankle joint before the torque attenuates with increased speed. Therefore, the torque output of the motor will be constant over the expected speed range of the ankle joint. This powertrain provides approximately 5.8 times the estimated torque for the swing cycle. Therefore only the micro-actuator will be required to move the ankle joint during swing phase. It is preferable that the drive system for the micro-actuator be backdriveable. This will help guard against the macro-actuator damaging the micro-drive, if actuated at the wrong time. If the micro-drive is not backdriveable it will need to be robust enough to resist the macro-actuator loading without breaking.

The macro-actuator of the HPAA is a pneumatic ram with a 31.8 mm (1.25 in.) bore and 76 mm (3.0 in) stroke. The air cylinder is pinned to the shank and to the ankle joint. A 76 mm connecting arm attaches the air cylinder to the ankle joint. This connecting rod is used to increase the ankle torque and range of motion of the foot. In this 3-link mechanism configuration, the angle between the air cylinder and connecting arm changes as the ankle joint rotates. This will cause the torque being applied by the macro-actuator to change as the ankle moves from heel strike to toe-off. Therefore, care was taken to configure the macro-actuator mechanism in a way that would increase the applied torque by the macro-actuator as the ankle moved from heel strike to toe-off. At toe-off the macro-actuator can produce as little as 7.4 Nm (66 lb-in) of torque at 140 kPa (20 psi) or as much as 25.5 Nm (225 lb-in) of torque at 480 kPA (70 psi).

The HPAA has the ability to operate as a single stepper motor actuator or as a dual hybrid actuator. The total torque range the HPAA is able to apply to the ankle joint is between 0 and 37.1 Nm (328 lb-in.) at 480 kPa (70 psi). Thus the approximate torque-to-mass[1] ratio is 18:1 for the HPAA. Figure 2.8.1, shows the HPAA mounted inside the shank of the Jaywalker robot.

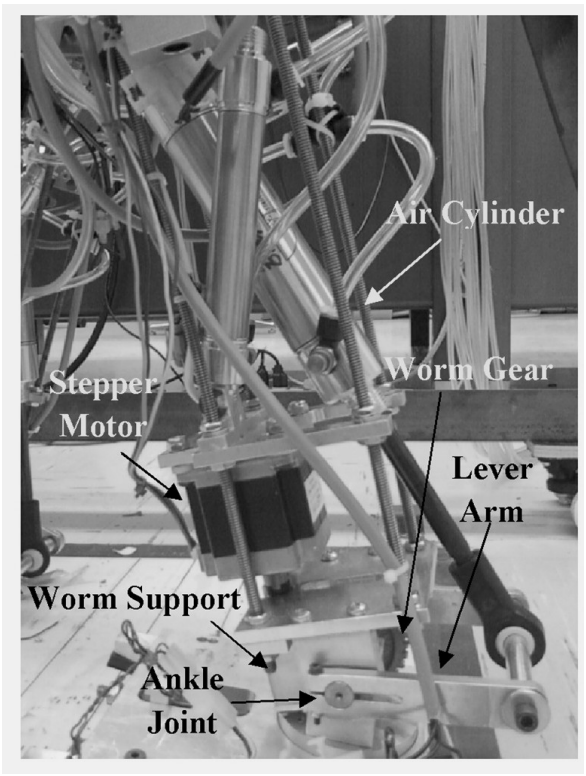

Figure 2.8.1: The HPAA mounted on the shank of the Jaywalker testbed.

The control of the HPAA on the robot is the same as the testbed. Except a positional control system is used to plantarflex the HPAA between heel strike and toe-off of the stance phase, and dorsiflexes between toe-off and heel strike during the swing phase. The downstream pneumatic circuit for the Jaywalker robot has 24% the total volume used in the test stand. Therefore the fill latency will be 24% the time of the test stand. The fill latency was estimated to be 27.2 ms based on the experimental data from the test stand.

[1] The mass of the shank is 2 kg (4 lb).

2.9 Jaywalker Testbed Development - Ankle Performance

Based on the maximum estimated ankle torque from section 2.8, it was determined the air pressure for the HPAA should be set at 345 kPA (50 psi) on the Jaywalker testbed. Figure 2.9.1, shows the estimated peak ankle torque relative to the upper and lower torque bounds of the HPAA at 345 kPA (50 psi) over the range of motion of the ankle. At this pressure the estimated ankle torque is approximately the average of the upper and lower torque limits over the ankle's range of motion. This was done to split the error difference of the estimated ankle torque. The HPAA successfully lifted the robot with a single foot onto its toe using this pressure. This confirms that the required ankle torque for walking is within the lower and upper limits of the HPAA set at 345 kPA (50 psi). Normal operating pressure during walk trials was 310 kPa (45 psi).

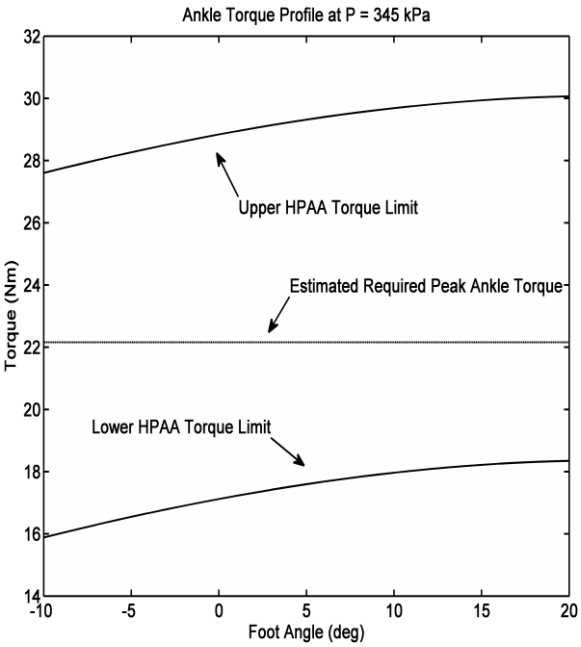

Figure 2.9.1: Calculated torque for HPAA and the estimated maximum required ankle torque.

The HPAA has powered the Jaywalker robot for over 250 walking trials on flat ground. During these walking trials, it was determined that the optimal speed for the HPAA was between 8 and 10 RPM to achieve ideal gait motion. HPAA trials were performed at 20 RPM. However, at this speed the HPAA simply threw the Jaywalker forward causing the gait to become unstable.

2.10 Conclusions

The HPAA is a hybrid parallel macro-micro actuator designed to provide an economical power source for positional control biped robots. It achieves this goal by having the micro-actuator control the speed and position of the actuator. This reduces the control costs of the actuator. Benchmark testing the HPAA with a stepper motor shows that it performs nearly the same as a stepper motor. The RMS position error is less than 1º and the absolute velocity error is less than 0.02 RPM for tested speeds and positions. The HPAA was then integrated into the Jaywalker biped robot testbed. Here it has demonstrated it can provide both the necessary torque and joint velocity for the Jaywalker to step forward.

Currently the HPAA can only plantarflex the ankle during stance phase. This is acceptable as it is this motion that moves the robot forward. However, during rough terrain testing it may be necessary to dorsiflex the ankle during stance phase. In order to accomplish this; the HPAA will act as a power damper. The micro-actuator will move the air cylinder piston to compress the air inside the cylinder. A feedback control strategy will be implemented to pulse the control valve open to relieve excess pressure during the process. This will allow the HPAA to have a full range of motion and minimize energy by not having to charge the opposite side of the air cylinder.

2.11 References

[1] Honda, "ASIMO's Specifications," at http://world.honda.com/ASIMO/technology/spec.html (last visited on March, 14 2010).

[2] Choi, H.-S., You, S.-S., Lee, S.-J., Kim, B.-G., Lim, G.-W., Ko, D.-Y. and Moon, W.-J., 2006, "A study on a new biped robot supporting heavy weight," Busan, South Korea, pp. 1180-1184.

[3] Pratt, J. and Krupp, B., 2008, "Design of a bipedal walking robot," Orlando, FL, United States, **6962**, pp. 69621.

[4] Robinson, D. W., Pratt, J. E., Paluska, D. J. and Pratt, G. A., 1999, "Series elastic actuator development for a biomimetic walking robot," IEEE/ASME International Conference on Advanced Intelligent Mechatronics, AIM, pp. 561-568.

[5] Spampinato, G. and Muscato, G., 2006, "DIEES biped robot: A bio-inspired pneumatic platform for human locomotion analysis and stiffness control," Genoa, Italy, pp. 478-483.

[6] Vanderborght, B., Verreist, B., Van Damme, M., Van Ham, R., Beyl, P. and Lefeber, D., 2006, "Locomotion control architecture for the pneumatic biped lucy consisting of a trajectory generator and joint trajectory tracking controller," Genoa, Italy, pp. 240-245.

[7] Yong, M., Jiaxin, W., Shi, L. and Zhuo, H., 2006, "Energy-efficient control of pneumatic muscle actuated biped robot joints," Dalian, China, **2**, pp. 8881-8885.

[8] Mills, J. K., 1993, "Hybrid Actuator for Robot Manipulators - Design, Control and Performance," Mechatronics, **3**(1), pp. 19-38.

[9] Takemura, F., Pandian, S. R., Nagase, Y., Mizutani, H., Hayakawa, Y. and Kawamura, S., 2000, "Control of a hybrid pneumatic/electric motor," Takamatsu, **1**, pp. 209-214.

[10] Shin, D., Sardellitti, I. and Khatib, O., 2008, "A hybrid actuation approach for human-friendly robot design," Pasadena, CA, United states, pp. 1747-1752.

[11] Morrel, J. D., 1996, "Parallel Coupled Micro-Macro Actuators," Massachusetts Institute of Technology, Cambridge.

[12] Perry, J., 1992, *Gait Analysis: Normal and Pathological Function*, Slack, Thorofare, N.J., pp. 52-53, Chap.

[13] Winter, D., 1990, *Biomechanics and Motor Control of Human Movement*, Wiley, pp. 91, Chap. 4.

3. MOTION ANALYSIS OF A 2D BIPED WALKING MACHINE WITH A PASSIVE HIP

3.1 Introduction

The Jaywalker 2D biped walking machine, shown in Figure 3.1.1, moves by actuating the inside leg to take a step, and then synchronously actuating the outside legs to take a step. All legs are constructed the same. This version of the testbed has actuated ankles and knees powered by the HPAA and knee pneumatic ram respectively, but the hip is a passive hip. This is accomplished by setting the HRS to its neutral state. The purpose of this configuration is to determine the Jaywalkers ability to utilize passive dynamics during the gait cycle.

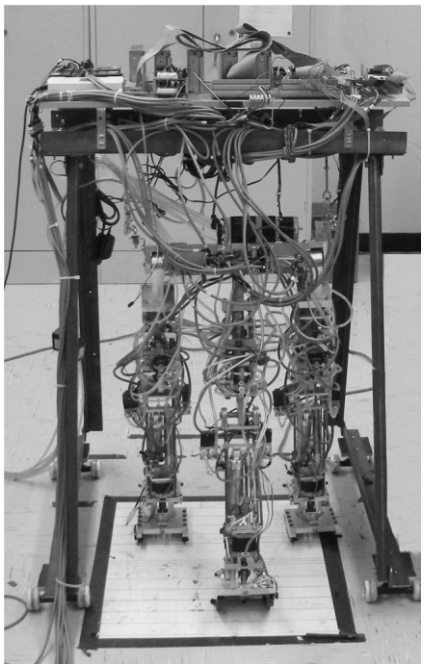

Figure 3.1.1: The Jaywalker 2D Walking Machine. It moves by actuating the inside leg for a step and then synchronously actuating the outside legs for a step.

Limit cycle walkers, like those referenced [1-2], are designed to utilize passive dynamics during walking. The principles that govern the design of these machines are derived from simple analytical models [3-5]. While there are differences between the referenced models, they all assume the leg mass is infinitesimal compared to the point mass at the hip. This assures that the motion of the swing leg does not affect the motion of the hip. Hobbelen et al. designed a limit cycle walker, and placed the actuators in the trunk and connected to the desired joint through a cable transmission [4]. The purpose of

Table 3.1.1: The mass distribution and general dimensions for the Jaywalker walking machine.

Jaywalker Body Mass Distribution				
	Mass	**Robot Dimensions (cm)**		
Segment	**m (kg)**	**Width**	**Depth**	**Height**
Hip	6.8	41.3	7.3	-
Thigh	2.6	7.6	7.6	35.2
Shank	2.0	8.6	8.6	37.0
Foot	1.4	12.7	17.8	6.0

this was to maintain the $m_{leg} << M_{hip}$ relationship. Table 3.1.1 shows the mass distribution of the Jaywalker walking machine. Obviously, its leg mass is not negligible, and may cause issues with the swing phase. The question is to what degree will the leg mass affect the Jaywalkers ability to walk with a passive hip? To answer this question the Jaywalker performance will be evaluated by analyzing its ability to take steps and then eventually progress to walking.

3.2 Step Background

One of the first major milestones in a young child's life is taking their first step. Typically within 4 months the child has learned to walk with reasonable success, but they are still prone to falls when uneven terrain is encountered, or they start to walk too fast. During this period of learning to walk, the child will use furniture and adults as tethers to help maintain stability. From a computational perspective this makes perfect sense, because humans can efficiently apply past experiences to solve new problems, but are not able to process complex mathematical models. Since the Jaywalker wants to mimic human motion, it should also mimic human control. Therefore intelligent control

techniques [6-7] will be employed to develop the controller for the Jaywalker, rather than traditional model techniques [5,8-9]. Specifically, the Jaywalker will utilize a fuzzy logic controller that uses human knowledge to develop the rules for motion, similar to reference [7]. The reason for selecting this type of controller is the future plans for the Jaywalker involve developing an embedded control system and self learning algorithms are too computationally expensive for these systems to solve.

Since the Jaywalker's motion and control are inspired by human behavior. The Jaywalker will be taught to walk in a similar manner as humans. Therefore the following tests will be performed to teach the Jaywalker to walk.

1. Single Step Test. The single step test is akin to a child's first step. It will be performed on both the inside and outside legs, and the purpose is to determine the appropriate initial step conditions as well as the step length for walking.
2. Double Step Test. The double step test is the precursor to attempting a continuous walk. The Jaywalker will take two successive single steps to determine if the step length of the first inside or outside legs will allow the Jaywalker to take a stable second step. The final step length of the second step will be evaluated to determine if a third step is feasible.
3. Continuous Test. If the Jaywalker is able to perform the double step test with a final step length suitable for a third step, then a continuous walk for one gait cycle test will be performed. If the robot is able to complete one continuous gait cycle, then the walking pattern will be repeated 5 times, allowing the robot to take 10 steps.

This particular walking machine prototype uses the passive hip mode of the HRS discussed in Chapter 1. This procedure for teaching the Jaywalker will not change regardless of actuator configuration. The Jaywalker is tethered to a wheeled cage to

prevent damage when an unstable event occurs. Although the walking machine is tethered, it is still possible for an awkward motion to cause damage to one or more components. The purpose of test 2 is to minimize the risk of any awkward motion that could damage the walker. It does this by ensuring the first step provides the proper initial conditions for the second step.

Figure 3.2.1: Motion capture of human walking at three key points during the gait cycle. (a) Shows the position of the legs at toe-off right before the back foot looses contact with the ground. (b) Shows the position of the legs at mid-swing right before the knee starts to extend. (c) Shows the position of the legs at heel strike right after contact with the ground has been made with the swing foot.

Since the Jaywalkers motion and control are inspired by humans. It is only logical to compare its step performance with a human step. This comparison was accomplished by qualitatively analyzing the step kinematics and quantifying the step length. Video was taken of the Jaywalker taking a step and compared with video of a human step. Toe-off, mid-swing and heel strike are the locations in the gait cycle of most kinematic interest. This is because they represent transition points from one phase of the gait cycle to another. These three transition locations are shown in Figure 3.2.1 for a human subject taking a step. Figure 3.2.1a shows toe-off. At this point in the gait cycle the knee is already flexing on the swing leg, which started when the foot rolled

over the ball of the foot. The stance leg is perpendicular to the ground. Figure 3.2.1b shows the mid-swing right before the knee starts to extend. The foot during the swing phase remains close to the ground, being lifted only high enough to reposition itself for heel strike, minimizing energy. Knee extension does not start until the swing thigh has passed the stance leg. The stance leg starts to lean forward in preparation for heel strike. The vertical position of the hip does not noticeably change from toe-off to this location in the gait cycle. Figure 3.2.1c shows heel strike. The angles between the front and back legs and the ground appear to be similar. The vertical hip position from the ground becomes noticeably shorter. The lowering of the hip started with knee extension, but appeared to suddenly stop once the swing leg was straight and the heel made contact with the ground. The thigh does not move from mid-swing to heel strike.

A consistent step length is important for the Jaywalker's ability to walk. When the walking machine is starting from rest, it has some initial step length; measured before the first swing phase. A terminal step length is measured after the swing phase is complete. Normally, a step is measured from heel-to-heel of the opposite feet. However, because of the curved foot on the Jaywalker it is difficult to get an accurate measurement at these

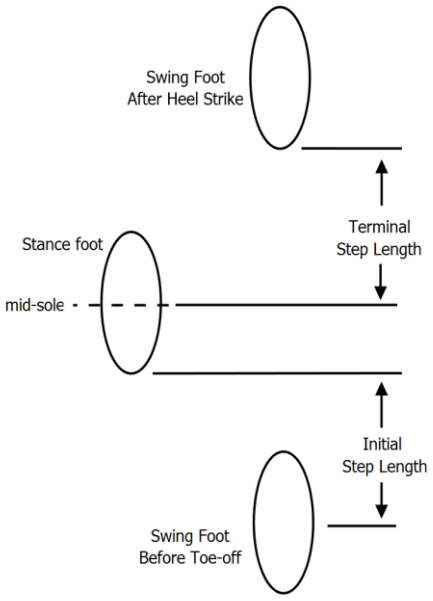

Figure 3.2.2: Pictorial definition of the initial and terminal step lengths used to evaluate the step performance of the Jaywalker.

points, because the back leg heel is often not contacting the ground. Therefore, to achieve a more accurate measurement, the step length was redefined to be measured from the heel of the front foot to the mid-sole of the back foot. Figure 3.2.2 shows a schematic of the initial and terminal step length definitions. The terminal step length for right leg will be the initial step length for the left and vice versa for continuous walking. So it is important that the initial step length and terminal step length be approximately equivalent to each other.

If the initial and terminal step lengths deviate significantly from one another, then an adjustment will need to be made by the walking machine. Modifying the toe-off position can effectively change the leg length to keep the stance leg vertical at toe-off. The hip can also be actuated to control the step length by adjusting the position and velocity of the swing leg. Unfortunately, the Jaywalker has a passive hip and no ability to dynamically change the toe-off position. Therefore if the Jaywalker's initial and

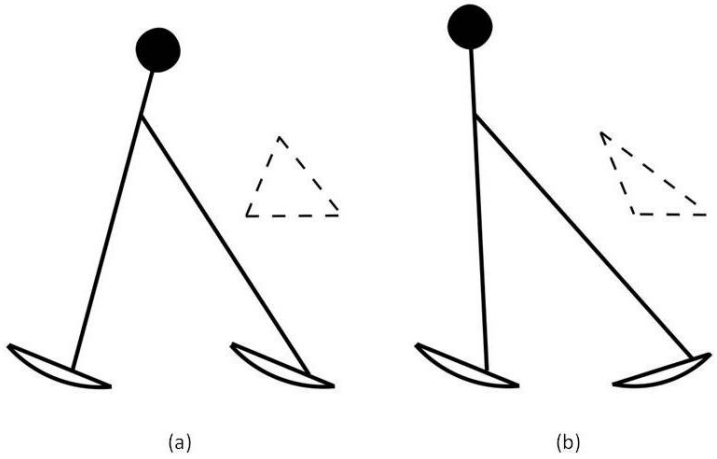

Figure 3.3.1: Simple representations of the initial step. (a) Shows the position of the hip mass when both legs are completely dorsiflexed. (b) Shows the position of the hip mass when the back leg is rolling to toe-off.

terminal step lengths deviate too much, the next step will have an invalid initial condition. This will cause the Jaywalker to become unstable.

3.3 Step Parameters

The geometry between the front leg, back leg and ground produces a triangle, and are considered to be pinned together. A change to the length of one side will cause a change in length of the other two sides. An unstable terminal step will occur if any combination of leg or step length, of this triangle, is changed to cause the hip mass to be too far forward or back when the gait transitions from the single support phase. There are several initial step parameters that can be adjusted to produce a stable terminal step. For example, toe-off position of the back foot can change the hip mass position. This is shown in Figure 3.3.1. Figure 3.3.1a shows the position of the hip mass when both ankles are completely dorsiflexed. However, without changing the position of the front foot, the back foot will start to increase the leg length, moving the hip mass over and past the stance leg, as it begins to plantarflex towards the toe-off set point. This is shown in Figure 3.3.1b. Depending upon when toe-off is triggered, during this motion, will determine the length of the back leg and thereby position of the hip mass.

Along with toe-off, the other prominent step parameter that effects terminal step stability is initial step length. This parameter works in concert with the toe-off position. If either the initial step length or toe-off position is changed without changing the other an unstable terminal step will most likely occur. However, when attempting to find a stable terminal step, one of these parameters should be fixed while adjusting the other.

Finding a stable terminal step with the Jaywalker is easiest when the toe-off position was fixed. However, toe-off position was changed whenever a specific initial step length was desired.

Changing the initial step length and toe-off position are not the only parameters that can change the Jaywalkers step geometry. The initial flex angle for the front foot will cause the front leg to change the height of the hip mass, as well as, a small change in the step length. This will in turn change the required back leg length needed to move the hip mass to the desired position. Typically this parameter is used to make small adjustments to the step performance. Since the back leg already plantarflexed to create thrust for walking, modifying its initial value is equivalent to changing the initial step length or toe-off position. Whereas plantarflexing the front leg changes the pivot point of the step cycle. The dorsiflex position is given as the number of step commands provided to the stepper motor by the control computer to plantarflex the foot from the maximum dorsiflexion limit. Figure 3.3.2 gives a brief review of foot flexion terms.

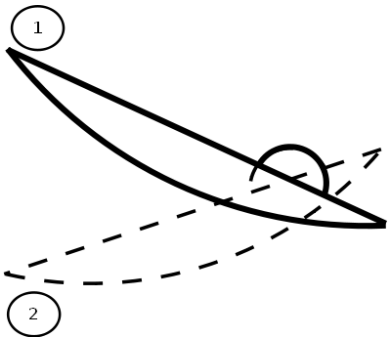

Figure 3.3.2: When the foot is flexed towards the shank, it is dorsiflexed. When the foot is flexed away from the shank, it is plantarflexed. Position 1 shows the foot in a dorsiflex position, and position 2 shows the foot in a plantarflex position

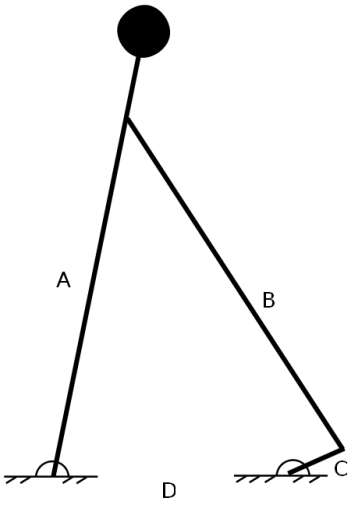

Figure 3.3.3: The double stance phase modeled as a 4-bar linkage.

The kinematics of the double stance phase of the gait cycle can be modeled as a four-bar linkage, shown in Figure 3.3.3. Changing link C's (back foot) rotational velocity will change link A's (front leg) rotational velocity, because they are coupled by link B. This means that the back leg ankle velocity will also affect the stability of the terminal step. If the back foot moves the hip mass too fast or too slow, the hip will be too far forward or backward for a stable terminal step to occur. The ankle velocity is given as the frequency (steps/s) of the control square wave sent to the stepper motor by the control computer.

In summary the principal parameters that will affect the Jaywalker taking a stable step are: toe-off, initial step length, stance foot flex and ankle velocity. Any combination of these parameters will yield a stable step, provided a stable step exists. To ensure the existence of a stable step an active hip controlling the stride length is necessary.

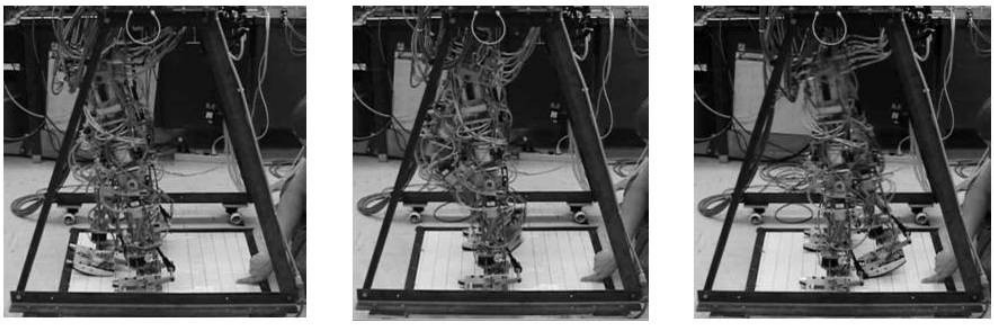

Figure 3.4.1: Motion capture of the Jaywalker inside step. (a) Shows the position of the Jaywalker's legs at toe-off. (b) Shows the position of the Jaywalker's legs at mid-swing just before knee extension. (c) Shows the position of the Jaywalker's legs at heel strike.

3.4 Single Step Results

Single step test trials were performed 103 times with the inside leg of the Jaywalker, with varying step parameters. The inside leg was able to achieve a stable terminal step for 54% of these trials. Figure 3.4.1 shows the motion capture at toe-off, mid-swing and heel strike from the walking video for one of these successful trials with an initial step length of 14.0 cm (5.50 in.) and a terminal step length of 6.77 cm (2.67 in.). Figure 3.4.1a shows the toe-off of the Jaywalker right before transitioning to the single stance phase. Comparing the position of its legs, with the human subject's leg position from Figure 3.2.1a yields the following observations.

- The walker's front leg is perpendicular to the ground, but the thigh appears to be slightly hyper-extended. This causes the hip joint to not align vertically with the ankle joint. Whereas the subject's stance leg flexes the knee; causing the leg to bow, but the hip appears to still align vertically with the ankle.
- The walker's back leg stays straight until the toe-off sensor is triggered, and then the foot looses contact with the ground. The subject's knee is bent while the foot is still making contact with the ground. This allows more of the foot to stay in contact with the ground, without pushing the hip too far forward. It also provides energy to propel the swing leg.

Figure 3.4.1b shows the inside leg of the Jaywalker at mid-swing just before knee extension. The following observations can be taken from comparing the walker's mid-swing with that of the human subject's mid-swing in Figure 3.2.1b.

- Both the stance legs of the walker and subject lean forward before knee extension. However, the Jaywalker's stance leg leans further forward, because the thigh is hyper-extended. The vertical position of the hip does not change noticeably

between toe-off and mid-swing. This similar behavior was observed by the subject between toe-off and mid-swing.

- The knee flex is more pronounce in the walker than the human subject right before knee extension. However, the subject continues to flex the hip while extending the knee. The Jaywalker has reached its apex of hip flexion at this moment.

Figure 3.4.1c shows the inside leg of the Jaywalker at heel strike. The actual heel strike position of the walker appears similar to the human subject's heel strike once allowances are made for differences in terminal step and leg lengths. The significant difference

Table 3.4.1: Single step testing results for the inside leg given the specified initial step length.

Stable Terminal Success Rate and Average Terminal Step Length for the Inside Step					
I.S. [cm (in)]	**Total Trials**	**Successful Trials**	**% Success**	**T.S. Avg [cm (in)]**	**T.S Std Dev [cm (in)]**
12.7 (5.00)	57	21	36.8	11.34 (4.466)	2.591 (1.020)
13.3 (5.25)	66	42	63.6	11.73 (4.652)	2.598 (1.023)
14.0 (5.50)	4	2	50.0	6.827 (2.688)	.223 (.088)

occurs during the terminal swing phase between mid-swing and heel strike. When the human subject's knee becomes fully extended the position of the thigh remains at its apex. Then he leans forward to induce heel strike. The Jaywalker reaches the apex of thigh flexion at the same point the knee starts to flex. As the knee starts to extend thigh starts to rotate downward until the foot contacts the floor.

The inside leg was tested over a range of initial steps lengths between 11.4 cm (4.50 in.) and 15.2 cm (6.00 in.). Table 3.4.1 shows the success rate, average step length and standard deviation of the terminal step for initial step lengths with at least one successful trial over this range. The two best terminal step results occurred using initial

step lengths of 12.7 (5.00 in.) and 13.3 cm (5.25 in.). Absolute error between the initial and terminal step lengths is smaller for the 12.7 cm initial step than the 13.3 cm initial step, 1.36 and 1.59 respectively. However, the success rate for the 13.3 cm initial step is 30% better than the 12.7 cm step. During single step testing for the inside leg; the inside leg ankle velocity was held constant at 5000 steps/s. The initial dorsiflexion position of the outside stance legs ranged between 0 and 1750 steps. Finally the toe-off ranged between 6.4 mm (.25 in.) and 8.9 mm (.35 in.). As the testing matured, over the final 25 inside step trials the dorsiflexion range narrowed to between 1600 and 1750 steps and the toe-off was fixed at 6.4 mm, using strictly the 13.3 cm initial step length. However, the

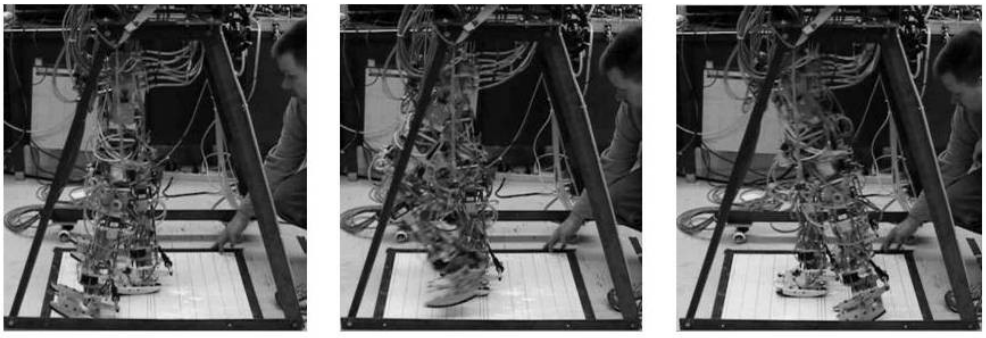

Figure 3.4.2: Motion capture of the Jaywalker outside step. (a) Shows the position of the Jaywalker's legs at toe-off. (b) Shows the position of the Jaywalker's legs at mid-swing just before knee extension. (c) Shows the position of the Jaywalker's legs at heel strike.

success rate improved by only 4.4% compared to the success rate of the 13.3 cm initial step in Table 3.4.1.

Similar to the inside leg single step test, the outside leg single step test was conducted varying the step parameters. Forty-four trials where conducted for the outside legs with initial step lengths ranging from 11.4 cm (4.5 in.) to 19.7 cm (7.75 in.). The

overall success rate for the outside leg single step test is 25%. Figure 3.4.2 shows the outside leg taking a stride with an initial step length of 14.0 cm (5.50 in.) and terminal step lengths of 9.50 cm (3.75 in.) and 11.4 cm (4.50 in.) respectively for the X leg[1] and Z leg[2]. Many of the same observations about the inside leg single step relative to the human subject's step apply to the outside leg. Therefore discussion of the observed kinematics of the outside leg will focus on differences between it and the human subject that vary from the inside leg single step observations.

Figure 3.4.2a shows the outside legs at toe-off. The position of the hip is much more forward at toe-off than the inside leg or human subject's hip positions. This is due to the inside stance foot slipping backwards. This shortens the initial step length, allowing the back leg to push the hip too far forward. Figure 3.4.2b shows the outside legs in mid-swing. The outside swing legs and inside stance leg positions of the walker almost parallels the inside swing leg and outside stance legs positions in Figure 3.4.1b. Figure 3.4.2c shows the Jaywalkers outside leg heel strike. When the outside legs contact the ground at approximately the same position; the position of the walking machine at heel strike closely aligns with the heel strike in Figure 3.4.1c. However, the difference between the X leg and Z leg step length was less than 2.54 cm (1.00 in.) in only 30% of the trials. The difference is that during the terminal swing phase between the mid-swing and heel strike positions; the supporting cage stops the forward momentum of the walking machine, allowing the legs time to extend to a stable step length.

---

[1] The X leg is outside leg farthest from the eye.
[2] The Z leg is the closest outside leg to the eye.

The inside stance leg slipping is caused by the outside legs. In this instance the summation of the vertical force components of the outside legs is enough to lift the robot. This causes the inside leg to slip backwards until its change in angle causes contact with the floor and prevents more slipping. The Jaywalker's outside leg step test and inside leg step test positions appear to be similar at mid-swing; this issue does not appear to be causing a serious problem with step performance. The problem of most concern is that the walking machine is not capable of a stable terminal step without using the support cage as a crutch. This problem and its significance will be discussed in detail in section 3.6. For the purposes of completeness in analyzing the step performance of the Jaywalker; the crutched step was considered a successful outside step.

Table 3.4.2: Single step testing results for the outside legs given the specified initial step length.

Stable Terminal Success Rate and Average Terminal Step Length for the Outside Step							
				T.S. X leg		T.S. Z leg	
I.S. [cm (in)]	Total Trials	Successful Trials	% Success	Avg [cm (in)]	Std Dev [cm (in)]	Avg [cm (in)]	Std Dev [cm (in)]
14.0 (5.50)	15	6	40.0	4.021 (1.583)	7.701 (3.032)	2.751 (1.083)	4.712 (1.855)
14.6 (5.75)	8	3	37.5	6.139 (2.417)	4.932 (1.942)	8.890 (3.500)	8.329 (3.279)
16.5 (6.50)	4	2	50.0	2.540 (1.000)	3.591 (1.414)	9.525 (3.750)	4.491 (1.768)
17.1 (6.75)	3	1	33.3	7.620 (3.000)	-	0	-

Table 3.4.2 shows outside leg terminal step length results over the specified initial step length range given at least one successful step. The 16.5 cm (6.50 in.) initial step length has the highest success rate of any of the trials. However, the 14.0 cm (5.50 in.) initial step length has the second highest success rate, and overlaps the successful initial step length range for the inside leg. During step testing the ankle velocity was varied

between 2500 and 5000 steps/s, the toe-off position between 6.4 mm(.25 in.) and 8.9 mm (.35 in.) and the inside leg initial plantarflexion was varied between 0 and 1700 steps. The parameters provided the most success taking an outside step where an ankle velocity of 5000 steps/s, toe-off position of 6.4 mm (.25 in.) and 0 plantarflexion.

3.5 Double Step Test Results

The purpose of the double step test is to determine if the terminal step of one leg will feed into the initial step of the other. This will determine how successful the Jaywalker will be at walking with a passive hip. Based on the single leg step test results it was determined the inside leg should always step first and then the outside leg. The justification for this is as follows:

1. The success rate for achieving a stable terminal step is on average 10% better for the inside leg than the outside leg.
2. The preferred initial step length range for both legs is between 13.3 cm (5.25 in) and 14.0 (5.5 in). The inside leg is capable of producing a terminal step within this range, unlike the outside legs.
3. The outside legs do not consistently end at the same terminal step length.
4. The inside leg takes a pure step without the aid of a "crutch".

The observed kinematics and step lengths for the double stance will be briefly discussed. However, the double step test is essentially two single step tests back-to-back. So the results do not vary significantly from the single step test. The overall success rate of the double step test and the success rate frequency (success/trials) are of most interest to show that within the limits of the walker's motion, the controller is becoming more robust. The test procedure for the double step is: 1) Trigger the inside legs to take a step

and measure the terminal step length; 2) Move all feet to the desired dorsiflexion position for the next step; 3) Trigger the outside legs to take a step and record the terminal step length. Figure 3.5.1 shows the inside and outside leg toe-off, mid-swing and heel strike positions during a double step test. The double step trial performance compared with the inside and outside single step trials, Figures 3.4.1 and 3.4.2, shows minimal differences in

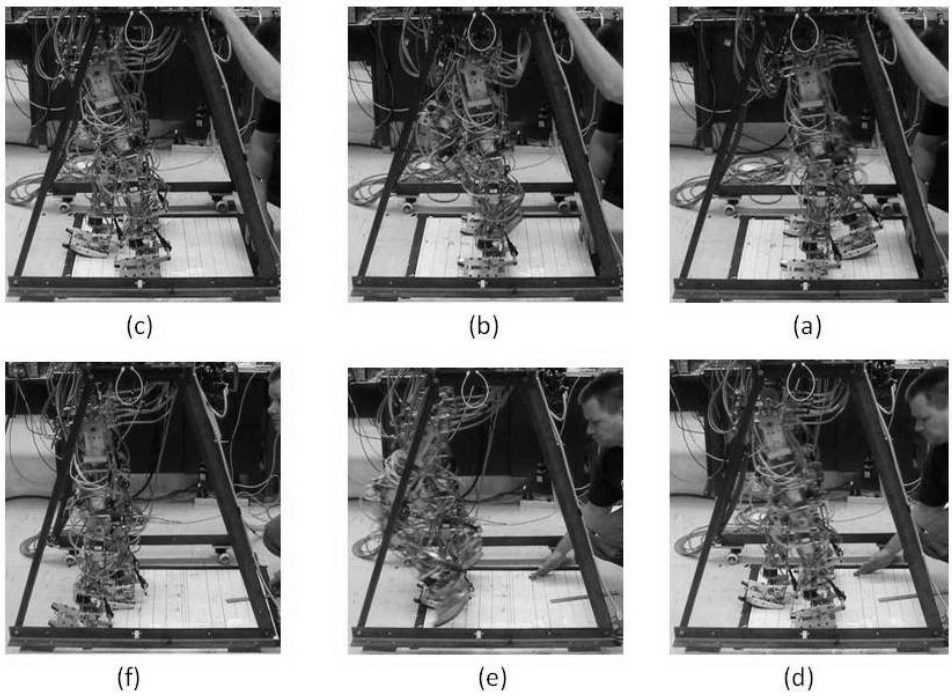

Figure 3.5.1: Motion capture of the inside and outside steps during double step testing. (a) Inside leg toe-off. (b) Inside leg mid-swing. (c) Inside leg heel strike. (d) Outside leg toe-off. (e) Outside leg mid-swing. (f) Outside leg heel strike.

the kinematic motion. The double step trial in Figure 3.5.1 had the ankle velocity and toe-off position set to 5000 steps/s and 6.4 mm (.25 in.) respectively for both the inside and outside legs. The outside legs were initially plantarflexed 1700 steps before the inside leg step, and the inside leg was initially plantarflexed 0 steps before the outside legs step. The inside leg step produced an ideal terminal step length of 13.3 cm (5.25 in.)

which was equal to its initial step length. The outside leg terminal step length was -2.54 cm (-1.00 in.) and 8.109 cm (3.19 in.) respectively for the X and Z legs. The negative distance indicates that the heel of the outside leg is behind the mid-sole of the inside leg. Figure 3.5.2 shows the step length results for the outside legs when the initial step length of the inside leg is set to 13.3 cm (5.25 in.). The X and Z leg trend lines show that as the initial outside leg step length increases the terminal outside leg step length decreases.

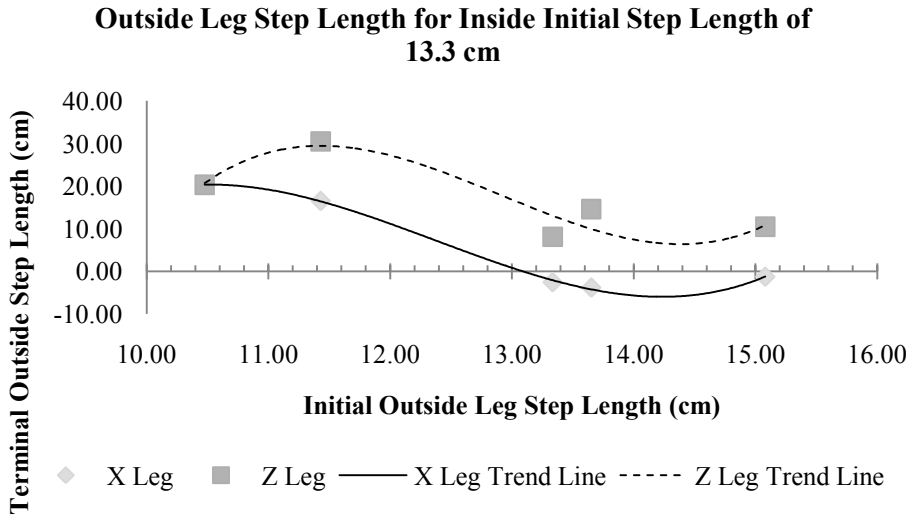

Figure 3.5.2: The outside leg step length results for the double step test with the inside leg initial step set at 13.3 cm (5.25 in.).

This is counter to the ideal curve where the terminal step length increases linearly with an increase in initial step length with a unit slope. The disagreement between the test results and the ideal can be explained by the crutch effect of the support cage. The shorter the initial step length the greater the toe-off. This causes the Jaywalker to lean too far forward requiring the support cage to prevent a fall. The legs then swing forward to support the walker. This yields a larger than expected terminal step.

The overall success rate for the double step test is 7.1%. However, the frequency distribution, Figure 3.5.3, shows a significant improvement in the success rate over time. This illustrates that as the understanding of the Jaywalker's motion improves; the controller is becoming more robust.

The results of the step testing strongly indicate that the Jaywalker is not capable of walking with a passive hip. Several exploratory attempts were made to have the Jaywalker take two continuous steps. However, this testing was suspended after it was determined detrimental to the health of the walker.

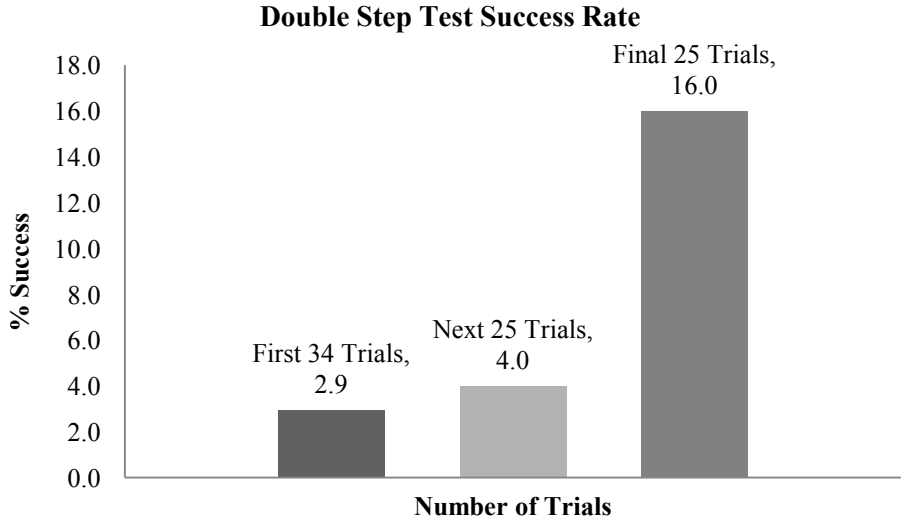

Figure 3.5.3: The frequency distribution of the double step success rate for the 84 total trials.

3.6 Step Dynamics

The observed kinematics during step testing of the Jaywalker, showed its motion to be similar to human motion for the double stance phase and single support phase up to

terminal swing. However, during terminal swing the kinematics of the walker stray from the desired human trajectories. As the knee actuator rotates the shank clockwise, extending the knee; the thigh is rotating counterclockwise, extending the hip. This is causing the Jaywalker to take a quick step. This quick step is the reason for the consistently shorter terminal step lengths. This event seriously affects outside leg performance requiring it to use a crutch for stable walking. Quick step is noticeable with the inside leg, but does not prevent the walker from taking independent stable steps. While the effects of this problem are observed in the Jaywalkers kinematics; the cause is in the walker's dynamics.

A velocity profile with respect to position was created using a simple energy model of the swing leg. The focus of this model is to clarify why the outside legs are more effected by quick step than the inside legs. The swing leg is modeled as a two-link multi-lumped mass pendulum pinned to a fix joint. As stated previously the scope of this model is to develop an angular velocity profile of the swing leg with respect to the angular position of the thigh. Therefore, the stance leg was neglected from the model, because it minimally affects the angular velocity or position of the swing leg.

The model starts in a maximum kinetic energy state, with the swing leg flexed and the thigh perpendicular to ground ($\theta = 0°$) and an initial hip angular velocity of 1.54 rad/s (14.7 RPM). This hip velocity is based on a walking speed of 1.1 m/s. The flexed leg swings forward, calculating the velocity for small increments in θ, until the kinetic energy becomes zero. At this point the knee is assumed to instantaneously extend. The final angular velocity and position for the flexed leg become the initial conditions for the

straight leg model. The angular velocity for the straight leg is then calculated for small decrements in θ, until the kinetic energy is maximized. Table 3.6.1 shows the initial and final velocity and position conditions based on maximum and minimum kinetic energy for the model.

Table 3.6.1: Boundary conditions for the energy model used to analyze the quick step behavior of the swing leg.

Swing Leg Boundary Conditions				
Leg Position	**θ_i (deg)**	**ω_i (rad/s)**	**θ_f (deg)**	**ω_f (rad/s)**
Flexed	0	1.54	-	0
Straight	θ_f	0	0	-

Figure 3.6.1 shows the different flexed and straight leg swing models used for the inside and outside legs. Figure 3.6.1a and Figure 3.6.1b show the flexed and straight leg models for the inside leg. Figure 3.6.1c and Figure 3.6.1d show the flexed and straight leg models for the outside legs. The reason the inside and outside legs require separate models is that the hip is rigidly connected to the inside leg. A majority of the total hip mass (66 %) can be assumed to be located around the hip joint. However, the other 44% of the hip mass consists of a stepper motor offset from the hip joint by 7.30 cm (2.88 in.). This mass is represented as m_1 on the inside leg models. Because the motor mass is rigidly connected to the inside leg on the opposite side of the pivot point, the motor mass will want to oppose the motion of the leg mass. The locations of the thigh and shank lumped masses in Figure 3.6.1 correspond to the actual center-of-gravity locations for the shank and thigh on the Jaywalker. For simplicity the foot mass was lumped in with the shank mass at the shank's center-of-gravity location.

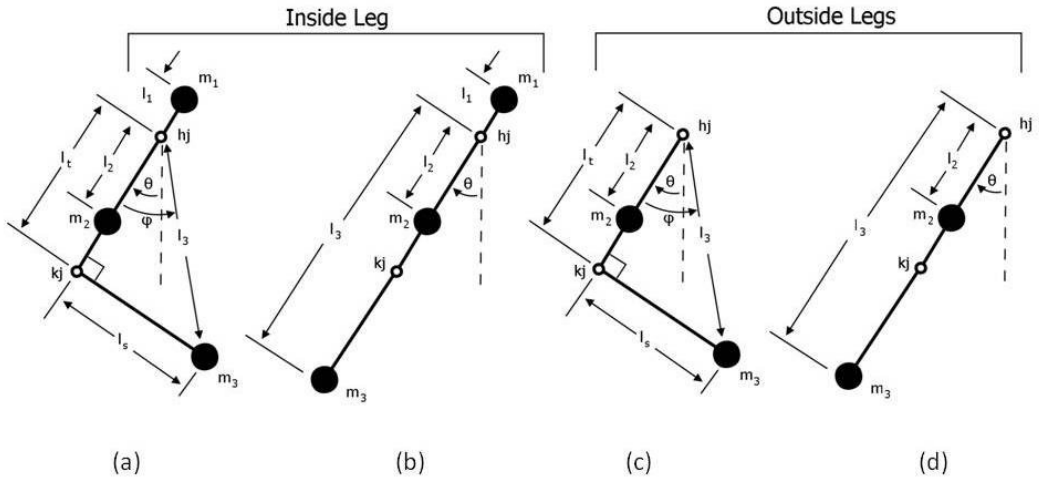

Figure 3.6.1: The lumped mass swing leg models. (a) Flexed knee model for the inside leg. (b) The straight leg model for the inside leg. (c) The flexed knee model for the outside leg. (d) The straight knee model for the outside leg.

After applying the initials conditions in Table 3.6.1 and assuming energy is conserved; the lumped model energy equations can be rewritten to express the angular velocity as a function of the current position. The equations for the inside leg flexed and straight swing velocities respectively are

$$\omega_j = \sqrt{\frac{(m_1 l_1^2 + m_2 l_2^2 + m_3 l_3^2)\omega_i^2 + 2g\{(m_1 l_1 - m_2 l_2)(1 - \mathrm{c}(\theta_i)) - m_3 l_3(\mathrm{c}(-\varphi) - \mathrm{c}(\theta_j - \varphi))\}}{(m_1 l_1^2 + m_2 l_2^2 + m_3 l_3^2)}} \tag{3.6.1}$$

and

$$\omega_j = \sqrt{\frac{2g(m_1 l_1 - m_2 l_2 - m_3 l_3)(\mathrm{c}(\theta_i) - \mathrm{c}(\theta_j))}{(m_1 l_1^2 + m_2 l_2^2 + m_3 l_3^2)}}, \tag{3.6.2}$$

The equations for the outside leg flexed and straight swing velocities respectively are

$$\omega_j = \sqrt{\frac{(m_2 l_2^2 + m_3 l_3^2)\omega_i^2 - 2g\{(m_2 l_2)(1 - \mathrm{c}(\theta_i)) + m_3 l_3(\mathrm{c}(-\varphi) - \mathrm{c}(\theta_j - \varphi))\}}{(m_1 l_1^2 + m_2 l_2^2 + m_3 l_3^2)}}, \tag{3.6.3}$$

and

$$\omega_j = \sqrt{\frac{2g(m_2 l_2 + m_3 l_3)(\mathrm{c}(\theta_j) - \mathrm{c}(\theta_i))}{(m_1 l_1^2 + m_2 l_2^2 + m_3 l_3^2)}}. \quad (3.6.4)$$

Most terms in the above equations are defined adequately in Figure 3.6.1. The c in equations 3.6.1-3.6.4 is an abbreviation for cosine. The θ and φ angles are the angles between the thigh and a vertical ground frame and the thigh and radial distance between the hip joint and m_3 respectively. As long as the knee is held in a fixed position, φ is constant.

Equations 3.6.1-3.6.4 and their respective mass and length values from Table 3.6.2 were input into a MATLAB simulation. Figure 3.6.2 shows the results of this simulation. Both the inside and outside flexed legs start with the same initial velocity of 1.54 rad/s, but the inside leg obtains a maximum hip angle of 60.8º whereas the outside leg's maximum hip angle is 55.9º. The inside and outside legs also have almost the same final hip velocity; 4.28 rad/s and 4.13 rad/s respectively. Therefore, the straight legs are moving approximately 273% faster at the point of maximum kinetic energy than the flexed legs. The difference between the maximum inside leg thigh angle and maximum outside leg thigh angle is 4.9 degrees. This means the inside leg thigh moves an additional 3.0 cm (1.2 in.) along the arc length at the knee. Figure 3.6.2 shows the inside leg velocity to be greater than the outside leg velocity at the same angle. It is difficult to compare straight leg velocities of the outside and inside legs because of the potential energy difference between the two starting points. The outside straight leg model was rerun with the inside leg initial conditions. This

Table 3.6.2: Jaywalker model parameters.

Model Parameters	
m_1	2.31 kg
m_2	2.60 kg
m_3	3.47 kg
l_1	0.073 m
l_2	0.183 m
$l_{3,f}$	0.421 m
$l_{3,s}$	0.582 m

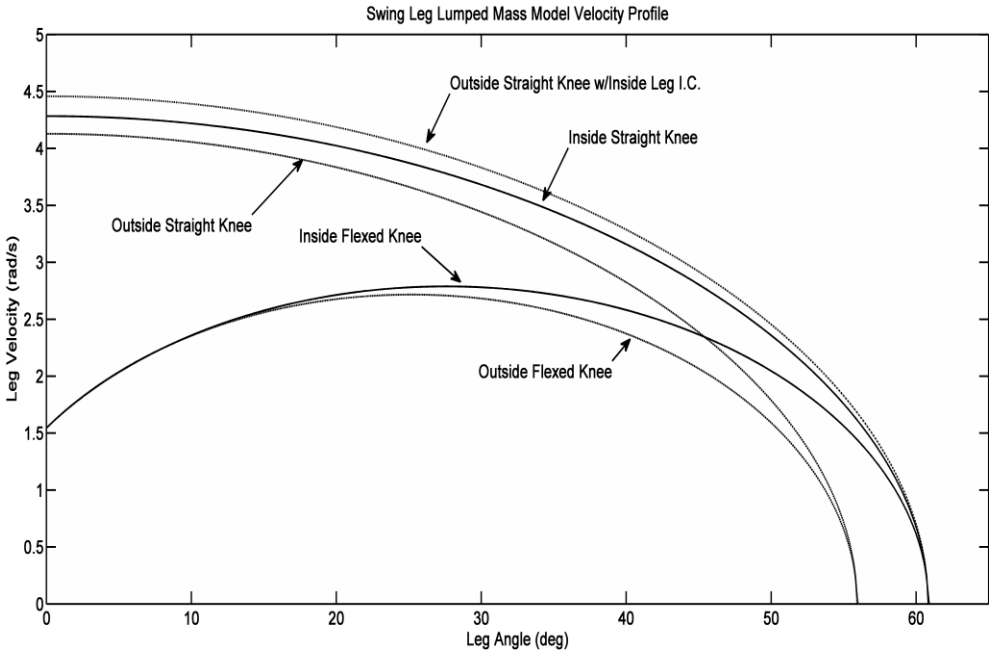

Figure 3.6.2: The velocity profiles for the inside and outside legs during swing phase.

allows for a velocity comparison from the same energy state. The velocity profile of this new outside straight leg is referenced in Figure 3.6.2. The velocity of the inside leg is clearly slower than the outside leg when both originate from the same energy state. This energy analysis shows that by increasing the thigh swing angle and decreasing the straight leg velocity the stepper motor mass has a positive effect on the Jaywalkers ability to take a step. However, the straight legs are still moving at a substantially faster rate than the flexed legs. This is contributing to the quick step problem during terminal swing.

The other contributing factor to quick step is reaction forces caused by inertial forces. The moment-of-inertia increases by approximately 180% between the flexed and straight knee states, for both the inside and outside legs. For the actual swing leg on the walker, the transition between the flexed knee and straight knee states do not occur instantaneously. The knee actuator applies a force to the shank causing it to accelerate

faster than gravitational acceleration, creating an inertial force. This inertial force creates an increasing reaction force at the knee joint, because of the increasing moment-of-inertia. This reaction force translates up the thigh and to the hip, essentially pulling the walker down. This is double trouble for the outside legs because they have twice the mass as the inside leg, causing twice the reaction force about the same hip mass. Therefore, the outside legs will pull the walker down twice as fast as the inside legs.

The quick step event during terminal swing phase is caused by an increase in leg velocity and the introduction of external reaction forces on the hip. The stepper motor mass acting as a counterbalance on the inside leg helps to resist these elements. This allows the Jaywalker to take stable independent steps. The outside legs have no counterbalance and twice the reaction forces at the hip. This causes an extremely short step, making the outside legs rely on a crutch to produce stable steps. These results do not determine which factor, the counterbalance or reaction forces, contribute most to the quick step. A counterbalance would need to be added to the outside legs and retested to determine which element of quick step is most affecting step performance.

3.7 Conclusions

The Jaywalker was not ultimately successful at producing a stable gait cycle with a passive hip. This is not surprising because the mass rule, $m_{leg} << M_{hip}$, was knowingly not followed in the design of the Jaywalker. Following this rule ensures that the leg inertial forces do not affect the dynamics of the hip. It is difficult at best to adherence to this rule with an actively controlled walker, because actuator masses will not be

negligible in the system. This leaves limit cycle walkers to take advantage of passive dynamics, but these walking machine are capable of only flat ground walking. It is the goal of this project to do more with the walking machine than flat ground walking. This is why the mass rule was overlooked during the designing of the Jaywalker.

Step testing for the inside leg of the Jaywalker showed that it is possible to take a stable independent step, and that this step is sufficiently long enough to allow the next step to be successful. A part of this success is the inside leg is rigidly connected to the hip. The stepper motor on top of the hip acts as a counterbalance reducing the effects of quick step during terminal swing. The outside legs step testing was less successful because they have no counterbalance and cause twice as large reaction force at the hip as the inside leg. While the quick step events that occur during the terminal swing prevent successful motion. The performance of both the inside and outside legs during the double stance and swing phases up to terminal swing are similar to human motion.

The first attempt at walking with a passive hip and significant leg mass did not conclude with a stable gait cycle. However, the successful step tests of the inside leg with a counterbalance, show that it may be possible to achieve a stable gait cycle. The following recommendations for future research efforts include:

- Add counterbalance to the outside legs to improve terminal step length, or implement the iHD discussed in Chapter 1.
- During the terminal stance phase, the swing thigh of the Jaywalker starts to rotate back towards the ground. A passive locking mechanism used to hold the thigh in place while the shank extends would improve the terminal step length.

- Development of a toe-off sensor array. This would be used to dynamically alter the amount of toe-off during individual steps. Allowing the walking machine a wider range of step lengths that can produce stable motion.

3.8 References

[1] Collins, S., Ruina, A., Tedrake, R. and Wisse, M., 2005, "Efficient bipedal robots based on passive-dynamic walkers," Science, **37**, pp. 1082-1085.

[2] McGeer, T., 1990, "Passive walking with knees," *Proceedings of the 1990 IEEE International Conference on Robotics and Automation, May 13-18 1990*, Cincinnati, OH, USA, pp. 1640-1645.

[3] Garcia, M., Chatterjee, A., Ruina, A. and Coleman, M., 1998, "The simplest walking model: Stability, complexity, and scaling," Journal of Biomechanical Engineering, **120**(Compendex), pp. 281-286.

[4] Hobbelen, D. G. E. and Wisse, M., 2008, "Ankle actuation for limit cycle walkers," International Journal of Robotics Research, **27**(Compendex), pp. 709-735.

[5] Kajita, S., Kanehiro, F., Kaneko, K., Fujiwara, K., Yokoi, K. and Hirukawa, H., 2003, "Biped walking pattern generation by a simple three-dimensional inverted pendulum model," Advanced Robotics, **17**(Compendex), pp. 131-147.

[6] Bebek, B. and Erbatur, K., 2003, "A Fuzzy System for Gait Adaptation of Biped Walking Robots," *in Proceedings of IEEE Conference on Control Applications (CCA)*, Istanbul, Turkey, **1**, pp. 669-673.

[7] Tabrizi, S. S. and Bagheri, S., 2004, "Robustness of A biped robot controller developed by human expertise extraction against changes in terrain," *Proceedings of the IASTED International Conference on Artificial Intelligence and Applications (as part of the 22nd IASTED International Multi-Conference on Applied Informatics, Febrary 16, 2004 - Febrary 18, 2004*, Innsbruck, Austria, pp. 68-73.

[8] Denk, J. and Schmidt, G., 2003, "Synthesis of walking primitive databases for biped robots in 3D-environments," *2003 IEEE International Conference on Robotics and Automation, Sep 14-19 2003*, Taipei, Taiwan, **1**, pp. 1343-1349.

[9] Honda, "ASIMO's Walking Control," at http://world.honda.com/ASIMO/technology/walking_02.html (last visited on March, 28 2010).

CONCLUSIONS AND RECOMMENDATIONS

The Jaywalker, 2D sagittal plane, walking machine was designed to study rough terrain locomotion. The principle components to the design were the Hip Ratchet System (HRS) and the Hybrid Parallel Ankle Actuator (HPAA). The HRS used a pawl and ratchet system to engage or disengage the walker's legs from the hip drive shaft. The HPAA consists of a pneumatic ram and stepper motor connected in parallel to the ankle joint. The purpose of this configuration is to produce a high torque actuator that can be controlled using just the stepper motor.

As the HPAA is a new type of actuator; the concept had to be tested to determine its ability to be controlled by the stepper motor. Therefore the open loop performance of the HPAA was compared to a baseline stepper motor open loop performance. The results of this testing showed the HPAA positional RMS tracking error to be less than 1°, and the absolute velocity error to be less than 0.7 RPM compared to the baseline stepper motor. These were better than expected results considering the HPAA was lifting between 9 and 18 times the load as the baseline stepper motor.

The Jaywalker struggled to walk with a passive hip. Specifically because the outside legs could not take a sufficiently long enough step. This is because during terminal swing phase the thigh and hip masses would start to rotate too far down while the knee was extending forward. This behavior was termed quick step. The identically constructed inside leg did not exhibit this same behavior. The only difference between the inside and outside legs is that the inside leg is fixed to the hip, and the hip has a stepper motor mass located above the hip joint. An energy analysis of the inside and

outside swing legs shows the stepper motor mass acts as a counterbalance that increases the thigh flexion angle and decreases the decent velocity. Therefore to improve the walking ability of the Jaywalker with a passive hip a counterbalance needs to be added to the outside legs.

Recommendations for future research efforts with the Jaywalker include the following:

- Implement the Independent Hip Drive (iHD) to provide active control of the hip joint to eliminate the outside leg quick step.
- Implement an embedded control system to facilitate untethered walking.
- Develop a pressure feedback control system for the HPAA to allow it to move in the dorsiflexion direction under load.
- Develop a foot contact sensor array. This would be used to dynamically adjust the amount of toe-off during individual steps. Giving the Jaywalker a more robust range of acceptable step lengths during walking.
- Fuzzify the leg extension actuation by incorporating both accelerometer and encoder data into the decision making process.

APPENDIX A: JAYWALKER DESIGN

Appendix A contains supplemental design information for the Jaywalker walking machine.

A.1 Lumped Mass Models of the Jaywalker in the Sagittal and Frontal Planes

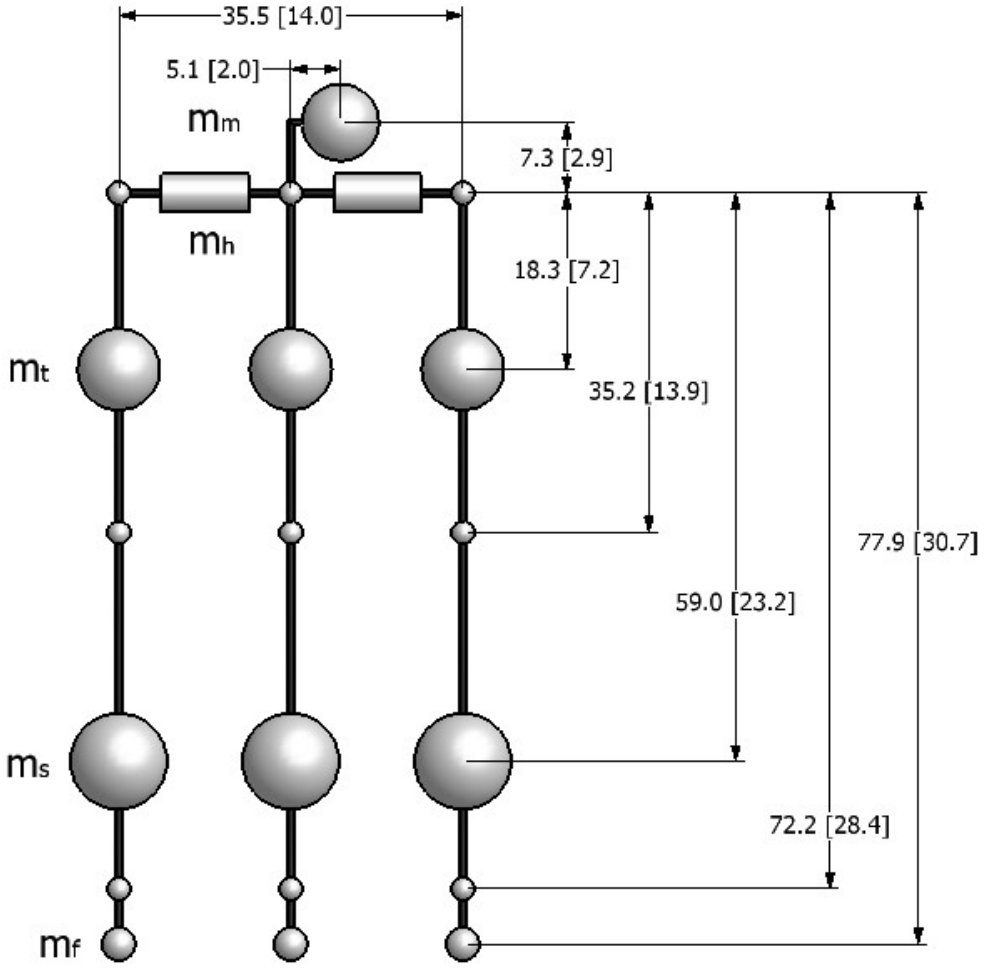

Figure A.1.1: Lumped mass model of the Jaywalker walking machine, showing the front locations of each mass point and joints relative to the hip (cm [in.]).

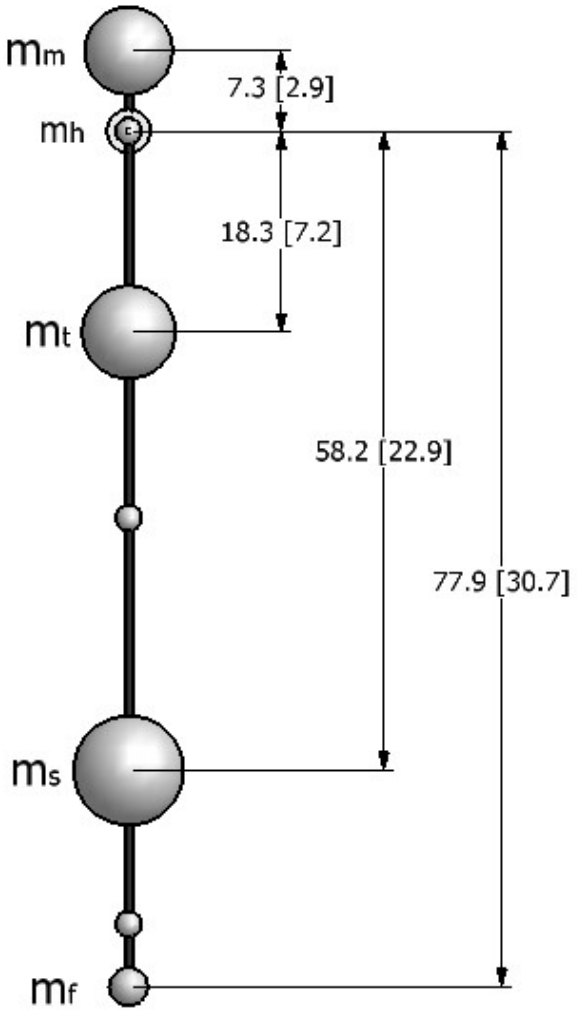

Figure A.1.2: Lumped mass model of the Jaywalker walking machine, showing the locations of each mass point relative to the hip in the sagittal plane (cm [in.]).

Note the only difference in the mass point locations between the frontal and sagittal plane occurs at the shank. The leg center-of-mass locations in the lower leg were measured using a blade test. The hip is symmetric and the mass is assumed to be evenly distributed along the frame.

A.2 Knee Actuation Mechanism Synthesis

The knee actuator mechanism was synthesized graphically using a 2:1 scaled drawing on 11"x17" graph paper for pneumatic ram stroke lengths ranging from 1.5 in. (3.8 cm) to 3.0 in. (7.6 cm). The drawings have been reduced to fit into this document and are not shown to scale. Line KA is the pneumatic ram. Line BC is the front of the shank where the ram is pinned. Points O_k and O_A are the knee and ankle joints respectively, and the line O_kO_A is the centerline of the shank. Line O_kK is the knee lever arm. Line O_kB is the offset from the knee joint to the front of the shank.

The knee is initially straight and the pneumatic ram is fully extended. The knee is then flexed between 60° and 90° about O_k. Line BC rotates with the knee offset by distance O_kB. Wherever line KA intersects line BC at the pneumatic rams retracted length, is the maximum flexion point of the knee. If line KA does not intersect line BC then no solution exists between 60° and 90° of knee flexion.

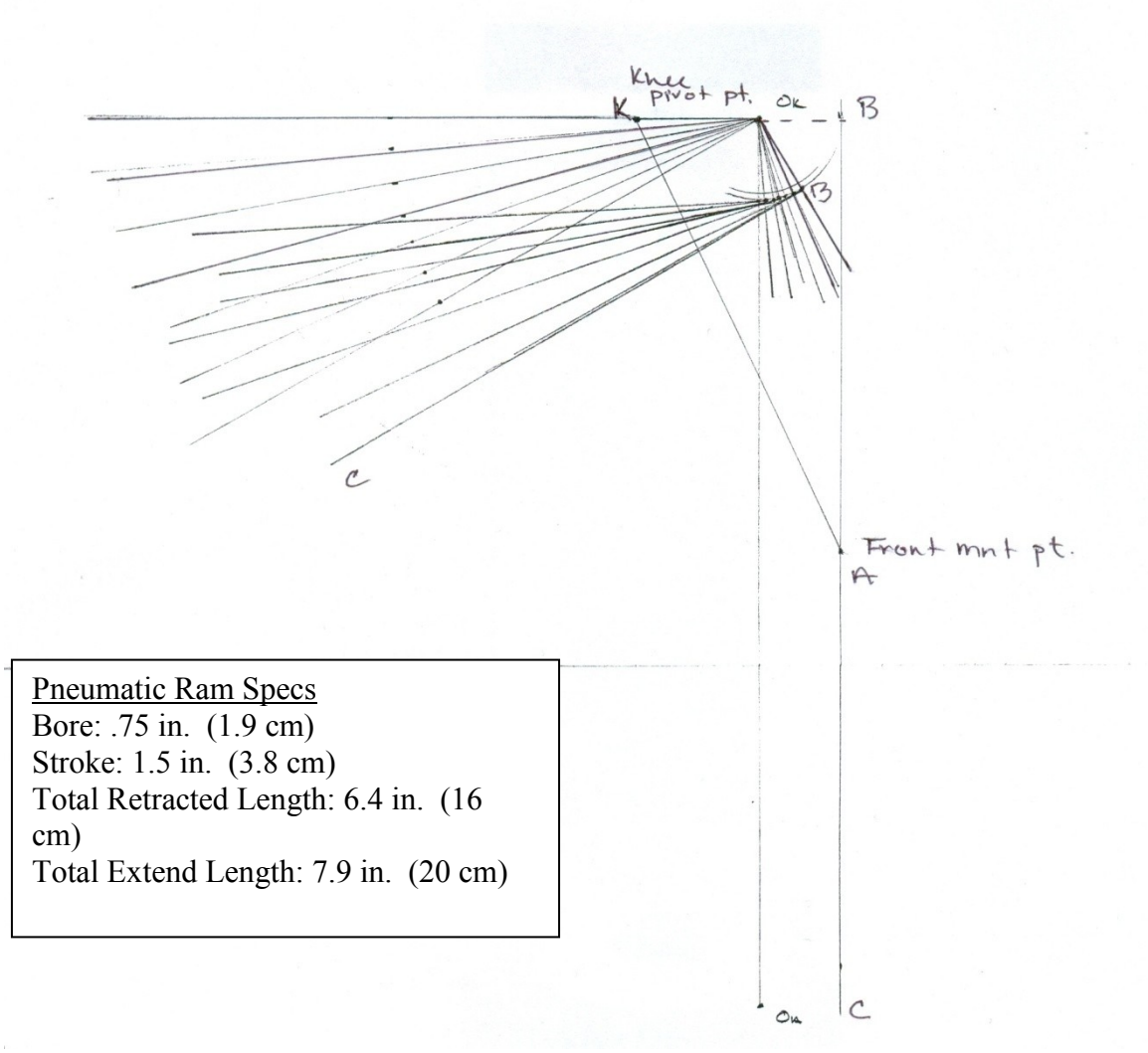

Pneumatic Ram Specs
Bore: .75 in. (1.9 cm)
Stroke: 1.5 in. (3.8 cm)
Total Retracted Length: 6.4 in. (16 cm)
Total Extend Length: 7.9 in. (20 cm)

Figure A.2.1: Synthesis of knee mechanism with a 1.5 in. (3.8 cm) stroke. The pneumatic ram KA does not intersect BC when it is retracted. Therefore no solution exists for this mechanism with the knee flexed between 60° and 90°.

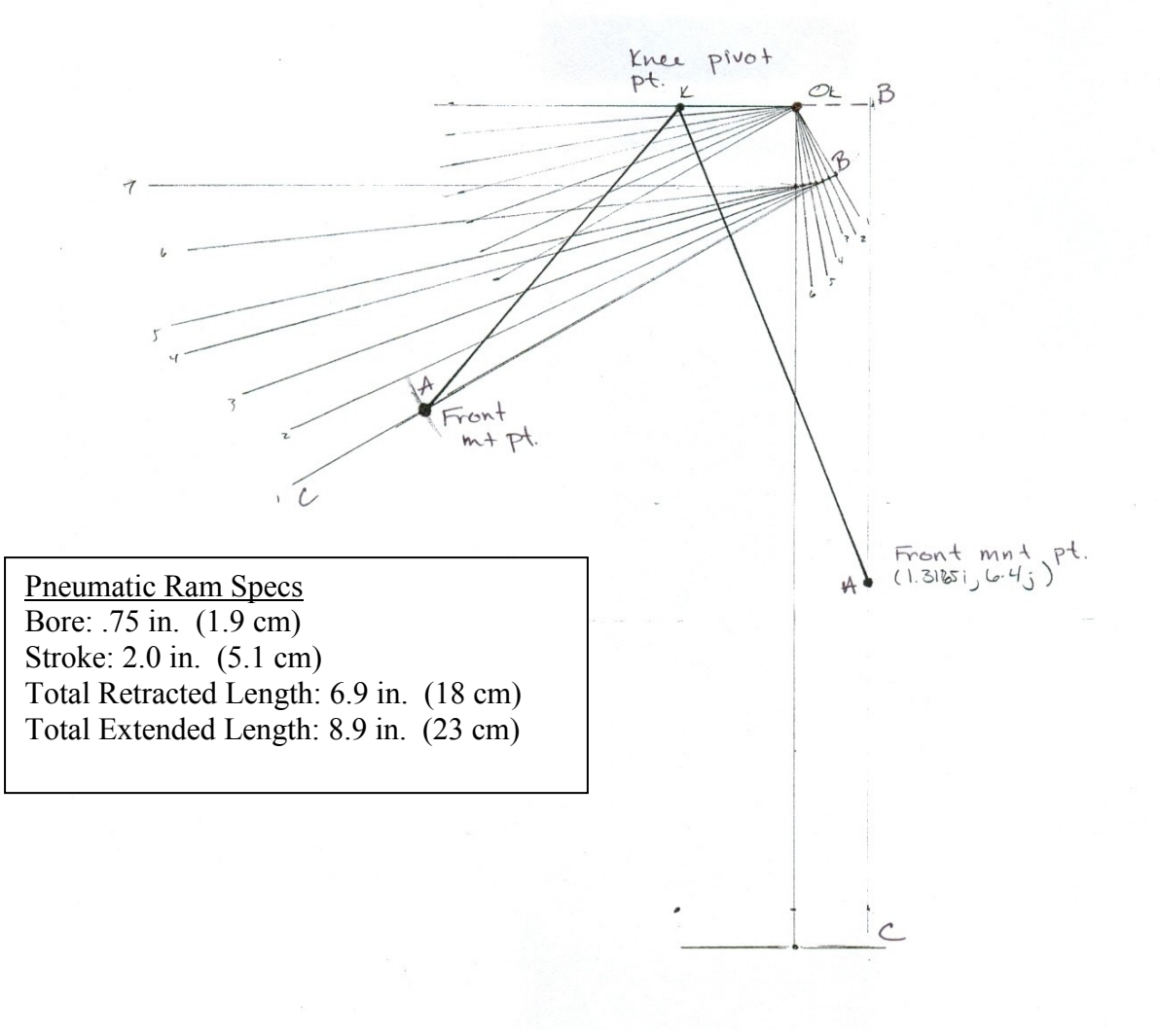

Pneumatic Ram Specs
Bore: .75 in. (1.9 cm)
Stroke: 2.0 in. (5.1 cm)
Total Retracted Length: 6.9 in. (18 cm)
Total Extended Length: 8.9 in. (23 cm)

Figure A.2.2: Synthesis of knee mechanism with a 2.0 in. (5.1 cm) stroke. The retracted pneumatic ram KA intersects the front of the shank BC at 60° of knee flexion.

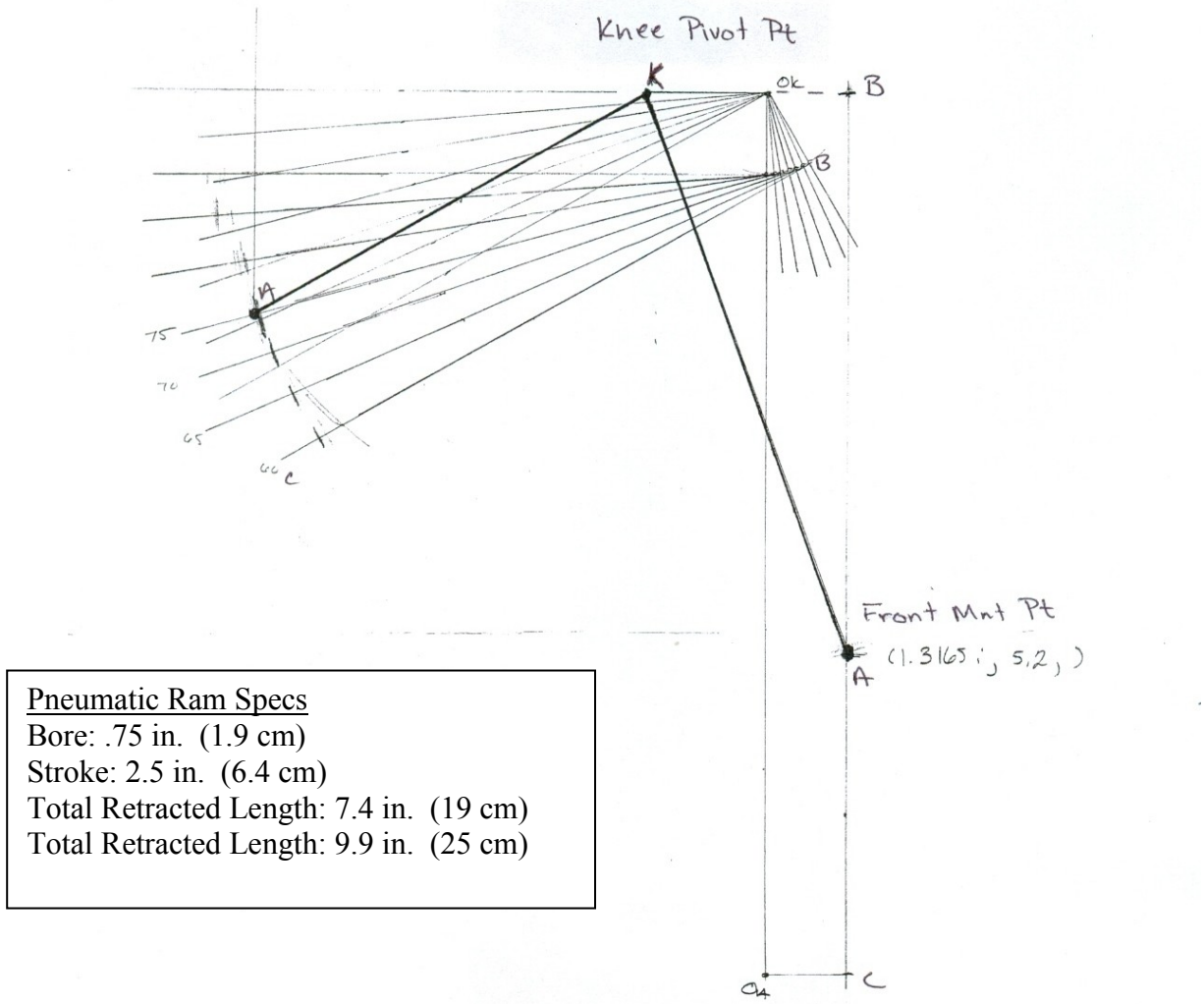

Pneumatic Ram Specs
Bore: .75 in. (1.9 cm)
Stroke: 2.5 in. (6.4 cm)
Total Retracted Length: 7.4 in. (19 cm)
Total Retracted Length: 9.9 in. (25 cm)

Figure A.2.3: Synthesis of knee mechanism with a 2.5 in (6.3 cm) stroke. The retracted pneumatic ram KA intersects the front of the shank BC at 75° of knee flexion.

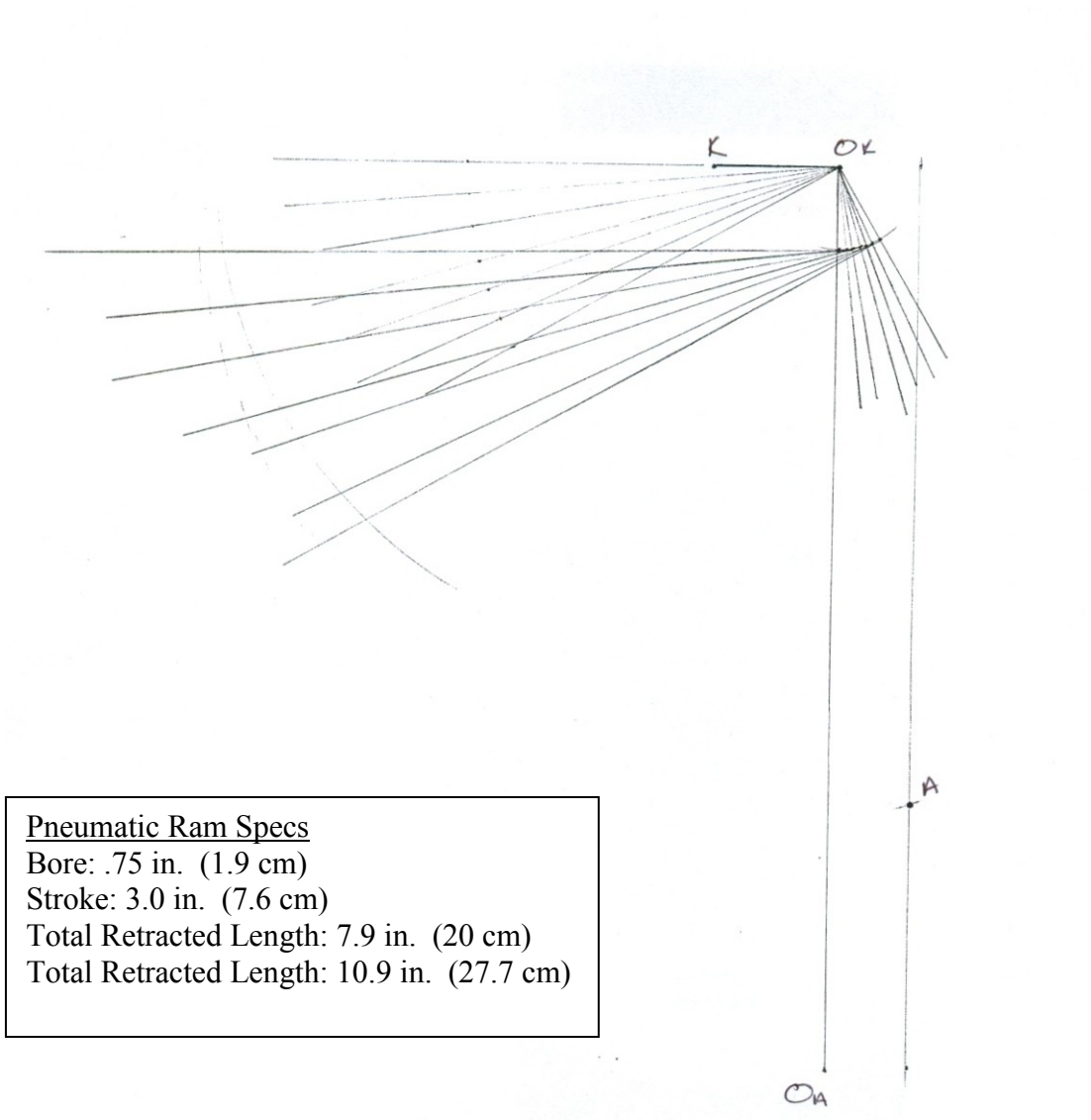

Pneumatic Ram Specs
Bore: .75 in. (1.9 cm)
Stroke: 3.0 in. (7.6 cm)
Total Retracted Length: 7.9 in. (20 cm)
Total Retracted Length: 10.9 in. (27.7 cm)

Figure A.2.4: Synthesis of knee mechanism with a 3.0 in. (3.8 cm) stroke. The pneumatic ram KA does not intersect BC when it is retracted. Therefore no solution exists for this mechanism with the knee flexed between 60° and 90°.

A.3 Ankle Actuation Mechanism Synthesis

The ankle actuator mechanism was synthesized graphically using a 2:1 scaled drawing on 11”x17” graph paper for a pneumatic ram with a stroke of 2.0 in (5.1 cm). The drawing has been reduced to fit in this document and is not shown to scale. Line AB is the pneumatic ram. Line O_AB is the lever arm. Line CD represents the front support rod on the shank. The pneumatic ram was positioned along the support rod at different positions until the desired range-of-motion for the ankle was achieved.

The final position of the ankle actuator was then graphically synthesized again at maximum dorsiflexion, maximum plantarflexion and neutral positions. This was done to improve the accuracy of the plantarflexion/dorsiflexion range-of-motion, as well as determine the values of the other angles in the mechanism.

Table A.3.1: Ankle mechanism synthesis results for three support locations.

Ankle Mechanism Synthesis Results			
Trial	**Plantarflexion**	**Dorsiflexion**	**Total**
1	55º	6º	61º
2	50º	12º	62º
3	45º	20º	65º

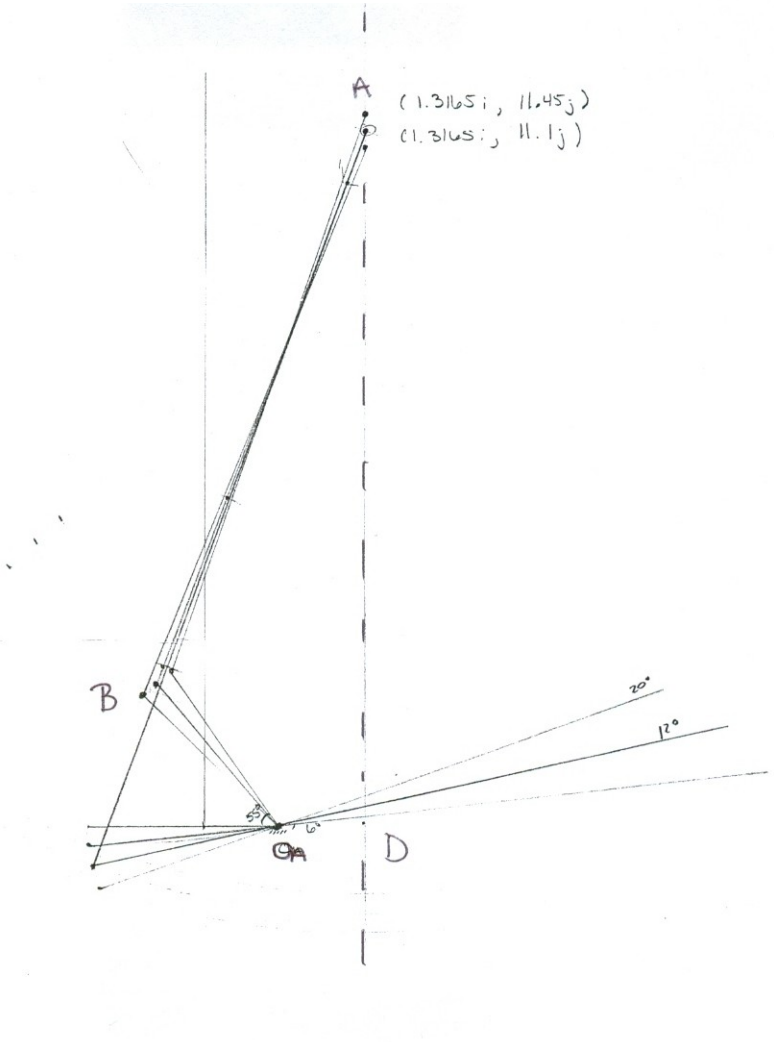

Figure A.3.1: Graphical synthesis of the ankle mechanism with the pivot point coincident with the support rod.

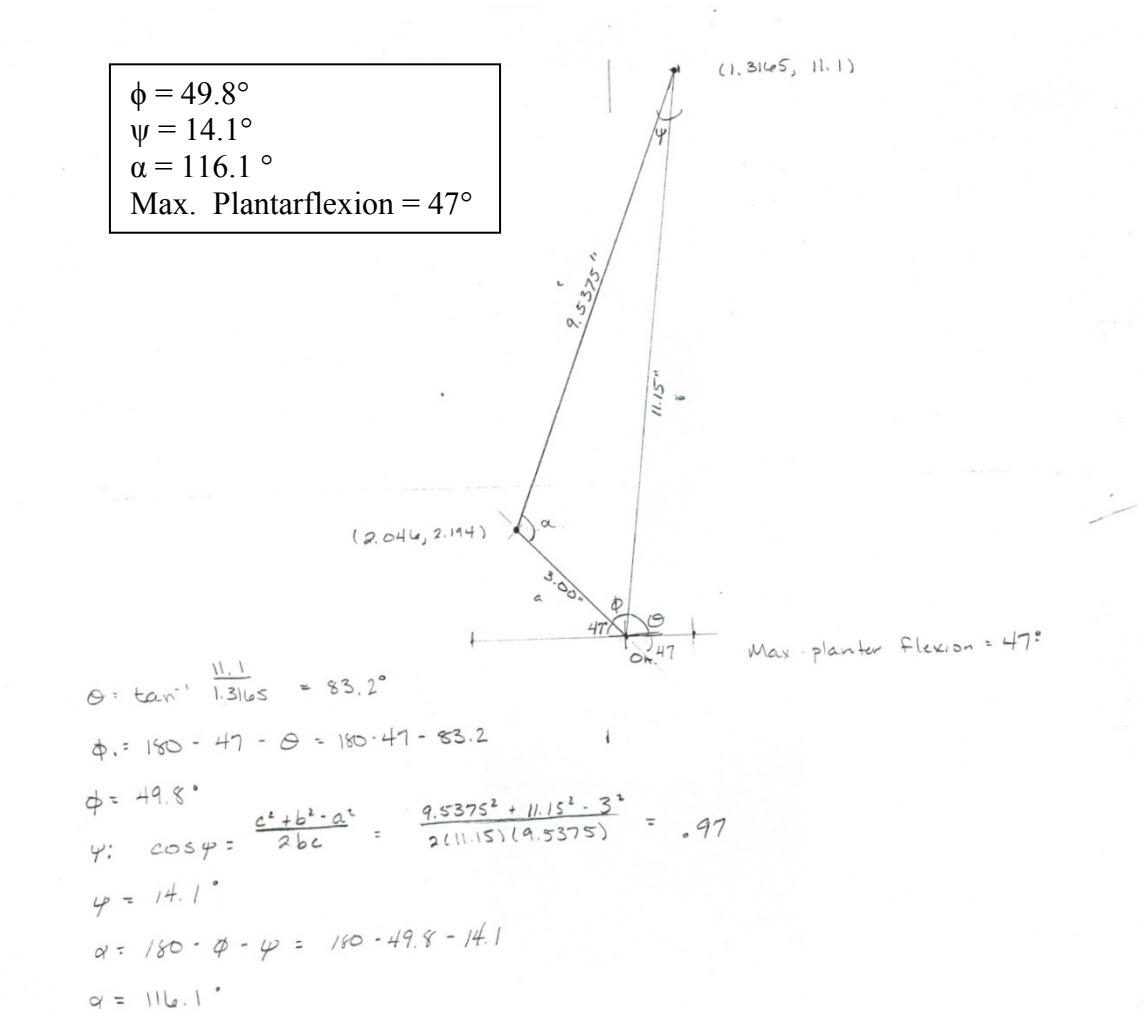

Figure A.3.2: Synthesis of ankle mechanism with foot completely plantarflexed. Maximum plantarflexion occurs when the pneumatic ram is retracted.

Applying Law of cosines.

$c^2 = a^2 + b^2 - 2ab\cos\phi$

$c^2 = 3.0^2 + 11.15^2 - 2(3.0)(11.15)\cos(96.8)$

$c^2 = 141.2$

$c = 11.9''$

$\phi = 96.8°$
$\psi = 14.1°$
$\alpha = 69.1°$
Ankle Flexion = 0°

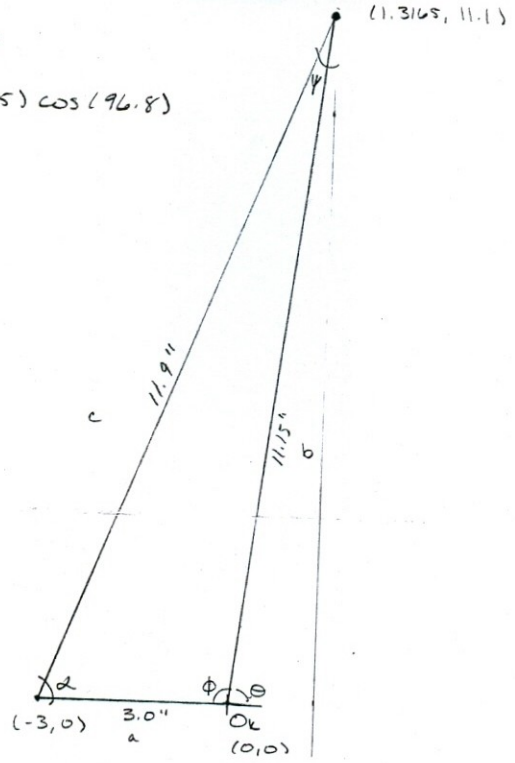

$\theta = \tan^{-1}\frac{11.1}{1.3165} =$

$\theta = 83.2°$

$\phi = 180 - \theta = 180 - 83.2$

$\phi = 96.8$

$\psi = \cos^{-1}\left\{\frac{c^2 + b^2 - a^2}{2bc}\right\} = \cos^{-1}\left\{\frac{11.9^2 + 11.15^2 - 3^2}{2(11.15)(11.9)}\right\} = .97$

$\psi = 14.1°$

$\alpha = 180 - \phi - \psi = 180 - 96.8 - 14.1$

$\alpha = 69.1°$

Figure A.3.3: Synthesis of ankle mechanism with foot in neutral postion.

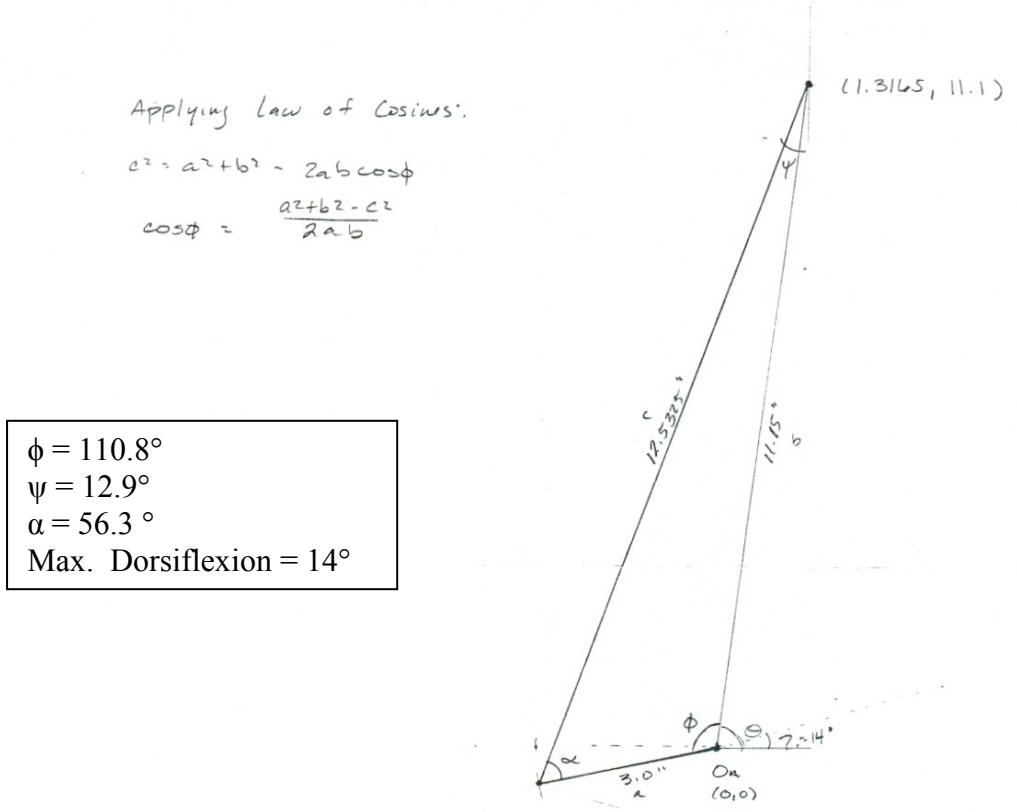

$\phi = 110.8°$
$\psi = 12.9°$
$\alpha = 56.3°$
Max. Dorsiflexion = 14°

$\theta = 83.2°$

$\phi = \cos^{-1}\left\{\frac{a^2+b^2-c^2}{2ab}\right\} = \cos^{-1}\left\{\frac{3^2+11.15^2-17.5325^2}{2(3.0)(11.15)}\right\}$

$\phi = 110.8°$

$\psi = \cos^{-1}\left\{\frac{c^2+b^2-a^2}{2bc}\right\} = \cos^{-1}\left\{\frac{12.5325^2+11.15^2-3^2}{2(11.15)(12.5325)}\right\}$

$\psi = 12.9°$

$\alpha = 180 - \phi - \psi = 180 - 110.8 - 12.9$

$\alpha = 56.3°$

Figure A.3.4: Synthesis of ankle mechanism with foot completely dorsiflexed. Maximum dorsiflexion occurs when the pneumatic ram is extended.

A.4 Knee Torque

The knee pneumatic ram does not align perpendicular to the fixed horizontal knee lever arm and angle varies as the knee flexes. Therefore only the vertical force component of the ram will apply a moment about the knee and will change as the knee flexes. Line a is the knee lever arm. Line b is the pneumatic ram. Line c is the difference between the origin of the knee joint and the location of the ram mount on the shank.

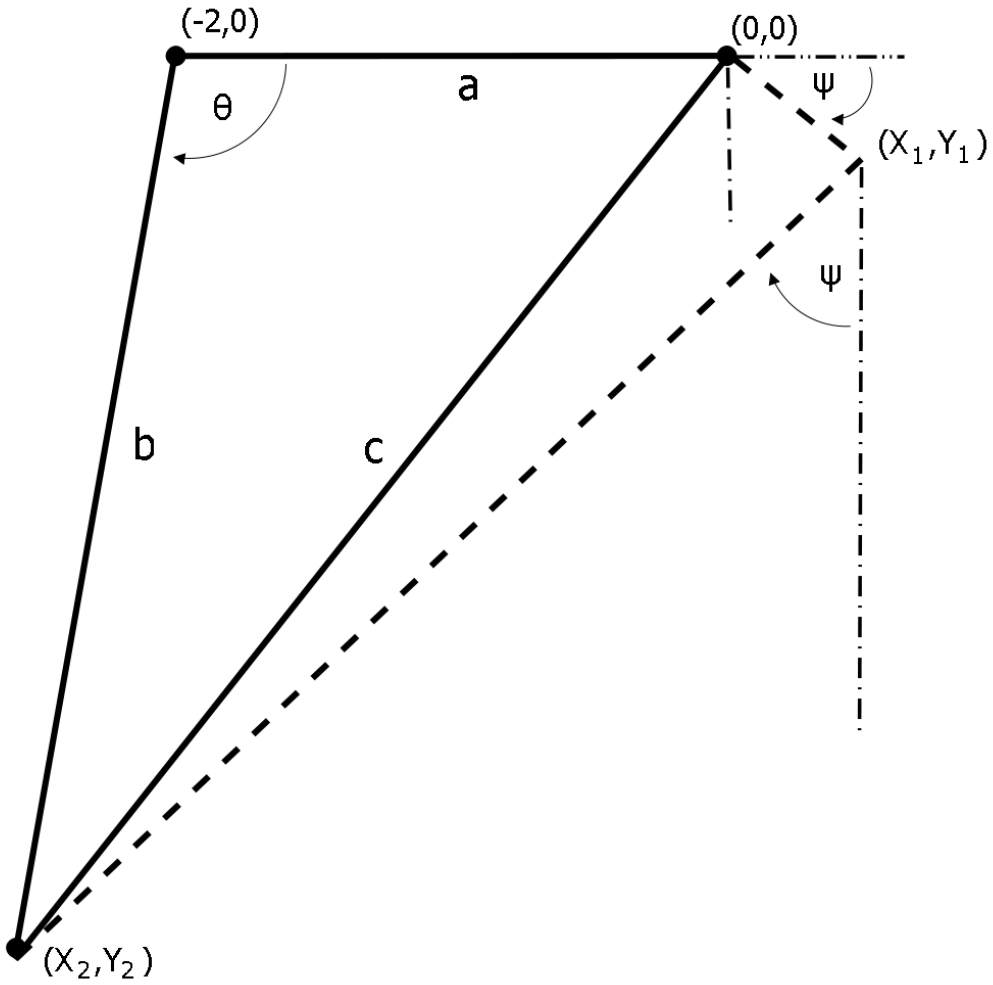

Figure A.4.1: Diagram of knee geometry used to evaluate the angle between the pneumatic ram and the lever arm as a function of knee flexion. The dimensions of this diagram are in inches.

The angle θ between the pneumatic ram and the lever arm can be determined using the law of cosines. However, the knee flexion angle ψ will need to be used to find the X_2 and Y_2 coordinates. The dashed lines, in Figure A.11, represent the shank front support structure mounted for the pneumatic ram. The location is of the mount is determined from the previous knee mechanism synthesis. All coordinates are in inches and degrees.

$$X_1 = 1.3\cos\psi \qquad \text{(A.4.1)}$$

$$Y_1 = -1.3 \sin \psi \quad \text{(A.4.2)}$$

$$X_2 = X_1 - 5.2 \sin \psi \quad \text{(A.4.3)}$$

$$Y_2 = -Y_1 - 5.2 \cos \psi \quad \text{(A.4.4)}$$

Use equations A4.1-A4.4 to find the magnitudes of lines a,b and c.

$$a = 2 \quad \text{(A.4.5)}$$

$$b = \sqrt{(X_2 + 2)^2 + (Y_2)^2} \quad \text{(A.4.6)}$$

$$c = \sqrt{(X_2)^2 + (Y_2)^2} \quad \text{(A.4.7)}$$

Apply the law of cosines to find calculate the pneumatic ram angle (θ).

$$\theta = \cos^{-1}\left(\frac{a^2+b^2-c^2}{2ab}\right) \quad \text{(A.4.8)}$$

Now determine the torque that is applied about the knee joint from the pneumatic ram along line b.

$$\tau_k = 2PA \sin \theta \quad \text{(A.4.9)}$$

Where P is the air pressure in psi and A is the cross-sectional area in square inches.

Figure A.12 shows the knee torque for the Jaywalker as the knee flexes through its range of motion. This knee profile was generated for the maximum cylinder pressure of 120 psi and the cylinder pressure during step testing. The peak knee torque approximations based on Winters were also plotted. These results show that the Winters knee torque approximations over estimate the required knee torque for the Jaywalker. In

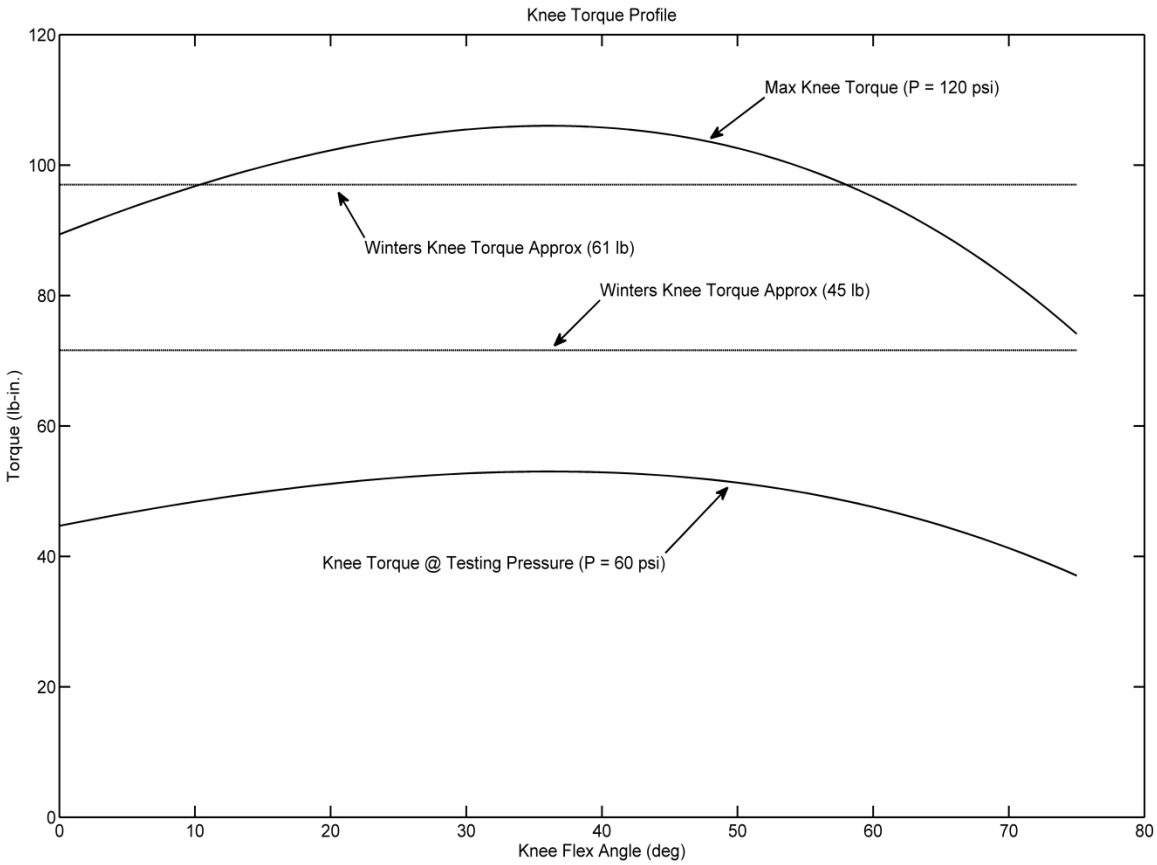

Figure A.4.2: Knee torque profile for the Jaywalker. The pneumatic ram generates a maximum knee torque when the cylinder pressure is set to its maximum value of 120 psi. The step testing was conducted with the knee cylinder pressure set to 60 psi. The Winters knee torque approximations are shown for the initial and final measured masses.

fact for the Jaywalker, the pneumatic sag in the swing phase dictated the knee pressure not the stance phase torque. Humans typically walk with a slight bend at the knee during the stance phase. This causes the hip COM to induce a moment about the knee. The

Jaywalker leg is straight during stance phase. Therefore the hip COM does not induce any moment. It is this difference that is most likely causing the Winters approximation to overestimate the peak knee torque.

A.5 Ankle Torque

The ankle torque is provided by a pneumatic ram and stepper motor attached to the ankle joint in parallel. The stepper motor applies up to 103 lb-in. of torque to the ankle joint. The pneumatic ram is placed such that as the ankle progresses from maximum dorsiflexion to maximum plantarflexion the pneumatic ram becomes almost orthogonal to the ankle joint. This causes the ankle joint to develop more torque as it approaches toe-off. Line a is the pneumatic ram. Line b is the lever arm. Line C is the vector between the ankle joint and the ram mount.

The angle θ between the ankle lever arm and pneumatic ram can be determined from the law of cosines. However, the ankle flexion angle ψ has to be known to compute the vector coordinates X_1 and Y_1. All coordinates are given in inches and all angles in degrees.

$$X_1 = 3\cos\psi \tag{A.5.1}$$

$$Y_1 = 3\sin\psi \tag{A.5.2}$$

Use equations A.5.1 and A.5.2 to find the magnitudes of lines a, b and c.

$$a = \sqrt{(X_1 + 1.3)^2 + (11.1 - Y_1)^2} \tag{A.5.3}$$

$$b = 3 \tag{A.5.4}$$

$$c = \sqrt{1.3^2 + 11.1^2} \tag{A.5.5}$$

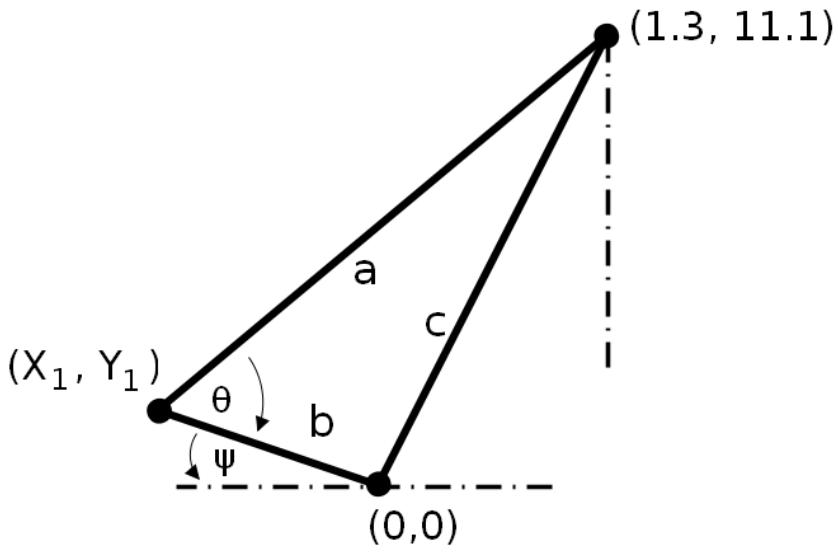

Figure A.5.1: Diagram of the ankle geometry used to determine the angle (θ) between the ankle lever arm and the pneumatic ram related to the ankle angle (ψ).

Apply the law of cosines to find the angle between the lever arm and pneumatic ram (θ). Refer to equation A.4.8 for the law of cosines. Now determine the minimum and maximum torque capable of being applied by the HPAA for any given pressure.

$$\tau_{min} = 3PA\sin\theta \qquad \text{(A.5.6)}$$

$$\tau_{max} = 3PA\sin\theta + \tau_m \qquad \text{(A.5.7)}$$

Where P is the pressure in psi and A is the cross-sectional area in square inches. The stepper motor torque is added to the pneumatic ram torque to obtain the maximum torque.

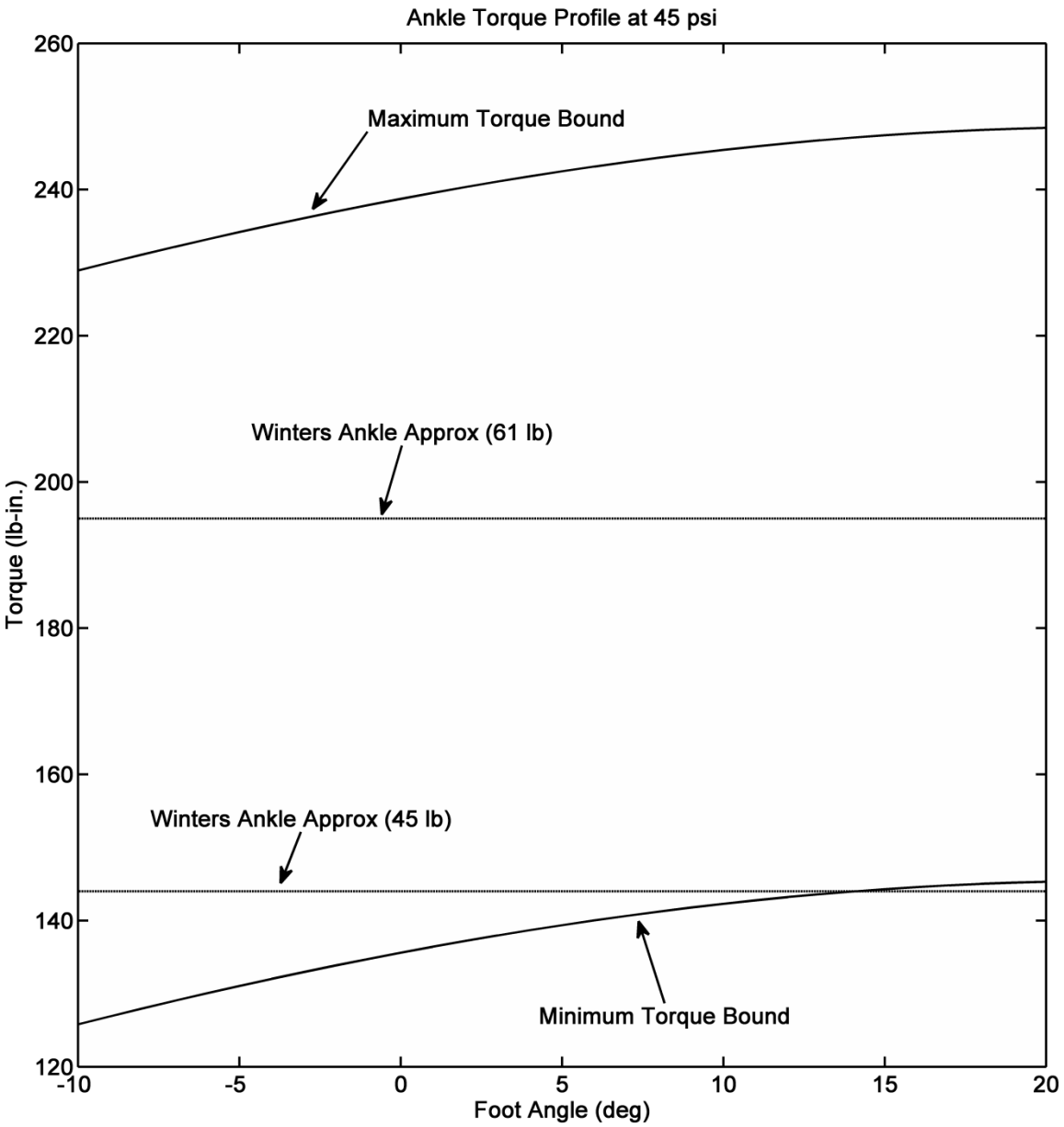

Figure A.5.2: The ankle torque profile for a cylinder pressure of 45 psi. The minimum torque bound is the torque applied by only the pneumatic ram. The maximum torque bound is the torque applied by the pneumatic ram and stepper motor. The peak Winters approximation torque for the initial and final walker weight are shown.

The Winters approximation for the final measured weight of the falls between the minimum and maximum torque bounds for the ankle actuator at 45 psi. Therefore, the Winters approximation reasonably approximates the ankle torque for the Jaywalker.

A.6 Joint Torque Approximation

The hip, knee and ankle peak joint torques were approximated using human data from Winter's Biomechanics and Motor Control of Human Movement [1]. The peak torques for the three joints during stance phase were take from Figure 4.13 on page 91 of Winter's book. These values were then used to linearly interpolate the Jaywalkers peak joint torques using body weight. The sex and weight of the test subject was not given by Winter. Therefore, it was assumed a 166 lb (75.3 kg) man was used as the test subject. This is the average of the 5^{th} and 95^{th} percentile weight for a man. From Winter's data the peak hip torque is 310 lb-in. (36 Nm), peak knee torque is 265 lb-in. (30 Nm) and the peak ankle torque is 531 lb-in. (60 Nm). The following are the three interpolation equations used to approximate the Jaywalker's peak joint torque.

$$\tau_{hip} = \frac{310}{166} w \qquad \text{(A.6.1)}$$

$$\tau_{knee} = \frac{265}{166} w \qquad \text{(A.6.2)}$$

$$\tau_{ankle} = \frac{531}{166} w \qquad \text{(A.6.3)}$$

Where w is the weight of the walking machine. These three equations (A.6.1-A.6.3) give the approximate joint torque for the Jaywalker, having a body weight of 45 lb, to be 84 lb-in, 72 lb-in. and 144 lb-in respectively for the hip, knee and ankle joints. The joint torque approximations for the Jaywalker weighing 61 lb are: 114 lb-in., 97 lb-in. and 195 lb-in. respectively for the hip, knee and ankle.

[1] Winter, D., 1990, *Biomechanics and Motor Control of Human Movement*, Wiley, pp. 91, Chap. 4.

A.7 Control Systems

The overall control system for Jaywalker discussed in Ch 1.11 contains three separate subsystems that the general computer uses to control the walking machine. These subsystems are: the SPI to parallel interface, solenoid control and motor control.

The SPI to parallel embedded system, Figure A.7.1, is used by the general control computer to read the values of the accelerometers. The NI-USB-6509 (NI I/O) provides I/O ports for the general control computer. However, it is not capable of toggling an I/O line fast enough to read SPI devices, like the accelerometers. Therefore a SX microprocessor was used to read the serial input of the accelerometers and output a parallel signal the general control computer can read. A bank of logical OR ICs were used to allow the general control computer to select which accelerometer to read, using the NI I/O board. The system can read up to 10 accelerometers, but only three are shown in Figure A.7.1.

The solenoid control circuit is shown in Figure A.7.2. It is simply an array of Darlington transistor to switch the knee and ankle solenoid valves on and off. To protect the NI I/O board from a current spike, it has been optically isolated from the rest of the circuit.

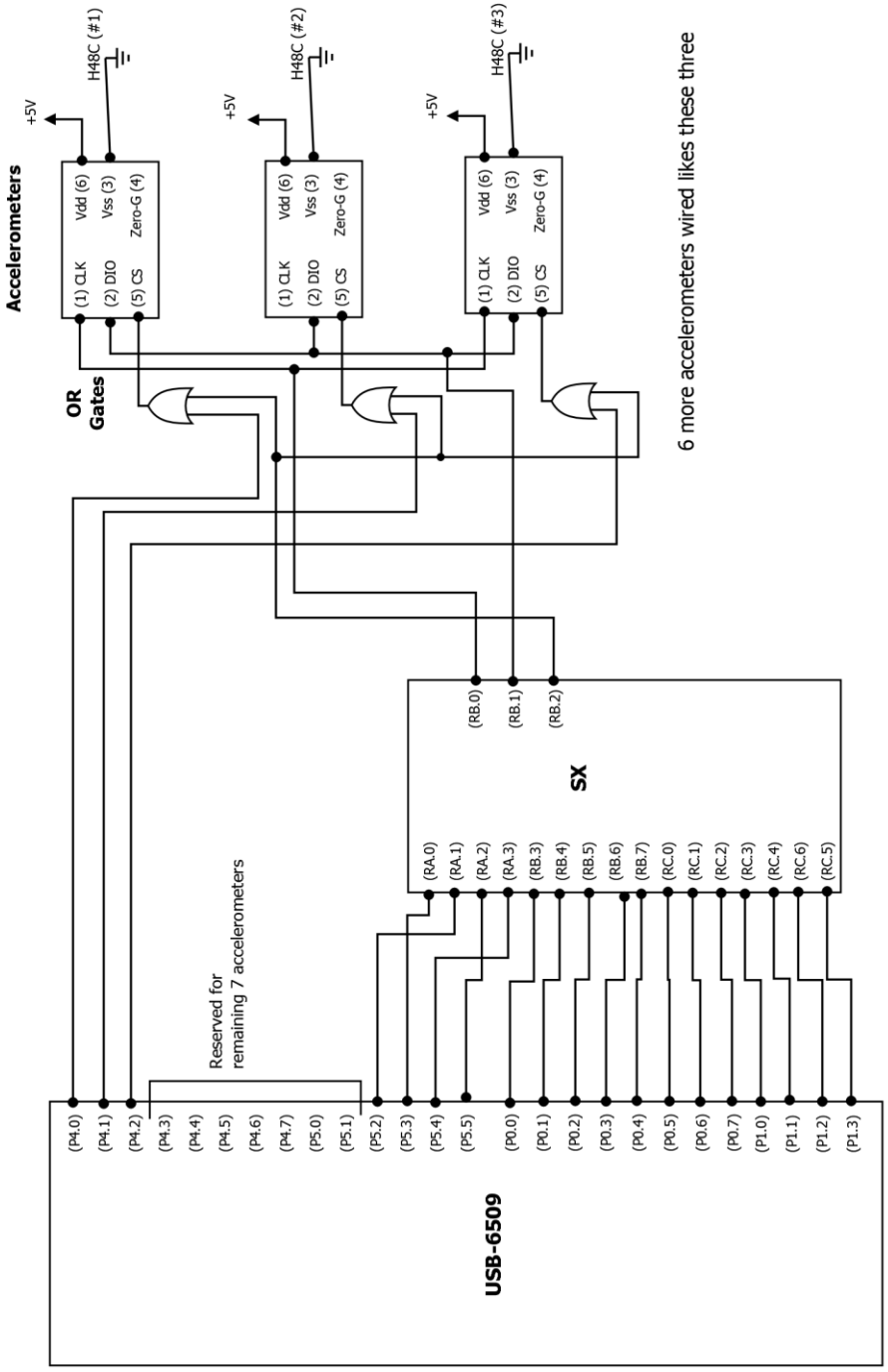

Figure A.7.1: Diagram of embedded system that reads the SPI protocol value from the accelerometer and converts into parallel data for NI board to read.

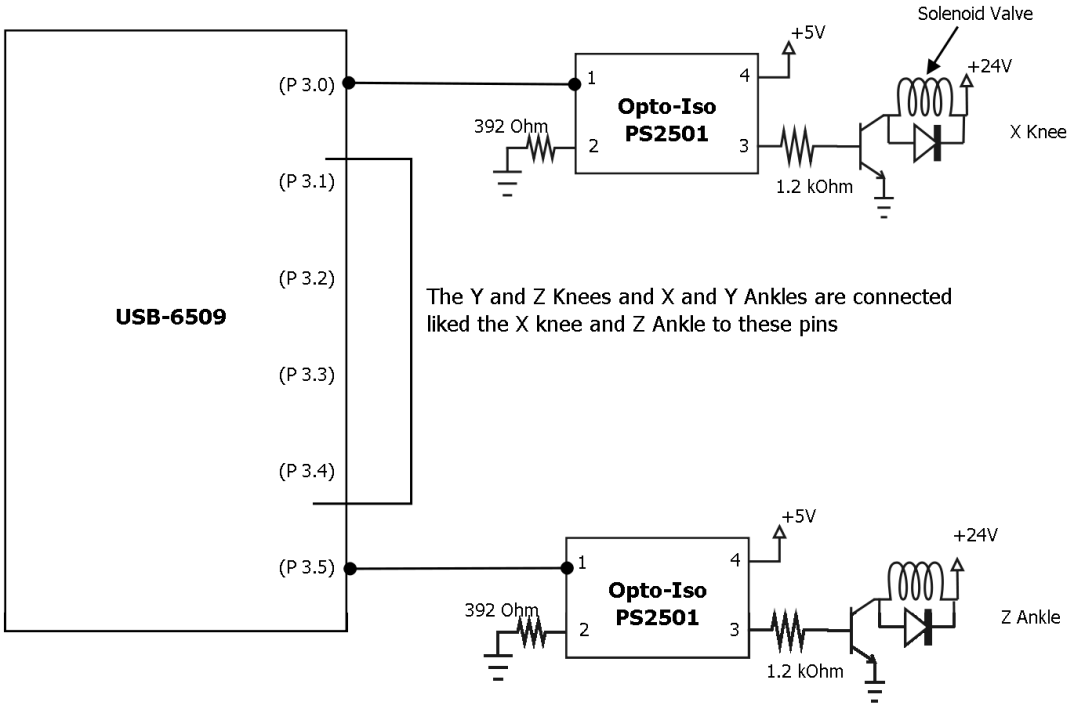

Figure A.7.2: Solenoid control circuit used to actuate the knee and ankle pneumatic rams on the Jaywalker.

The hip and ankle stepper motors are controlled an OMS Maxp motion control that was installed inside the general control computer. This control card sends the PWM and direction signals to the US Digital MD1 micro-step drive. The MD1 then sends the correct step sequence to the US Digital MS23 stepper motors. This circuit is shown in Figure A.7.3 for 1 axis.

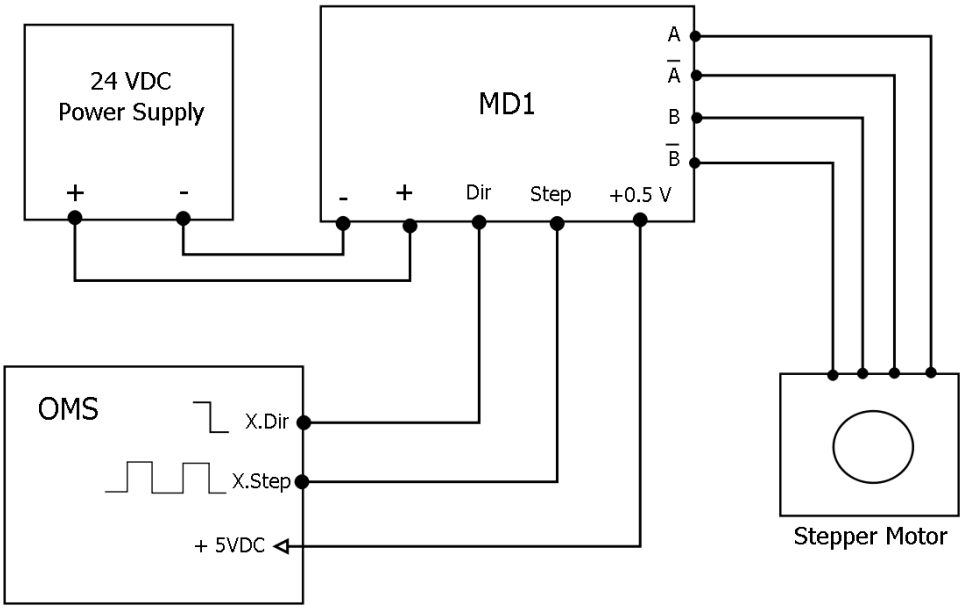

Figure A.7.3: The stepper motor drive circuit for 1 control axis.

A.8 SPI to Parallel Translator Code

```
' Filename: NI Serial to Parallel.SXB
' Written by: Bryce Baker
'-----------------------------------------------------------------
' Description: This program uses the SX to convert the serial data
' obtained from the Hitachi 48 accelerometer into parallel data for
' the NI USB-6509

' This program sends %101010101010 to confirm that the accelerometer
' is done reading.

' This program is set to read only the z axis on the x and y thigh
' legs.
'-----------------------------------------------------------------
DEVICE SX28, TURBO, STACKX, OPTIONX,OSCXT2
FREQ  4_000_000
ID       "NI_Par"
'-----------------------------------------------------------------
' [ Mask SX Pins ]
b_12            PIN     RC.6
b_11            PIN     RC.5
b_10            PIN     RC.4
b_09            PIN     RC.3
b_08            PIN     RC.2
b_07            PIN     RC.1
b_06            PIN     RC.0
b_05            PIN     RB.7
b_04            PIN     RB.6
b_03            PIN     RB.5
b_02            PIN     RB.4
b_01            PIN     RB.3
cs              PIN     RB.2
dio             PIN     RB.1
clk             PIN     RB.0
axisBit1        PIN     RA.3
axisBit0        PIN     RA.2
sx_talk         PIN     RA.1
usb_talk        PIN     RA.0
'-----------------------------------------------------------------------
' [ Constants ]
Xaxis   CON   0
Yaxis   CON   1
Zaxis   CON   2
Vref    CON   3
```

```
XselectCON   %101
YselectCON   %110
ZselectCON   %111
DselectCON   %011
Rdata  CON   %100
'-----------------------------------------------------------------------
' [ Variables ]
startFlag       VAR   BIT
XonceFlag       VAR   BIT
YonceFlag       VAR   BIT
ZonceFlag       VAR   BIT

startAccel      VAR   BYTE
axis            VAR   BYTE
axisSelect      VAR   BYTE
rvCountMSB  VAR   BYTE
rvCountLSB  VAR   BYTE
axCountMSB  VAR   BYTE
axCountLSB  VAR   BYTE

rvCount             VAR   WORD
axCount             VAR   WORD
dCountX             VAR   WORD
dCountY             VAR   WORD
dCountZ             VAR   WORD
'-----------------------------------------------------------------------
Get_H48c      sub     0
Done_H48c     sub    0
Send_H48c     sub     0
Read_Xaxis    sub     0
Read_Yaxis    sub     0
Read_Zaxis    sub     0
Get_Break     sub     0
'-----------------------------------------------------------------------
PROGRAM Start
Start:
'-----------------------------------------------------------------------
' [ I/O Directions ]
INPUTusb_talk
INPUT   axisBit0
INPUT   axisBit1
OUTPUT       sx_talk
OUTPUT       b_01
OUTPUT       b_02
OUTPUT       b_03
```

```
OUTPUT      b_04
OUTPUT      b_05
OUTPUT      b_06
OUTPUT      b_07
OUTPUT      b_08
OUTPUT      b_09
OUTPUT      b_10
OUTPUT      b_11
OUTPUT      b_12
' cs, dio and clk pins will be defined using low and high commands
' [ Subroutine Declarations ]
'-----------------------------------------------------------------------
' [ Initialize ]
' Initialize output pin values
Initialize:
HIGH cs
b_01 = 0
b_02 = 0
b_03 = 0
b_04 = 0
b_05 = 0
b_06 = 0
b_07 = 0
b_08 = 0
b_09 = 0
b_10 = 0
b_11 = 0
b_12 = 0

sx_talk = 0
axisSelect = 0
startAccel = 0
startFlag = 1
XonceFlag = 0
YonceFlag = 0
ZonceFlag = 0
dCountX = 0
dCountY = 0
dCountZ = 0
rvCount = 0
axCount = 0

watch dCountX,16,sdec
watch dCountY,16,sdec
watch dCountZ,16,sdec
```

```
watch usb_talk,1,ubin
watch sx_talk,1,ubin
watch startAccel,8,ubin
watch axisSelect,8,ubin

' [ Main ]
Main:
 startAccel.0 = axisBit0
 startAccel.1 = axisBit1
 startAccel.2 = usb_talk

IF startAccel = Rdata THEN
 FOR axis = Xaxis TO Zaxis
  GOSUB Get_H48c

 NEXT

GOSUB Done_H48c
GOSUB Send_H48c
GOSUB Get_Break
ENDIF

GOTO Main                       ' the program is re-initialized and waits to read
accel.  again
'-----------------------------------------------------------------
' [ Subroutines ]

' The Get_H48c subroutine gets the reference and axis count for the specified axis in the
the
' Read_Accel subroutine.

Get_H48c:
'Reads the reference count for the accelerometer
LOW cs                          ' activates the accelerometer chip
'(#1)
SHIFTOUT dio,clk,MSBFIRST,%11\2
SHIFTOUT dio,clk,MSBFIRST,Vref\3
'(#2)
SHIFTIN dio, clk,msbpost,rvCountMSB\5
SHIFTIN dio, clk,msbpost,rvCountLSB
HIGH cs                         ' deactivates the accelerometer chip

PAUSE 1

' Reads the axis count for the accelerometer
```

```
LOW cs
'(#3)
SHIFTOUT dio,clk,MSBFIRST,%11\2
SHIFTOUT dio,clk,MSBFIRST,Zaxis\3
' This shiftin sequence does the same thing as the previous, but with the axis count values
SHIFTIN dio,clk,msbpost,axCountMSB\5
SHIFTIN dio,clk,msbpost,axCountLSB
HIGH cs
' Combines the two byte variables into one word variable.

PUT @rvCount,rvCountLSB,rvCountMSB
PUT @axCount,axCountLSB,axCountMSB

RETURN

'--------------------------------------------------------------------
Done_H48c:

b_01 = 0
b_02 = 1
b_03 = 0
b_04 = 1
b_05 = 0
b_06 = 1
b_07 = 0
b_08 = 1
b_09 = 0
b_10 = 1
b_11 = 0
b_12 = 1

RETURN
'--------------------------------------------------------------------
Send_H48c:

checkAxis:
  axisSelect.0 = axisBit0
  axisSelect.1 = axisBit1
  axisSelect.2 = usb_talk

IF axisSelect = Xselect THEN
 GOSUB Read_Xaxis
ELSEIF axisSelect = Yselect THEN
 GOSUB Read_Yaxis
ELSEIF axisSelect = Zselect THEN
```

```
 GOSUB Read_Zaxis
ELSEIF axisSelect = Dselect THEN
 sx_talk = 0
 XonceFlag = 0
 YonceFlag = 0
 ZonceFlag = 0
 GOTO doneCheck
ENDIF

GOTO checkAxis

doneCheck:
RETURN
'--------------------------------------------------------------------
Read_Xaxis:
'IF XonceFlag = 0 THEN
'  sx_talk = 0
'  b_01 = dCountX.0
'  b_02 = dCountX.1
'  b_03 = dCountX.2
'  b_04 = dCountX.3
'  b_05 = dCountX.4
'  b_06 = dCountX.5
'  b_07 = dCountX.6
'  b_08 = dCountX.7
'  b_09 = dCountX.8
'  b_10 = dCountX.9
'  b_11 = dCountX.10
'  b_12 = dCountX.11
'  sx_talk = 1
'  XonceFlag = 1
'  YonceFlag = 0
'  ZonceFlag = 0
'ENDIF
RETURN
'--------------------------------------------------------------------
Read_Yaxis:
'IF YonceFlag = 0 THEN
'  sx_talk = 0
'  b_01 = dCountY.0
'  b_02 = dCountY.1
'  b_03 = dCountY.2
'  b_04 = dCountY.3
'  b_05 = dCountY.4
'  b_06 = dCountY.5
```

```
'  b_07 = dCountY.6
'  b_08 = dCountY.7
'  b_09 = dCountY.8
'  b_10 = dCountY.9
'  b_11 = dCountY.10
'  b_12 = dCountY.11
'  sx_talk = 1
'  XonceFlag = 0
'  YonceFlag = 1
'  ZonceFlag = 0
'ENDIF
RETURN
'--------------------------------------------------------------------
Read_Zaxis:
IF ZonceFlag = 0 THEN
  sx_talk = 0
  b_01 = dCountZ.0
  b_02 = dCountZ.1
  b_03 = dCountZ.2
  b_04 = dCountZ.3
  b_05 = dCountZ.4
  b_06 = dCountZ.5
  b_07 = dCountZ.6
  b_08 = dCountZ.7
  b_09 = dCountZ.8
  b_10 = dCountZ.9
  b_11 = dCountZ.10
  b_12 = dCountZ.11
  sx_talk = 1
  XonceFlag = 0
  YonceFlag = 0
  ZonceFlag = 1
ENDIF
RETURN
'--------------------------------------------------------------------
Get_Break:
BREAK
RETURN
'--------------------------------------------------------------------
' [ Long Comments ]

' (#1)
' The shiftout must send a %11011 value to tell the accelerometer to read the reference
' voltage count.  The first shiftout sends the %11 and the second shiftout sends %011 to
```

```
' complete the %11011 value.  This could be done with one shiftout command, but
decided to
' keep the code consistent with the axis read, which has to vary this value.

' (#2)
' The shiftin command can only read a byte.  Therefore two bytes have to be used to read
' the 12 bit signal coming from the accelerometer.  The first shiftin reads in the upper
' 5 most bits including the null bit.  The second shiftin reads in the lower 8 bits of the
' the count value.

' (#3)
' The shiftout must send either %11000, %11001 or %11010 to the accelerometer to read
' the X, Y and Z axes respectively.  This is done by shifting out %11 permanently and
' then shifting out the three right most bits of the axis variable to generate the
' %000, %001 and %010 values needed to activate an axis.
```

APPENDIX B: HPAA DEVELOPMENT

Appendix B contains supplemental design and development information for testing and implementing the Hybrid Parallel Ankle Actuator on the Jaywalker walking machine.

B.1 Actuator Test Stand

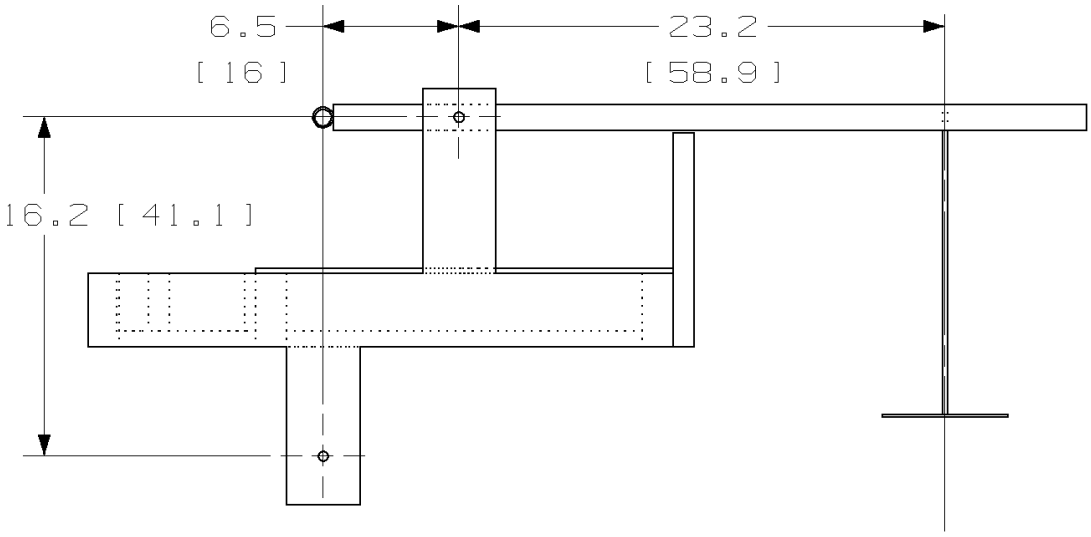

Figure B.1.1: Shows the three key dimensions of the actuator test stand. These dimensions are: the distance from the drive shaft to the weight hanger and the distances from drive shaft to the pneumatic ram mount location.

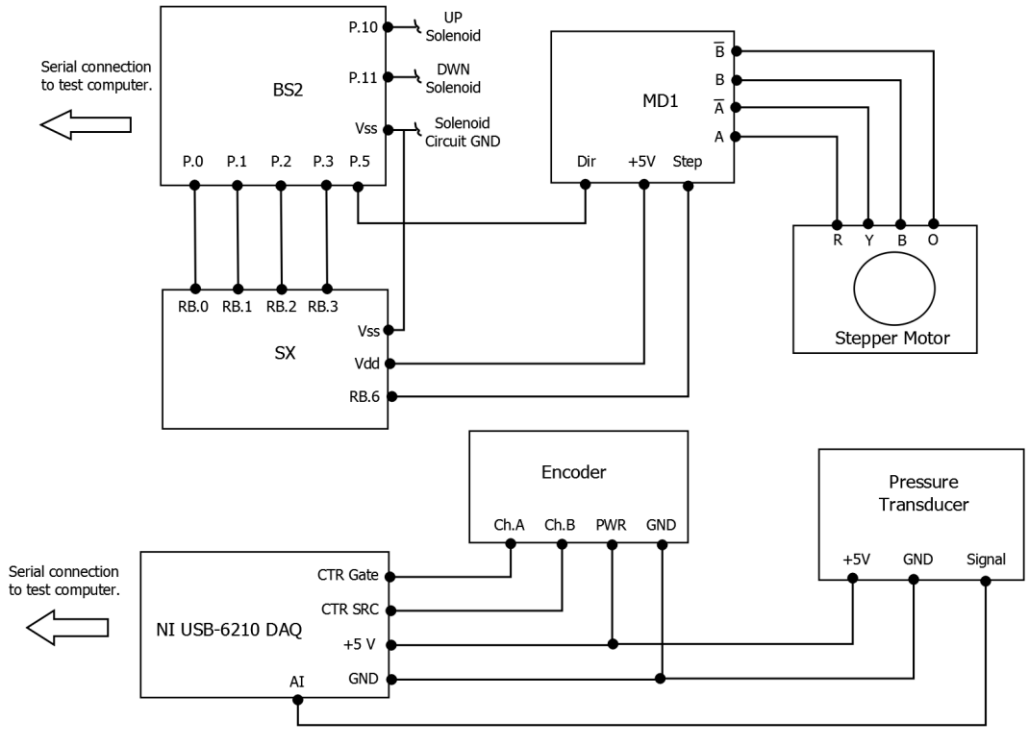

Figure B.1.2: Shows the control and DAQ systems for the actuator testbed. A Basic Stamp MP is used as the main controller for the system, and interfaces with the general test computer using a RS232 connection. It controls the solenoid valves to the pneumatic ram as well as when to actuate the stepper motor and at what speed. The PWM for the stepper motor is offloaded to an SX MP. The encoder and pressure transducer are read by a NI USB-6210 DAQ board and interfaces with the general test computer using an USB connection. LabVIEW is used to read and record the encoder and pressure transducer data.

B.2 Test Stand Main Controller Basic Stamp Code

```
' {$STAMP BS2}
' {$PBASIC 2.5}
' ================================================================
' Filename: HPA_Control.bs2
' Written by: Bryce Baker
' Description: This program is used to control the HPA testbed with the 3.6 timing belt
ratio.
'================================================================

'------ Declare Variables -----
serDec       VAR Byte
idx          VAR Nib

'------- Set Pin Names -----
shaftSpeed_2rpm     PIN 0
shaftSpeed_4rpm     PIN 1
shaftSpeed_6rpm     PIN 2
shaftSpeed_8rpm     PIN 3
armDir              PIN 5
UpValve             PIN 10

'----- Set I/O Pins -----
OUTPUT shaftSpeed_2rpm
OUTPUT shaftSpeed_4rpm
OUTPUT shaftSpeed_6rpm
OUTPUT shaftSpeed_8rpm
OUTPUT armDir
OUTPUT UpValve

'----- Initialize Pins -----
shaftSpeed_2rpm = 0
shaftSpeed_4rpm = 0
shaftSpeed_6rpm = 0
shaftSpeed_8rpm = 0
armDir  = 0
UpValve = 0

main:
check_input:
'======================= Create Screen=====================
DEBUG "Select Arm Speed ",CR,"1) 2 RPM Up",CR,"2) 2 RPM Dwn",CR
DEBUG"-------------------------------------------------------",CR
DEBUG "3) 4 RPM Up", CR, "4) 4 RPM Dwn",CR
```

```
DEBUG"------------------------------------------------------------",CR
DEBUG "5) 6 RPM Up", CR, "6) 6 RPM Dwn",CR
DEBUG"------------------------------------------------------------",CR
DEBUG "7) 10 RPM Up", CR, "8) 10 RPM Dwn",CR
DEBUG"------------------------------------------------------------",CR
DEBUG "9) Turn Off Solenoid",CR,"10) End Program",CR
DEBUG "Make Selection: "
SERIN 16, 16468, [DEC serDec] ' input from debug screen
DEBUG CLS
'---------------------- Check Input User Selection From Screen -------------------------------

SELECT serDec
 CASE 1
   armDir = 0
   UpValve = 1
   PAUSE 0
   FOR idx = 0 TO 1
     TOGGLE shaftSpeed_2rpm
     PAUSE 1
   NEXT
 CASE 2
   armDir = 1
   FOR idx = 0 TO 1
     TOGGLE shaftSpeed_2rpm
     PAUSE 1
   NEXT
 CASE 3
   armDir = 0
   UpValve = 1
   PAUSE 0
   FOR idx = 0 TO 1
     TOGGLE shaftSpeed_4rpm
     PAUSE 1
   NEXT
 CASE 4
   armDir = 1
   FOR idx = 0 TO 1
     TOGGLE shaftSpeed_4rpm
     PAUSE 1
   NEXT
 CASE 5
   armDir = 0
   UpValve = 1
   PAUSE 500
   FOR idx = 0 TO 1
```

```
    TOGGLE shaftSpeed_6rpm
    PAUSE 1
  NEXT
 CASE 6
  armDir = 1
  FOR idx = 0 TO 1
    TOGGLE shaftSpeed_6rpm
    PAUSE 1
  NEXT
 CASE 7
  armDir = 0
  UpValve = 1
  PAUSE 5
  FOR idx = 0 TO 1
    TOGGLE shaftSpeed_8rpm
    PAUSE 1
  NEXT
 CASE 8
  armDir = 1
  FOR idx = 0 TO 1
    TOGGLE shaftSpeed_8rpm
    PAUSE 1
  NEXT
 CASE 9
  UpValve = 0
 CASE 10
  GOTO end_program

ENDSELECT
GOTO check_input

end_program:
UpValve = 0

STOP
```

B.3 Test Stand PWM Controller SX Code

```
' Filename: MD1_Drive_Control.SXB
' Written by: Bryce Baker
'=================================================================
' Description:
' This program is written to generate a pulse-train for a MD1 microstep used to control
the stepper motor for the HPA
' testbed.   It will generate a pulse upto a frequency of 100 kHz.   The duty cycle of the
pulse-train is set at 50%.

' This specific program is written for the HPA test stand with the timing belt with a 7.2
ratio is attached.
'=================================================================
' DEVICE Settings
'=================================================================
DEVICE      SX28, OSC4MHZ, TURBO, STACKX, OPTIONX,OSCXT2
FREQ  4_000_000
ID      "HPA_CTRL"

'=================================================================
' IO PINS
'=================================================================
Trigger480    var     RB.0
Trigger960    var     RB.1
Trigger1440   var     RB.2
Trigger2400   var     RB.3
PulsePin      var     RB.6          'Masks Pin 7 of port RB
'=================================================================
' Constants
'=================================================================
numPulses     con     2000          'Sets the number of pulses for the pulsetrain
        (1045 Pulses for 50 deg)
                                    '                                          (215
Pulses for 10 deg testing)

'=================================================================
' Variable Declarations
'=================================================================
delay_outside var     byte          'variable used for the outside loop of the nested
delay loop
delay_inside  var     byte          'variable used for the inside loop of the nested delay
loop
counter       var     word
cntPulses     var     word
```

```
'====================================================================
' Subroutine Prototypes
'====================================================================
freq480                 sub 0
freq960                 sub 0
freq1440        sub 0
freq2400        sub 0
delay           sub 2

'====================================================================
'Program Code
'====================================================================
PROGRAM Initialize          ' Sets the execution point of the program

' Initialize variables to be used in program
Initialize:
output PulsePin
input Trigger480
input Trigger960
input Trigger1440
input Trigger2400

PulsePin = 0
delay_outside = 0
delay_inside = 0

cntPulses = 2*numPulses

Main:
check:
if Trigger480 = 1 then
 freq480
elseif Trigger960 = 1 then
 freq960
elseif Trigger1440 = 1 then
 freq1440
elseif Trigger2400 = 1 then
 freq2400
else
 'Do Nothing
endif
goto check
end
```

```
'=============================================================
' Subroutines
'=============================================================
' One pass through the frequency subroutine loop generates either the high or low
segment of a pulse (1/2 the pulse).
'Therefore, for a 2000 pulse pulsetrain, the frequency subroutine loop must execute 4000
times.

sub freq480
pause 1
for counter = 0 to cntPulses step 1
  toggle PulsePin                       ' It takes two passes of the inside loop to
generate one full pulse
   delay 106, 9                         ' (high/low) of the pulse-train.   Therefore to
generate 10 pulses
next                                    ' the inisde loop executes 20 times.
PulsePin = 0
endsub
'-------------------------------------------------------------------------------------------------

sub freq960
pause 1
for counter = 0 to cntPulses step 1
  toggle PulsePin                       ' It takes two passes of the inside loop to
generate one full pulse
   delay 52, 9                          ' (high/low) of the pulse-train.   Therefore to
generate 10 pulses
next                                    ' the inisde loop executes 20 times.
PulsePin = 0
endsub
'-------------------------------------------------------------------------------------------------

sub freq1440
pause 1
for counter = 0 to cntPulses step 1
  toggle PulsePin                       ' It takes two passes of the inside loop to
generate one full pulse
   delay 57, 5                          ' (high/low) of the pulse-train.   Therefore to
generate 10 pulses
next                                    ' the inisde loop executes 20 times.
PulsePin = 0
endsub

'-------------------------------------------------------------------------------------------------
```

```
sub freq2400
pause 1
for counter = 0 to cntPulses step 1
  toggle PulsePin                                ' It takes two passes of the inside loop to
generate one full pulse
   delay 50, 3                                 ' (high/low) of the pulse-train.   Therefore to
generate 10 pulses
next                                             ' the inisde loop executes 20 times.
PulsePin = 0
endsub

'-------------------------------------------------------------------------------------------------------
sub delay
'freqDelayIL = __param2
asm
          mov     delay_outside,__param1       ' sets delay_outside = variable freqDelay,
This value varies to change delay time
oloop   mov     delay_inside,__param2          ' sets delay_inside = 9, Inner loop always
equals 9 to yield 19 instructions
wloop  djnz     delay_inside,wloop             ' or approximately 5 microseconds.
          djnz     delay_outside,oloop
endasm
endsub
```

B.4 HPAA Step Response Curves

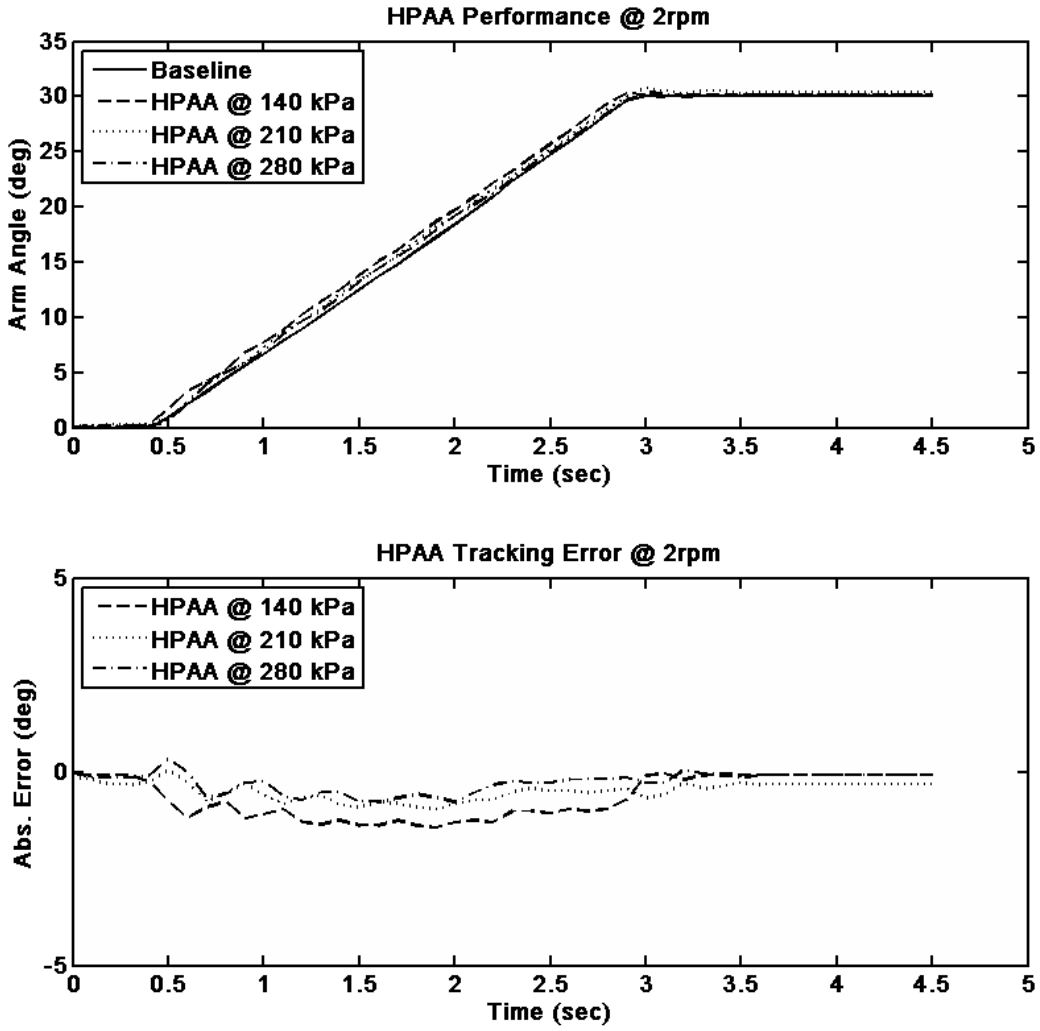

Figure B.4.1: Enlarged reproduction of HPAA step response results from Figure 2.6.1a.

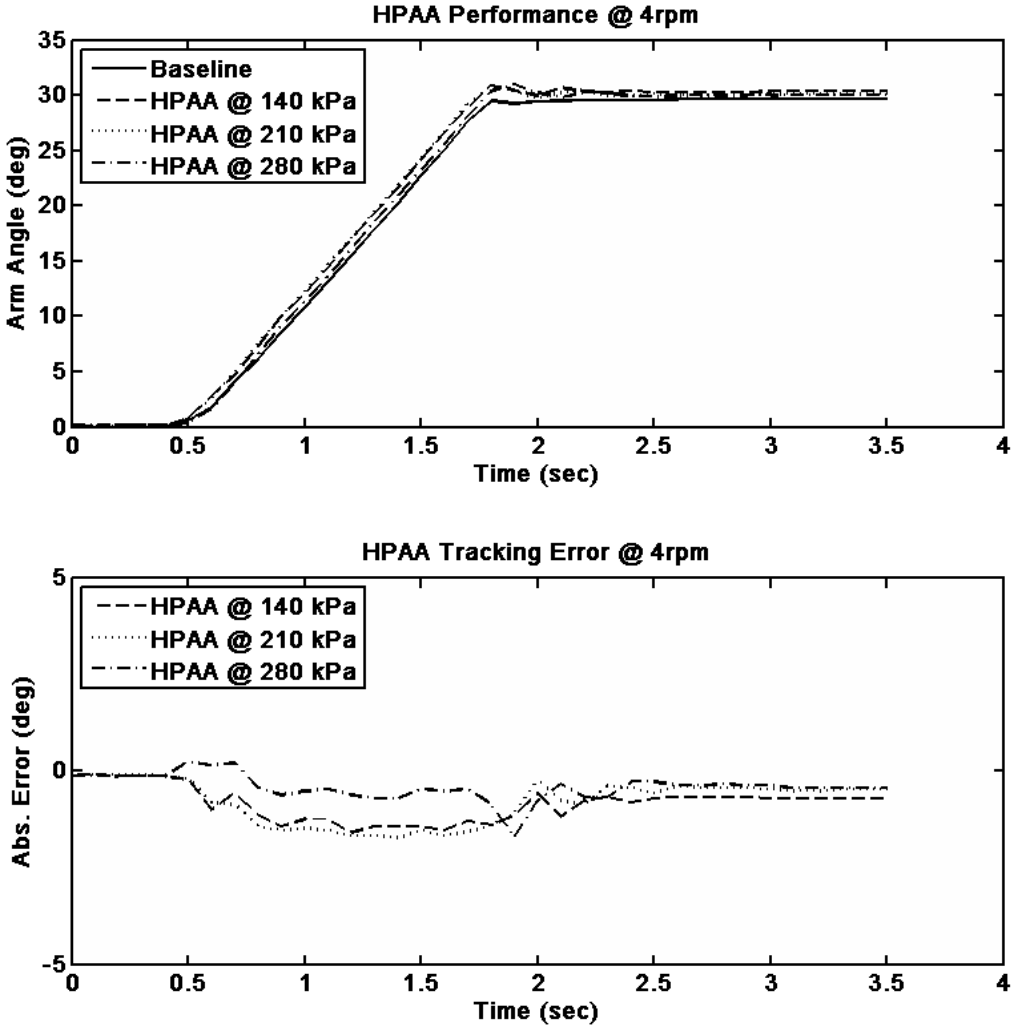

Figure B.4.2: Enlarged reproduction of HPAA step response results from Figure 2.6.1b.

B.5 Pneumatic Latency Analysis of HPAA

The pneumatic latency of the HPAA, discussed in chapter 2; sections 3, 6, and 8 was determined experimentally on the actuator test stand. The experiment procedure was: 1) locking the lever arm to the test stand; 2) Start the data acquisition system; 3) Open the solenoid valve to the pneumatic ram; 4) Record the time required to get to the set pressure. This experiment was conducted for multiple trials over a pressure range of

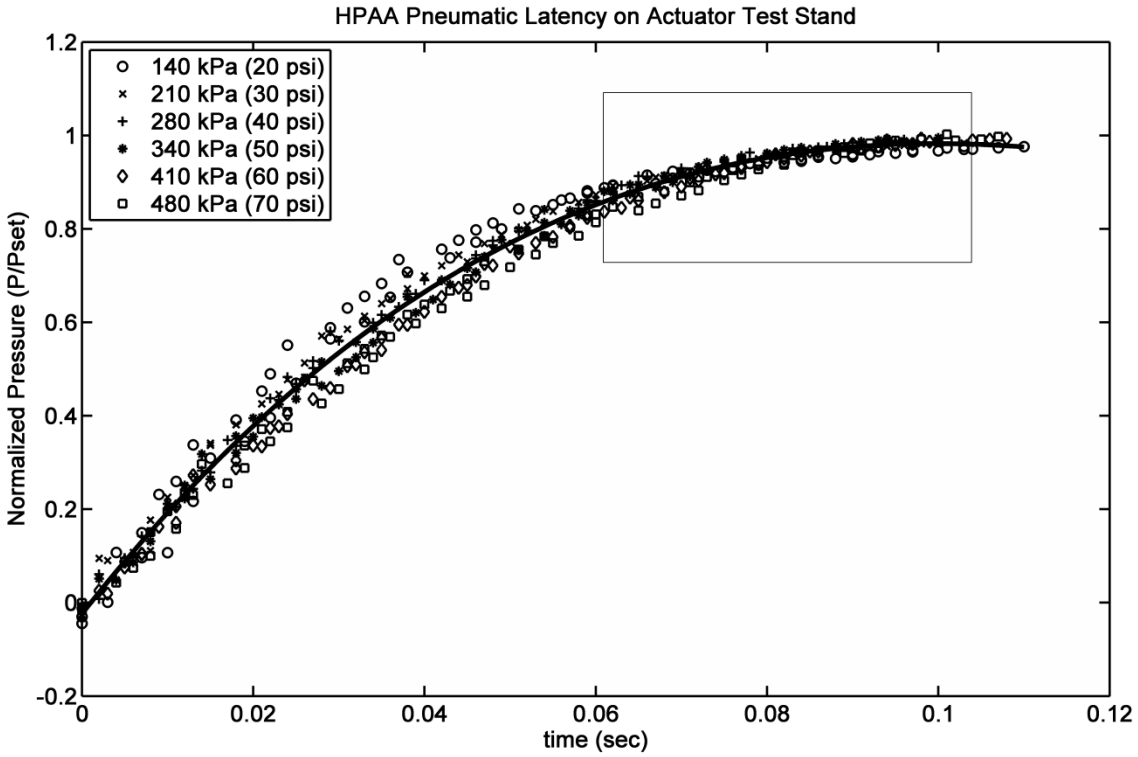

Figure B.5.1: The pneumatic latency test results for the HPAA on the actuator test stand. This test was conducted for pressures between 140 kPa and 480 kPa. The normalized pressure results show the latency time is approximately the same for all tested pressures.

140 kPa (20 psi) to 480 kPa (70 psi). The results show in Figure B.5.1, show that all the pressures start to converge after 0.06s and reach their set pressures around 0.1s. Showing, the pneumatic latency is approximately constant over the range of tested pressure.

B.6 HPAA Down Cycle Discussion

Currently, the HPAA is a unidirectional actuator capable of producing plantarflexion motion. This motion is sufficient for almost all types of walking and terrain. However, there are a few situations that may require an alternative actuation method by the HPAA. Any motion that requires the toe to contact the ground before the heel, like hopping, will require a change in actuation method by the HPAA. Figure

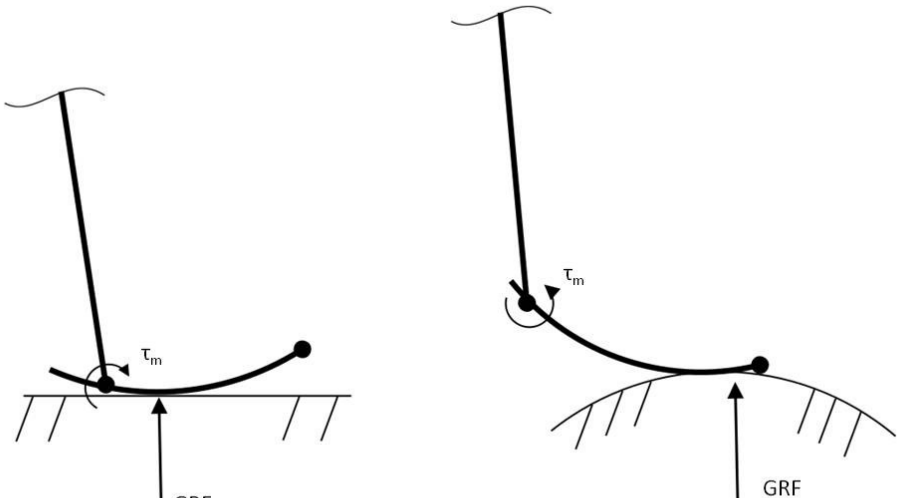

Figure B.6.1: Shows the loading conditions for the ankle during walk and hop motions. (a) Shows the ankle motor torque opposing the ground reaction force (GRF) during normal walk. (b) Shows the ankle motor torque in the same direction as the GRF during the landing of a hop.

B.6.1 shows the direction of HPAA micro-actuator torque for both normal walking and toe-first motion. Controlling toe-first motion is not about applying a force to generate dorsiflexion, but to damping the rate at which the ankle naturally wants to dorsiflex. Therefore, for these situations where toe-first motion is preferred; the HPAA will become a power damper.

The HPAA power damper will work by using the stepper motor in tandem with the GRF to compress the air in the pneumatic ram. Consequently, as the ram is compressed the opposing force will increase with pressure. A bleed valve and threshold pressure feedback controller will be used in conjunction to prevent the pressure build up from stopping motion. Figure B.6.2 shows the electro-pneumatic control circuit for the HPAA pneumatic ram. Figure B.6.2a shows the control circuit during normal walking, and Figure B.6.2b shows the control circuit during power damping. The difference between the two states is that during normal walking the bleed valve and PWM controller are off, and the main valve is on. However, during power damping the PWM controller reads the pressure and pulses the bleed valve on/off to maintain a set range of pressure. The main valve is closed during this operation.

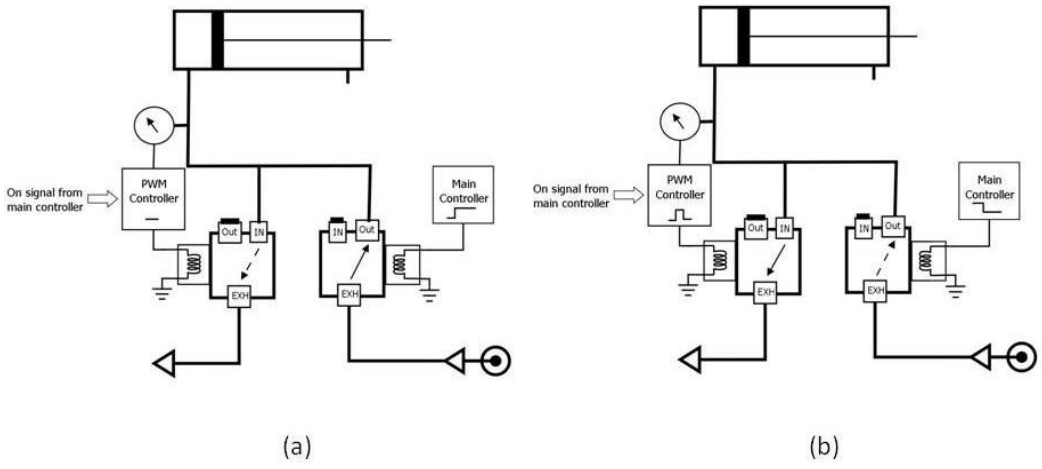

Figure B.6.2: The electro-pneumatic circuit for the HPAA for both normal walking and power damping phases. (a) Shows the state of the control circuit during normal walking. (b) Shows the state of the control circuit during power damping.

APPENDIX C: JAYWALKER STEP TESTING

This appendix contains supplemental information about the step testing and dynamics of the Jaywalker walking machine.

C.1 Secondary Step Parameters

The initial stance leg plantarflexion (steps) and ankle velocity (steps/s) are given in terms of values inputted into the controller. The following examples show how to covert these values into RPM and degrees about the ankle shaft.

Example 1: Converting control steps into degrees of ankle rotation.

Sending a10 step pulse train from the control computer will cause the stepper motor to take 1 step. This is because of the micro-step controller used to drive the stepper motor. The stepper motor advances the output shaft 1.8° for every step. Due to the 15:1 worm gear reduction between the stepper motor and ankle joint; 1.8° of motor shaft rotation moves the ankle joint 0.10°. Therefore, for every 10 steps sent from the control computer; the ankle will move 0.10°.

$$Ankle\ Rotation\ (\text{deg}) = \frac{(No.of\ Steps \times 1.8°)}{(10 \times 15)} \qquad \text{(C.1.1)}$$

Example 2: Converting control velocity into RPM of ankle joint.

Sending a 100 (step/s) pulse train from the control computer will cause the stepper motor to move at 10 (steps/s). Again, this is because of the stepper motors micro-step

controller. There are 200 steps per revolution for the motor drive shaft. This corresponds to 3000 steps per revolution for the ankle joint, because of the 15:1 gear reduction. Therefore, a 100 (step/s) frequency sent from the control computer will cause the ankle to move at 2 RPM.

$$Ankel\ Vel\ (RPM) = \frac{(Step\ Freq \times 60)}{(10 \times 200 \times 15)} \qquad \text{(C.1.2)}$$

The initial ankle angle for the front leg is defined by how far the foot is plantarflexed relative to its maximum dorsiflexion position. Figure C.1.1 shows the initial ankle angle of the front foot during step testing. This value ranged from 0 to 1750 steps (0 -21°) during step testing.

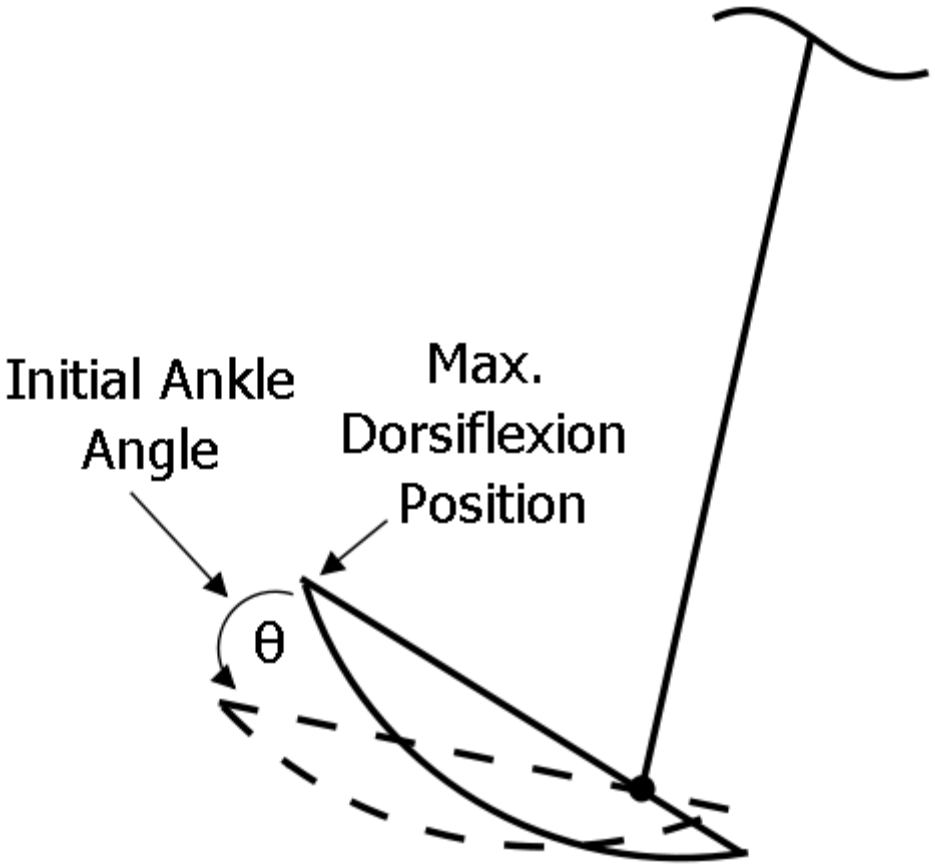

Figure C.1.1: Shows the initial ankle angle for the front leg the during step test.

C.2 Step Testing Decision Chart

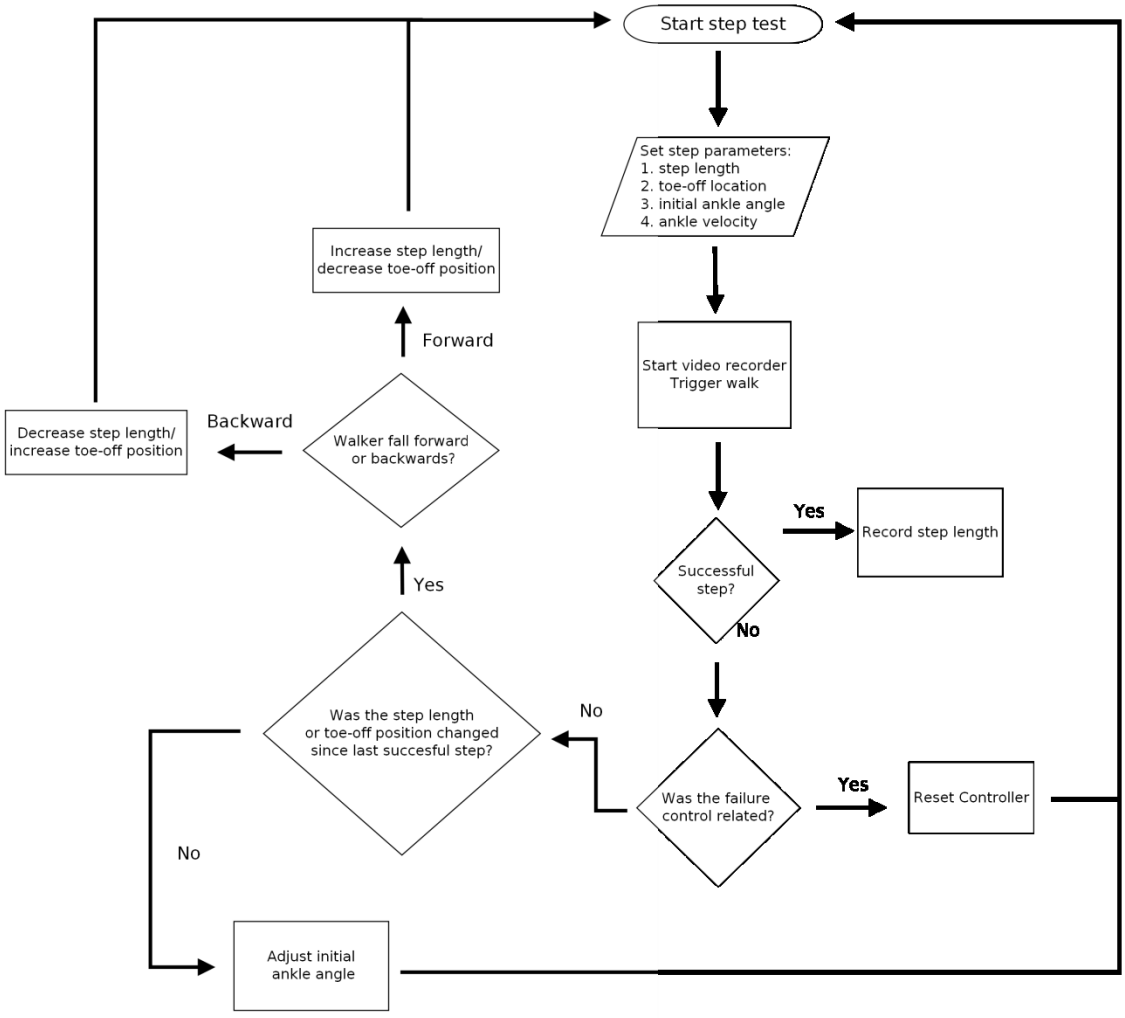

Figure C.2.1: Decision logic used in step testing to determine which parameters to vary during testing.

C.3 Jaywalker Equations of Motion

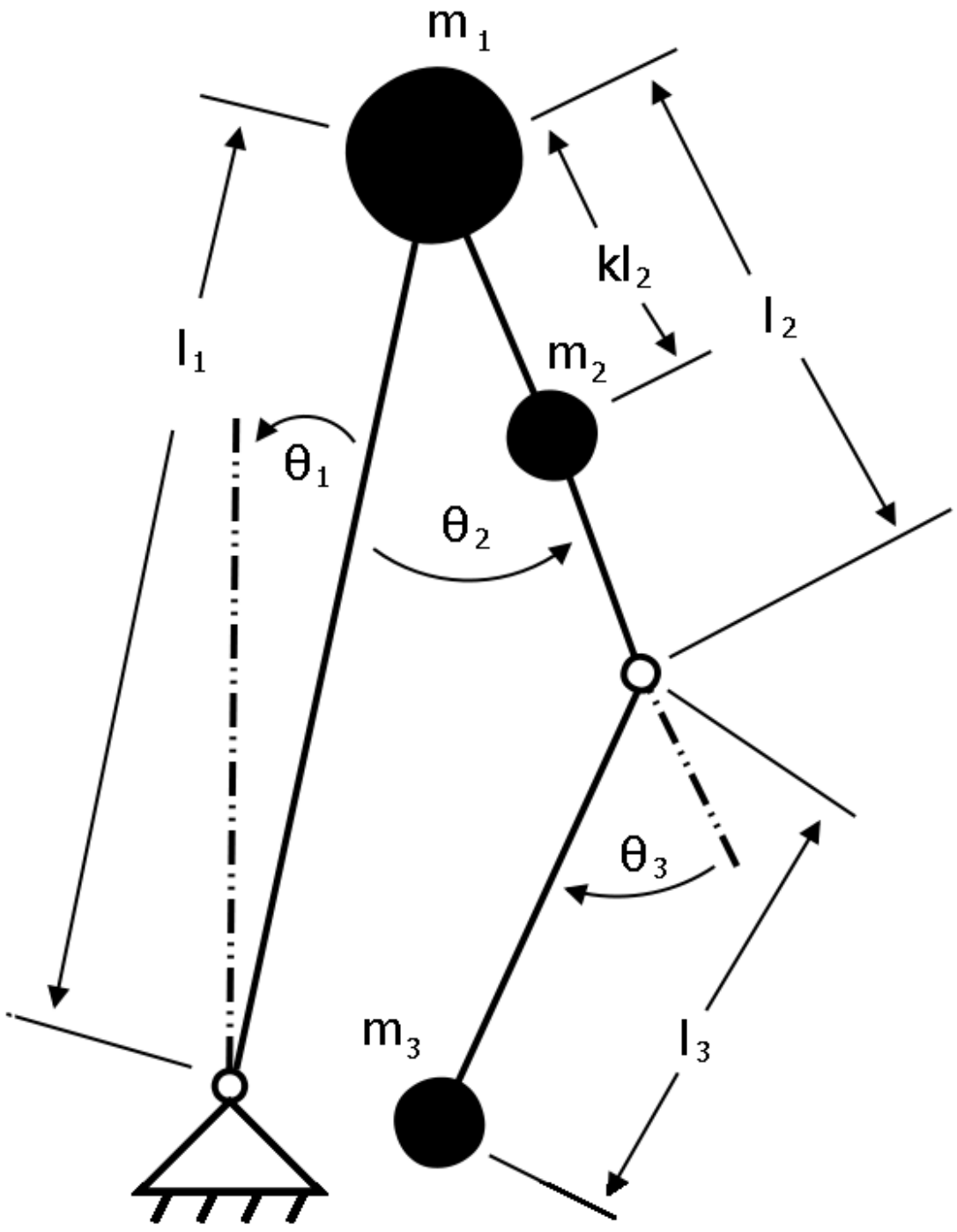

Figure C.3.1: Simplified lumped mass model used to derive the equations of motion for the Jaywalker walking machine.

A simplified 3-link lumped mass model was used to derive the equations of motion for the Jaywalker walking machine. The center-of-mass of the thigh is not located at the distal end of the link. It is located at some fractional distance away from the hip. The variable k, represents this unknown fraction. A single mass is used to represent the foot and shank mass at the distal end of link 3. This is shown in Figure C.3.1.

The equations-of-motion where solved using the following Lagrange equation,

$$\frac{d}{dt}\left(\frac{\partial \mathcal{L}}{\partial \dot{q}_i}\right) - \frac{\partial \mathcal{L}}{\partial q_i} = Q_i', \qquad \text{(C.3.1)}$$

where $\mathcal{L}$ is the Lagrangian function, q_i is the general coordinate and Q_i' is the applied force not able to be converted into a potential energy. The Lagrangian function is the difference between the total kinetic energy (T) and the total potential energy (V) of the system,

$$\mathcal{L} = T - V. \qquad \text{(C.3.2)}$$

The serial chain kinematics and Lagrange equation can become very lengthy. The following abbreviations of trigonometric functions are made to allow the equations to better fit c

$$\cos(\theta_1) = c_1$$
$$\cos(\theta_2) = c_2$$
$$\cos(\theta_3) = c_3$$
$$\cos(\theta_2 - \theta_3) = c_{23}$$

$$\sin(\theta_1) = s_1$$
$$\sin(\theta_2) = s_2$$
$$\sin(\theta_3) = s_3$$
$$\sin(\theta_2 - \theta_1) = s_{21}$$
$$\sin(\theta_2 - \theta_3) = s_{23}$$
$$\sin(\theta_2 - \theta_1 - \theta_3) = s_{213}$$

The serial kinematic chain velocities are:

$$\dot{R}_1^2 = l_1^2\dot{\theta}_1^2, \tag{C.3.3}$$

$$\dot{R}_2^2 = l_1^2\dot{\theta}_1^2 + k^2 l_2^2\left(\dot{\theta}_2 - \dot{\theta}_1\right)^2 + 2kl_1l_2\left(\dot{\theta}_1\dot{\theta}_2 - \dot{\theta}_1^2\right)c_2, \tag{C.3.4}$$

$$\dot{R}_3^2 = l_1^2\dot{\theta}_1^2 + l_2^2\left(\dot{\theta}_2 - \dot{\theta}_1\right)^2 + l_3^2\left(\dot{\theta}_2 - \dot{\theta}_1 - \dot{\theta}_3\right)^2 + 2l_1l_2\left(\dot{\theta}_1\dot{\theta}_2 - \dot{\theta}_1^2\right)c_2 + 2l_1l_3\left(\dot{\theta}_1\dot{\theta}_2 - \dot{\theta}_1^2 - \dot{\theta}_1\dot{\theta}_3\right)c_{23} + 2l_2l_3(\theta_2 - \theta_1)\left(\dot{\theta}_2 - \dot{\theta}_1 - \dot{\theta}_3\right)c_3, \tag{C.3.5}$$

where R is the position vector of the point mass. The total kinetic energy is

$$T = \sum_{i=1}^{3}\frac{1}{2}m_i\dot{R}_i^2, \tag{C.3.6}$$

and the total potential energy is

$$V = \sum_{i=1}^{3} m_1 g R_{y,i}, \tag{C.3.7}$$

where $R_{y,i}$ is the vertical component of the point mass position vector. Applying equations C3.2 – C.3.7 to C.3.1 yield the following equations of motion:

$$\tau_1 = \left[(m_1 + m_2 + m_3)l_1^2 + (km_2 + m_3)(l_2^2 - 2l_1l_2c_2) + m_3\left(l_3^2 - 2l_3(l_1c_{23} - l_2c_3)\right)\right]\ddot{\theta}_1 - [(km_2 + m_3)(l_2^2 - l_1l_2c_2) - m_3l_2(l_1c_{23} - 2l_3c_3)]\ddot{\theta}_2 + [m_3l_3(l_3 - l_1c_{23} + l_2c_3)]\ddot{\theta}_3 - [(km_2 + m_3)l_1l_2s_2 + m_3l_1l_3s_{23}]\dot{\theta}_2^2 - [m_3l_3(l_1s_{23} + l_2s_3)]\dot{\theta}_3^2 + \left[2l_1\left((km_2 + m_3)l_2s_2 + m_3l_3s_{23}\right)\right]\dot{\theta}_1\dot{\theta}_2 - [2m_3l_3(l_1s_{23} + l_2s_3)]\left[\dot{\theta}_1\dot{\theta}_3 + \dot{\theta}_2\dot{\theta}_3\right] - (m_1 + m_2 + m_3)gl_1s_1 - (km_2 + m_3)gl_2s_{21} - m_3gl_3s_{213}\,, \tag{C.3.8}$$

$$\tau_2 = [(km_2 + m_3)(l_2^2 - l_1l_2c_2) + m_3l_3(l_3 + l_1c_{23} + 2l_2c_3)]\ddot{\theta}_1 + [(km_2 + m_3)l_2^2 + m_3l_3(l_3 + 2l_2c_3)]\ddot{\theta}_2 - [m_3l_3(l_3 + l_2c_2)]\ddot{\theta}_3 - [(km_2 + m_3)l_1l_2s_2 + m_3l_1l_3s_{23}]\dot{\theta}_1^2 + m_3l_2l_3s_3\dot{\theta}_3^2 + 2m_3l_3s_3\dot{\theta}_1\dot{\theta}_3 - 2m_3l_2l_3s_3\dot{\theta}_2\dot{\theta}_3 + (km_2 + m_3)gl_2s_{21} + m_3gl_3s_{213}\,, \tag{C.3.9}$$

and

$$\tau_3 = [m_3 l_3(l_3 - l_1 c_{23} + l_2 c_3)]\ddot{\theta}_1 - [m_3 l_3(l_3 + l_2 c_3)]\ddot{\theta}_2 + m_3 l_3^2 \ddot{\theta}_3 + [m_3 l_3(l_1 l_{23} + l_2 s_3)]\dot{\theta}_1^2 + m_3 l_2 l_3 s_3 \dot{\theta}_2^2 - 2m_3 l_2 l_3 s_3 \dot{\theta}_1 \dot{\theta}_2 - m_3 l_3 s_{213} \ . \quad \text{(C.3.10)}$$

τ_1, τ_2 and τ_3 are the torques generated about the ankle, hip and knee joints respectively.

When analyzing passive walkers with the assumption that $m_{leg} << M_{hip}$; the equations simplify that of a single inverted pendulum and the torque is zero. The legs essentially become kinematic restraints that define the motion of the hip mass.

Equations C.3.8-C.3.10 were developed to be used with accelerometer data to indirectly measure the joint torque of the Jaywalker. So that the walking machines actuators can be optimized for rough terrain.